January 2011

Nonuniform Power Changes and Spatial, Temporal and Spectral Diversity in High Gamma Band (>60 Hz) Signals in Human Electrocorticography

Charles Gaona
Washington University in St. Louis

WASHINGTON UNIVERSITY IN ST. LOUIS

School of Engineering and Applied Science

Department of Biomedical Engineering

Dissertation Examination Committee:
Eric C. Leuthardt, Chair
Dennis L. Barbour
Daniel W. Moran
Abraham Z. Snyder
Larry H. Snyder
Kilian Q. Weinberger

NONUNIFORM POWER CHANGES AND SPATIAL, TEMPORAL AND SPECTRAL DIVERSITY IN HIGH GAMMA BAND (>60 HZ) SIGNALS IN HUMAN ELECTROCORTICOGRAPHY

by

Charles Michael Gaona

A dissertation presented to the Graduate School of Arts and Sciences
of Washington University in partial fulfillment of the
requirements for the degree of

DOCTOR OF PHILOSOPHY

August 2011
Saint Louis, Missouri

The views expressed in this article are those of the author and do not reflect the official policy or position of the United States Air Force, Department of Defense, or the U.S. Government.

ABSTRACT OF THE DISSERTATION

Nonuniform power changes and spatial, temporal and spectral diversity in high gamma band (>60 Hz) signals in human electrocorticography

by

Charles Michael Gaona

Doctor of Philosophy in Biomedical Engineering

Washington University in St. Louis, 2011

Research Advisor: Professor Eric Claude Leuthardt, M.D.

High-gamma band (>60Hz) power changes in cortical electrophysiology are a reliable indicator of focal, event-related cortical activity. In spite of discoveries of oscillatory subthreshold and synchronous suprathreshold activity at the cellular level, there is an increasingly popular view that high-gamma band amplitude changes recorded from cellular ensembles are the result of asynchronous firing activity that yields wideband and uniform power increases. Others have demonstrated independence of power changes in the low- and high-gamma bands, but to date, no studies have shown evidence of any such independence above 60Hz. Based on non-uniformities in time-frequency analyses of electrocorticographic (ECoG) signals, we hypothesized that induced high-gamma band (60-500Hz) power changes are more heterogeneous than currently understood. We quantified this spectral non-uniformity with two different approaches using single-word repetition tasks in human subjects. First, we showed that the functional responsiveness of different ECoG high-gamma sub-bands can discriminate cognitive tasks (e.g., hearing, reading, speaking) and cortical locations. Power changes in these sub-bands of the high-gamma

range are consistently present within single trials and have statistically different time courses within the trial structure. Moreover, when consolidated across all subjects within three task-relevant anatomic regions (sensorimotor, Broca's area, and superior temporal gyrus), these behavior- and location- dependent power changes evidenced nonuniform trends across the population of subjects. Second, we studied the dynamics of multiple frequency bands in order to quantify the diversity present in the ECoG signals. Using a matched filter construct and receiver operating characteristic (ROC) analysis we show that power modulations correlated with phonemic content in spoken and heard words are represented diffusely in space, time and frequency. Correlating power modulation in multiple frequency bands above 60 Hz over broad cortical areas, with time varying envelopes significantly improved performed area under the ROC curve scores in phoneme prediction experiments. Finally we show preliminary evidence supporting our hypothesis in microarray ECoG data. Taken together, the nonuniformity of high frequency power changes and the information content captured in the spatio-temporal dynamics of those frequencies suggests that a new approach to evaluating high-gamma band cortical activity is necessary. These findings show that in addition to time and location, frequency is another fundamental dimension of high-gamma dynamics.

Acknowledgments

At the culmination of three years of work, and upon reflecting on the outstanding experience I have had studying here at Wash U, there are many people that come to mind that deserve thanks and appreciation for helping me complete the work that I have documented in this dissertation.

First, I need to acknowledge the United States Air Force and the US Air Force Academy for providing me this opportunity. I would also like to thank Dr. Frank Yin and Dr Dan Moran for welcoming me into the Biomedical Engineering program even with the constraints I brought. Next, I would like to thank the patients that participated in this research and their families. Thank you for your invaluable efforts and for allowing me to share a little bit of your lives. I am also very grateful for the technicians and staff of the Barnes and Children's EEG Monitoring Units. Thank you for your patience and support, especially in the evenings and on weekends when you allowed us to interrupt your time off while we worked with your patients. To the Moran Lab: thanks for your keen eyes and thoughtful discussions as this research took shape. I also need to thank the many members of the Leuthardt Lab who have rotated through over the last three years. Thank you for all you have taught me, for making the lab a great home away from home, and for the friendships we have built along the way. Thanks also to my committee, for the thoughtful insights that truly improved this research. Most importantly, I would like to thank my mentor, Eric. For your enthusiastic leadership, steadfast encouragement and friendship I am truly grateful. Thanks for reminding me that there's always a bright side.

I owe an even greater debt to my beloved family, who kept me going through this experience. First, to my wife Jenny: thank you for your love and patience through this process. I love being your husband and am so glad to belong to you. To our four beautiful children, Matthew, Emma, Mikey and Daniel: thank you for the joyful homecomings you gave me each night. Your love brought a smile to my face even on the toughest of days. Finally, to my Maker and Redeemer: thank you for allowing me to pursue You through science and through so many wonderful friendships along the way.

Charles Michael Gaona

Washington University in St. Louis

August 2011

Dedicated to my five reasons: Jenny, Matthew, Emma, Michael and Daniel.

Contents

List of Tables

List of Figures

1 Introduction and Specific Aims

1.1 Introduction

Clinical use of electrocorticography (ECoG) has provided a unique opportunity to study human cortical electrophysiology with high spatial resolution, temporal resolution and signal fidelity for over 70 years. While primarily used as a clinical tool for functional mapping and seizure focus identification, ECoG is also used for studies of surface cortical electrophysiology and is considered a robust brain computer interface (BCI) platform with prospects for long term viability (Leuthardt, Schalk et al. 2004; Chao, Nagasaka et al. 2010). Over the last decade, studies using ECoG and other modalities have identified gamma band power modulation as a reliable and specific phenomenon that localizes event-related neural activity in anatomy and time (Crone, Miglioretti et al. 1998; Leuthardt, Miller et al. 2007). Until now, most ECoG studies have only examined phenomena that occur below 250 Hz and nearly all treat the high-gamma range (>60 Hz) of ECoG signals as a spectrally uniform indicator of cortical activity. However, there is an abundance of evidence from microscale[1] and macroscale electrophysiological research showing oscillatory activity exists above 60 Hz (Sukov and Barth 1998; Jones, MacDonald et al. 2000; Baker, Gabriel et al. 2003). There is need to establish whether ECoG is capable of capturing this oscillatory activity in the high-gamma range and whether these high frequency oscillations are correlated with behavioral.

---

[1] Electrophysiological recordings with spatial scales < 1mm are referred to here as microscale recordings. While there are similarities, ensemble recordings from larger scales are distinguished here from microscale recordings from penetrating microelectrodes or from the cortical surface.

We propose to challenge the paradigm that high-gamma band ECoG signals are a spectrally uniform indicator of cortical activity and is limited to frequencies below 250 Hz. The overall objective of this research is to examine the extent of behaviorally relevant electrophysiological phenomena in the high-gamma range of ECoG signals. To this end, we will study power modulation in several sub-bands of the high-gamma band and their subsequent correlations with several hierarchical levels of behavior. The central hypothesis of this work is that the high-gamma band in ECoG contains behaviorally relevant information in multiple sub-bands above 60 Hz. Based on preliminary evidence from human language studies by our group, we believe that there is substantial diversity in the ECoG signal above 60 Hz. Using an experimental task that allows us to categorize both behavioral stimuli and responses at several hierarchical levels, we will examine the level of information coded in sub-bands of the high-gamma range of ECoG. To help bridge the gap between macro and microscale electrophysiology, we will also utilize ECoG microarrays to examine the extent of high-gamma diversity at a finer spatial resolution. The rationale for this research is that further defining the behavior of the ECoG high-gamma band may reveal previously untapped electrophysiological information that may improve clinical, scientific and BCI applications.

1.2 Specific Aims

We will test the central hypothesis via three specific aims:

Aim 1: Determine whether high-gamma band ECoG (>60 Hz) is a spectrally uniform indicator of cognitive activity. The hypothesis for this aim is that high-gamma activity is spectrally non-uniform and that different cognitive activities can evoke distinct spectral responses in separate sub-bands of the high-gamma range.

Aim 2: Determine whether the spatio-temporal dynamics of multiple frequency bands above 60 Hz encode information about individual cognitive activities under study. The hypothesis for this aim is that information encoded in the spatio-temporal dynamics of multiple frequency bands (> 60 Hz) can improve the ability to categorize the phonemic class of particular cognitive activities under study.

Aim 3: Examine spectral power change patterns and information coding in microarray ECoG. The working hypotheses for this aim are 1) high-gamma range microarray ECoG is spectrally non-uniform and different cognitive activities can evoke distinct spectral patterns in separate sub-bands of the high-gamma range, and 2) information encoded in the temporal dynamics of microarray high-gamma bands can improve the ability to categorize the phonemic class of particular cognitive activities under study.

The expected outcome of this research is that a new approach will be necessary to evaluate high-gamma range electrophysiology. In addition to the time and cortical location of power changes, the specific frequency band within the high-gamma range is another fundamental dimension of cortical electrophysiology for both traditional and microarray ECoG. The discovery of frequency diversity in the high-gamma range will provide the opportunity to explore the dynamics of these high-gamma sub-bands and their behavioral and neuronal correlates which may better facilitate the continuing synthesis of cellular, ensemble, and behavioral neuroscience.

1.3 Dissertation Overview and Organization

This thesis is divided into seven chapters. The second chapter provides the background and significance of the research. A review of relevant literature on electrophysiology recording techniques and relationships to functional imaging provides the context for the

research. Then, evidence of high-gamma band spectral, spatial and temporal diversity is presented in support of the three hypotheses. The chapter concludes with a discussion of the clinical and scientific significance of this work.

Chapter 3 describes the methods used in this research. The chapter is subdivided into four major sections. First common methods to all three aims are explained. The subsequent sections detail the experimental set up and analysis techniques used to test each of the three major hypotheses of this work.

Chapter 4 addresses the first hypothesis: that there is spectral diversity in the gamma band above 60 Hz. The results for individual subjects and then summaries across the subject population show that nonuniformities in high-gamma band power changes can dissociate cognitive tasks and anatomy.

Chapter 5 covers the second major hypothesis: that the spatio-temporal dynamics of multiple frequency bands above 60 Hz encode behaviorally relevant information. The results show that ECoG signals contain enough information to predict phonemic content in the context of a single word repetition experiment. The amount of information encoded in each domain is then quantified using a matched filter correlator. The results here show that phonemic information is encoded diversely in the spatial, temporal and spectral domains of ECoG signals.

Chapter 6 shows the results after testing the third major hypothesis: that microscale surface potentials have spectral diversity above 60 Hz and that the dynamics of high frequency rhythms encode information. Preliminary results in one subject demonstrate that there is sufficient spectral diversity in microarray ECoG signals to dissociate anatomic locations separated by as little as 1 mm. Further, there is sufficient information to discriminate

phonemic content in the spatial, temporal and spectral patterns of power modulations within a $9mm^2$ cortical location.

Chapter 7 concludes the work with a discussion of these findings in the context of the existing body of research, the implications of this work and suggested directions for future studies.

1.4 References

Baker, S., C. Gabriel and R. Lemon (2003). "Eeg oscillations at 600 hz are macroscopic markers for cortical spike bursts." The Journal of Physiology **550**(2): 529.

Chao, Z., Y. Nagasaka and N. Fujii (2010). "Long-term asynchronous decoding of arm motion using electrocorticographic signals in monkeys."

Crone, N., D. Miglioretti, B. Gordon and R. Lesser (1998). "Functional mapping of human sensorimotor cortex with electrocorticographic spectral analysis. Ii. Event-related synchronization in the gamma band." Brain **121**(12): 2301-2315.

Jones, M. S., K. D. MacDonald, B. Choi, F. E. Dudek and D. S. Barth (2000). "Intracellular correlates of fast (>200 hz) electrical oscillations in rat somatosensory cortex." J Neurophysiol **84**(3): 1505-1518.

Leuthardt, E. C., K. Miller, N. R. Anderson, G. Schalk, J. Dowling, J. Miller, D. W. Moran and J. G. Ojemann (2007). "Electrocorticographic frequency alteration mapping: A clinical technique for mapping the motor cortex." Neurosurgery **60**(4): 260-271

Leuthardt, E. C., G. Schalk, J. R. Wolpaw, J. G. Ojemann and D. W. Moran (2004). "A brain-computer interface using electrocorticographic signals in humans." Journal of Neural Engineering **1**(2): 63-71.

Sukov, W. and D. S. Barth (1998). "Three-dimensional analysis of spontaneous and thalamically evoked gamma oscillations in auditory cortex." J Neurophysiol **79**(6): 2875-2884.

2 Background and Significance

This chapter provides an overview of electrophysiological research techniques at different spatial scales and their relationships to each other as well as functional imaging techniques. This section will place this dissertation in the context of the existing body of literature. We then cover supporting evidence for each of the three aims of this dissertation as a basis for each of the three associated hypotheses. Finally, this chapter will discuss the clinical and scientific significance of this research.

2.1 Techniques for Recording Cortical Activity

There are several techniques for studying brain activity by measuring electrical activity directly and indirectly. Here they are categorized by spatial scale. Each has advantages and disadvantages, but all have made significant contributions to the understanding of cortical function. The primary focus of this review is on electrophysiological methods; however, since there is such a large body of brain research performed with magnetic resonance imaging (MRI), the relationship of the electrophysiological methods to the blood oxygenation level dependence (BOLD) signal is also covered.

2.1.1 Microscale Electrophysiology

In this dissertation, the term microscale refers to linear spatial scales less than 1 mm. This distinction is made because the diameter of a cortical column is approximately 0.1mm (Kandel, Schwartz et al. 2000). Therefore, when considering measurements using electrodes with diameters of 1mm or more, the dynamics of cortical columns become aggregated into mesosources, the spiking activity of individual neurons is no longer

detectable and the interpretation of electrophysiological signals must be viewed in a different way (Nunez and Srinivasan 2006).

2.1.1.1 Intracellular Recordings

At the finest spatial scale of electrophysiology, intracellular recordings using glass micropipettes or patch clamps measure electric potentials inside the cell membrane. Intracellular neuronal recordings started with Hodgkin and Huxley's work in characterizing the cell membrane characteristics of the giant squid axon (Hodgkin and Huxley 1939). Recordings of intracellular potentials can capture both action potential firing and oscillatory behavior in a single neuron (Ylinen, Bragin et al. 1995; Jones, MacDonald et al. 2000). These recordings also have the highest signal to noise ratios, capturing signals on the order of 100 mV (Malmivuo and Plonsey 1995). Studies using these techniques commonly examine the properties and dynamics of neurotransmitters, ion channels and cell membranes (Neher, Sakmann et al. 1978; Cahalan and Neher 1992). They have also been used to correlated intracellular electrophysiology with extracellular phenomena (Jones, MacDonald et al. 2000).

2.1.1.2 Extracellular Recordings

Recordings from microwires that penetrate the cortex to capture electric potentials from the intraparenchymal space are commonly referred to as extracellular, single unit activity, multiunit activity (MUA) or laminar recordings. The electrode dimensions range from 1s–10s μm and can capture action potential firing from one or more neurons (Hubel and Wiesel 1959) as well as subthreshold fluctuations in the extracellular field commonly referred to as local field potentials (LFP) (Renshaw, Forbes et al. 1940). The signal levels in these recordings vary according to the distance from the cell soma and typically range

from 100μV to 1mV (Jones, MacDonald et al. 2000). As technology has advanced, arrays of penetrating microelectrodes have made recording from multiple neurons and the associated LFPs possible as well (Buzsáki 2004). Studies of extracellular recordings have been used to study correlations of neural activity with sensory stimuli (Hubel and Wiesel 1959), physical location (O'Keefe and Dostrovsky 1971) and motor movements (Georgopoulos, Schwartz et al. 1986). They have also been shown to correlate with higher levels of cognitive function such as object attribute representation (Maunsell and Van Essen 1983), motor planning (Lawrence, White et al. 2005), decision thresholds (Gold and Shadlen 2001) and attention (Corbetta, Akbudak et al. 1998). Within the last decade, single and multiunit microscale extracellular recordings have been used as successful brain computer interface (BCI) platforms in human and nonhuman primates (Taylor, Tillery et al. 2002; Hochberg, Serruya et al. 2006; Velliste, Perel et al. 2008).

2.1.1.3 Microscale Epipial Recordings

Microscale recordings are also possible from the cortical surface (pia mater). Using nonpenetrating microwire electrodes with diameters ranging from 10-100 μm, these recordings capture electrophysiological dynamics from populations of cells and have been referred using terms such as epipial encephalography (EEG) and cortical potentials. At the cortical surface, potentials have magnitudes on the order of 100 μV (Jones, MacDonald et al. 2000). Studies using this modality have examined somatosensory responses in rodent whisker barrel cortex (Staba, Ard et al. 2005), mammalian olfactory bulb (Freeman and Baird 1987), and monkey visual cortex (Freeman and van Dijk 1987) amongst others. Recent research using microscale pial recordings in humans have correlated surface LFPs at multiple frequencies with contra- and ipsilateral motor movements (Leuthardt,

Freudenberg et al. 2009) and spoken words (Kellis, Miller et al. 2010). Recordings at this scale have also been used as a capable platform for brain computer interfaces in both human and non-human primates (Heldman 2007; Leuthardt, Gaona et al. 2011).

2.1.1.4 Integrative Microscale Research

The various phenomena captured by these techniques are inter-related at the microscale and across spatial scales. Many have studied how oscillatory synchrony in LFPs affects action potential firing (Gray, König et al. 1989; Buzsaki and Draguhn 2004), and the resulting implications of that relationship as a means of modulating sensitivity to neuronal inputs, temporally coordinating groups of neurons into assemblies, facilitating synaptic plasticity and consolidating information into long-term memory (Fries, Nikolic et al. 2007; Uhlhaas, Pipa et al. 2009). Additionally, cross-modality studies have revealed intracellular correlates of extracellular and cortical surface phenomena (Jones, MacDonald et al. 2000). The relationship of microscale electrophysiology to the functional MRI BOLD signal has been elucidated. Simultaneous recordings of BOLD and multiunit activity in anesthetized monkeys correlated both multiunit firing and LFP fluctuations with BOLD responses (Logothetis, Pauls et al. 2001).

2.1.2 Macroscale Electrophysiology

Macroscale recordings capture activity from multiple columns including 10^7 or more neurons depending on the specific technique. Because these techniques do not invade the parenchymal space, they are less invasive and therefore have clinical as well as scientific uses.

2.1.2.1 Scalp Recordings

Both electric and magnetic fields emanating from neural activity can be recorded from the scalp. Because they record from neural populations on the same orders of magnitude, scalp EEG and magnetoencephalography (MEG) are discussed together even though they most likely record from complimentary neural populations. Scalp EEG electrodes recording electric fields from the brain are mostly likely to record dipole current generators that are oriented normal to the scalp surface. In contrast, MEG is most likely to capture magnetic fields emanating from dipoles oriented tangentially to the scalp (Nunez and Srinivasan 2006). Therefore it is most likely that EEG captures cortical activity from the crowns of neocortical gyri, while MEG captures activity from within the sulci. The benefits of scalp recordings are the ability to study healthy human subjects, while obtaining recordings from broad cortical areas. However the primary disadvantage of studying scalp recordings is a low signal to noise ratio. It has been reported that approximately 6 cm^2 of cortex must become synchronized for electric signals to be recordable at the scalp (Nunez and Srinivasan 2006). The actual voltage levels and magnetic field strengths recorded at the scalp range between 10-100 μV (Nunez and Srinivasan 2006) or 10-100 fT (Dhond, Witzel et al. 2005) which makes these signals especially susceptible to environmental, electrooculographic and electromyographic contamination. Clinically, EEG has been used as a diagnostic for sleep disorders, epileptic seizure identification and localization (Blum and Rutkove 2007) and, though not without controversy, as a confirmatory test of coma and brain death (Roest, van Bets et al. 2009; Wijdicks 2010). MEG is being studied as a potential clinical diagnostic tool for several brain disorders (Georgopoulos, Karageorgiou et al. 2007).

The analysis techniques applied to scalp recordings generally study time-domain waveforms or specific frequency bands. Low pass time domain responses to stimuli are commonly referred to as event related potentials (ERP) (Makeig, Westerfield et al. 2002). Different features of these waveforms have been attributed to specific activities during cognitive processing (Salmelin 2007) and their spatial organization provides insight into specific cortical locations associated with these processes (Dhond, Witzel et al. 2005). Observation of oscillatory power modulations in specific bands (generally below 40 Hz, though as high 100 Hz) has been termed event related synchronization/ desynchronization (ERS/ERD) and has been correlated with motor movements (Pfurtscheller and Lopes da Silva 1999). While many scalp recorded studies focus on oscillatory activity below 40 Hz, both MEG and EEG have been used to examine gamma band (>40 Hz) activity as well (Kaiser and Lutzenberger 2003; Herrmann, Fründ et al. 2010). Because scalp recordings can encompass the entire outer surface of the cerebral cortex, they have also been used to study oscillatory synchrony on large scales (Pockett, Bold et al. 2009). EEG has also been used for more than two decades as a BCI platform for humans (Farwell and Donchin 1988; Wolpaw, McFarland et al. 1991), although because of low signal to noise ratios, they typically demand long training periods (Leuthardt, Miller et al. 2006). Integrative studies using EEG have also helped link scalp recorded phenomena with other electrophysiological scales. Simultaneous recordings of EEG and MUA have correlated the combination of gamma band power increases and negative delta phase from EEG with MUA aggregate firing rate (Whittingstall and Logothetis 2009).

2.1.2.2 Macroscale Subdural Recordings

Macroscale recordings directly from the cortical surface are known as Electrocorticography (ECoG), as well as intracranial EEG (iEEG), subdural EEG, and epipial EEG. This technique captures neuronal population dynamics from the gyral crowns. In humans, the most common electrodes have 2.4 mm diameters and 10 mm interelectrode spacing, though other form factors exist (Ad-Tech 2008; Blakely, Miller et al. 2008). Typical grids span areas as large as 8 cm x 8 cm and therefore cover relatively broad cortical areas. Because subdural electrodes are 1.5 mm away from the layer V pyramidal cells which putatively generate most of the dipole currents sensed at the surface, typical amplitudes reach 100s μV (Nunez and Srinivasan 2006). Penetrating macroscale depth electrodes used in clinical care are also categorized at this spatial scale. These linear arrays of cylindrical electrodes typically have 1.1 mm diameters and 2.3 mm heights, with 5-10 mm interelectrode spacings (Ad-Tech 2008). Although these electrodes pass through both gray and white matter in the cortex, because of their size, they capture population dynamics on the same scales as cortical surface electrodes. Clinically, ECoG is routinely used to identify epileptic seizure foci and for functional mapping prior to neurosurgical resections (Goldring and Gregorie 1984).

Research studies using ECoG use many of the same techniques applied to scalp and microscale LFP recordings: ERP analysis, band limited power changes and phase synchrony. The body of ECoG-based research has examined the neural substrates of many cognitive activities: contra- and ipsilateral motor systems (Crone 2000; Pfurtscheller, Graimann et al. 2003; Leuthardt, Miller et al. 2007; Wisneski, Anderson et al. 2008; Miller, Zanos et al. 2009), selective attention (Brovelli, Lachaux et al. 2005; Tallon-Baudry,

Bertrand et al. 2005; Ray, Niebur et al. 2008), memory (Fell, Klaver et al. 2001; Sederberg, Kahana et al. 2003; Mormann, Fell et al. 2005; Anderson, Rajagovindan et al. 2009), visual stimuli (Lachaux, George et al. 2005), auditory stimuli (Crone, Boatman et al. 2001; Trautner, Rosburg et al. 2006; Canolty, Soltani et al. 2007; Edwards, Soltani et al. 2009) human language (Crone, Hao et al. 2001; Canolty, Soltani et al. 2007; Mainy, Jung et al. 2008; Towle, Yoon et al. 2008). ECoG has also been explored as a BCI platform because of high signal to noise ratios, prospects for long term viability and a cortical coverage that may allow a broad range of behavioral modalities for control signals (Leuthardt, Schalk et al. 2009). A number of human studies using ECoG as a BCI have achieved one-dimensional (Leuthardt, Schalk et al. 2004; Leuthardt, Miller et al. 2006) and two-dimensional (Schalk, Miller et al. 2008; Rouse and Moran 2009) control of a cursor on a computer screen. Because of the reliability and fidelity of the control features, the human subjects using ECoG-based BCIs were able to achieve control with performance above chance after 3-24 minutes of training (Leuthardt, Schalk et al. 2004). Non-human primate studies examining the longevity and stability of ECoG signals in the context of a three-dimensional reaching task have also reported that the cortical dynamics remained stable for up to 5 months (Chao, Nagasaka et al. 2010).

Integrative studies across modalities using ECoG have also been accomplished. Slow cortical potentials and gamma band correlation structures from ECoG recordings have been shown to be similar in structure to BOLD functional connectivity maps (He, Snyder et al. 2008). ECoG gamma band power decreases have been correlated with task-related default network BOLD signal decreases as well (Miller, Weaver et al. 2009). Additional studies have also highlighted correlations between neuronal activity indicators in ECoG and BOLD (Brovelli, Lachaux et al. 2005).

In summary, while the different electrophysiology recordings techniques have their strengths and weaknesses, they capture the same physiological phenomena at different scales and therefore should be viewed synergistically. It is also clear that there are correlations between electrophysiological recordings from single units up through scalp electrodes with the fMRI BOLD signal which has been used as a measurement technique for a vast amount of neuroscience research.

2.2 Research Supporting the Three Aims

This section of the literature review focuses on specific research relevant to the discussion of the three aims of this dissertation. First, we will examine gamma band literature, the associated evidence for oscillatory phenomena in the high range of the gamma band, and emerging views on uniform broadband power changes in macroscale electrophysiology. Second, we review literature illustrating spatial and temporal diversity in the neural correlates of cognitive activity associated with language. Finally, we address the third aim of this dissertation and review the evidence for spatial diversity in microscale electrophysiological recordings.

2.2.1 Nonuniform Power Changes Above 60 Hz in Macroscale Recordings

It is commonly accepted that different low frequency bands in macroscale electrophysiological signals are indicators of different physiological phenomena. Slow cortical potentials (<0.5 Hz) have been studied as a correlate of BOLD functional connectivity networks and are thought to be an indicator of fundamental cortical structure (He, Snyder et al. 2008). Local frequency potentials (0.5-10 Hz) over motor cortex have been correlated with arm reaching and finger movements (Schalk, Kubanek et al. 2007;

Acharya, Fifer et al. 2010). Alpha rhythms (8-12 Hz) have been correlated with relaxation (Blum and Rutkove 2007), and the suppression of alpha rhythms is usually associated with somatosensory cortical activity (Crone, Miglioretti et al. 1998). Cortically broad beta rhythm (12-30 Hz) suppressions are typically associated with cognitive activity and sensorimotor activation (Crone, Miglioretti et al. 1998; Nunez and Srinivasan 2006). Gamma rhythms are spatially and temporally focal indicators of cortical processing associated with several cognitive tasks (Spydell, Ford et al. 1979; Pfurtscheller, Neuper et al. 1993; Crone, Miglioretti et al. 1998). Additionally, gamma rhythms have been subparcellated into low-gamma (30-60 Hz) and high-gamma (>60 Hz) bands in the macroscale literature because they have been shown to activate independently (Crone, Boatman et al. 2001; Edwards, Soltani et al. 2005).

In spite of the existence of these low frequency rhythms, the notion of band specific oscillatory activity has not been widely extended to the high-gamma range (>60 Hz) in the macroscale literature. The primary question for Aim 1 is the existence of nonuniform power modulation (presumably caused by oscillatory activity) above 60 Hz. In support of our hypothesis, there are several examples of electrophysiological evidence of neuronal activity at various frequencies above 60 Hz. It is not uncommon for single neurons to fire at rates reaching several hundred Hertz. Intrinsic bursting cells have been reported to fire at 200 Hz for brief periods, while fast repetitive bursting cells can reach rates up to 600 Hz (Contreras 2004). Microscale LFP recordings have also revealed evidence of high frequency oscillatory activity. Jones et al. have shown that high frequency oscillations in rat barrel cortex somatosensory evoked potentials (SSEP) between 200-600 Hz have both intra- and extracellular correlates. The oscillations between 200-400 Hz appear to result from intracortical connections (Staba, Ard et al. 2005), and have been proposed as a

mechanism for synchronizing timing on a sub millisecond scale (Barth 2003). The very high frequency oscillations in epipial recordings between 400-600 Hz were shown to correlate well with summated action potentials from populations of neurons (Jones, MacDonald et al. 2000). Very high frequency oscillations (600 Hz) have also been reported in human scalp SSEPs (Curio 2000) and nonhuman primate epidural SSEPs (Baker, Gabriel et al. 2003). The primate epidural oscillations were phase locked with simultaneously recorded single unit action potentials initiated by both electrical and tactile stimulation. Evidence for high frequency LFPs has not been confined to somatosensory cortex. Several studies have examined high frequency oscillations (approx 200 Hz) in the hippocampus referred to as sharp wave ripples (Ylinen, Bragin et al. 1995). Some have reported a possible association between sharp wave ripples and memory (Ponomarenko, Chepurnova et al. 2002), while others have studied their relationships to the pathology of epilepsy (Bragin, Wilson et al. 2002). Thus, there is microscale evidence of action potential firing and LFP oscillations at very high frequencies that appears to cross spatial scales.

Data from macroscale studies of the gamma band have shown indications of nonuniform power modulations above 60 Hz as well. In many cases, high frequency bands appear to activate nonuniformly in exemplar time-frequency analyses, but subsequent analyses in the studies only examine the total power in a relatively wide range of frequencies (e.g., 60-200 Hz) as a uniform entity (Brown, Rothermel et al. 2008; Korzeniewska, Crainiceanu et al. 2008; Mainy, Jung et al. 2008). One study of a single patient showed distinctions in time-frequency analyses and studied power changes within various narrow bands ranging from 70-200 Hz: however, the differences in these bands were not discussed (Brovelli, Lachaux et al. 2005). Another study highlighted individual patient differences in peak activation frequencies in the gamma band between two anatomic locations (Tallon-Baudry, Bertrand

et al. 2005). Although not often discussed, the macroscale literature also contains evidence of nonuniform power modulations above 60 Hz.

In spite of this evidence, there is growing interest in uniform and broadband (5-200 Hz) power increases, putatively caused by increases in asynchronous neuronal firing activity (Manning, Jacobs et al. 2009; Miller, Zanos et al. 2009; Miller 2010). The purpose of Aim 1 is to test the hypothesis that nonuniform power modulations in sub-bands of the high-gamma range (60-500 Hz) can dissociate cognitive phases of a task or anatomic locations. This concept is illustrated in Figure 2.1. If ECoG can only capture uniform broadband power changes, then the induced spectra should look like those presented in Figure 2.1C. However, if ECoG can capture nonuniform power changes, presumably caused by synchronous oscillatory or suprathreshold activity, the induced spectral power change may occur in distinct frequency bands (yellow and blue bars in Figure 2.1D) and may dissociate cognitive behavior or anatomy.

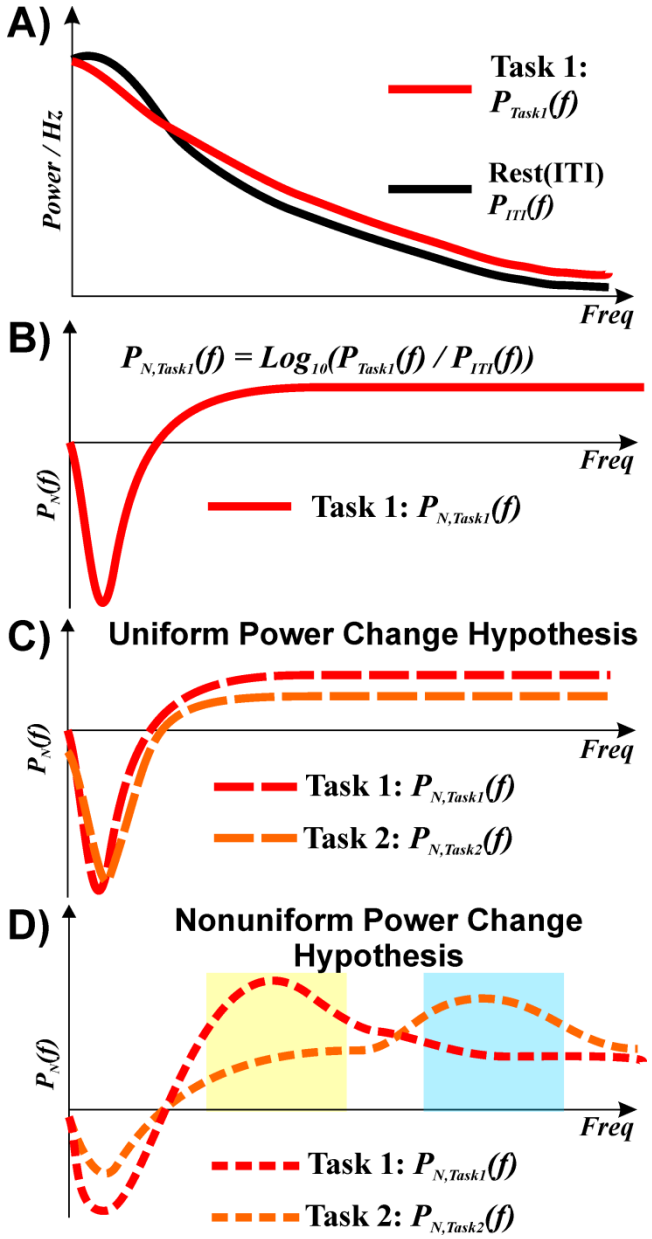

Figure 2.1 Schematic representations of power change paradigms
A) A typical set of power spectral densities. $P_{Task}(f)$ represents the task under observation and $P_{ITI}(f)$ represents the corresponding intertrial interval that is the basis for comparison. B) The normalized power spectrum defined in equation form and illustrated schematically. This method of normalization shows the direction and magnitude of power change with reference to a resting state over a range of frequencies. C) Schematic normalized spectra illustrating the hypothesis that high-gamma power change is uniform in nature. Low frequencies (μ, β, <30 Hz) tend to show power decreases for cognitive task while high frequencies have power increases. D) Schematic normalized spectra illustrating the hypothesis that high-frequency power change is nonuniform. Both spectra have power changes in specific bands that distinguish one cognitive task from another.

2.3 Diversity in the Neural Motif

One of the goals of behavioral neuroscience is to identify the neural correlates of behavior in hopes of revealing how the cortex processes and represents information. The neural correlates of interest depend on the experimental methodology, but generally tend toward indentifying specific cortical locations and patterns of neural activity. For electrophysiological studies, the indicators of neural activity have been temporal waveforms, band limited power and phase, or their inter-relationships. Several lines of research have shown that the neocortex represents information in a broadly distributed manner. Specifically, we mean that behaviors have neural correlates at several spatial locations, time frames and frequency bands. In this dissertation, we refer to the collection of neural correlates of behavior as the ***neural motif***, and the broad distribution of those neural correlates in the dimensions of space, time and frequency as ***diversity***. The hypothesis of Aim 2 is essentially that diversity in the neural motif above 60 Hz contains meaningful neural correlates of behavior. Here we examine the evidence in support of that hypothesis. Since we have previously discussed the findings that support the existence of diversity in the spectral dimension, we focus on the evidence for spatial and temporal diversity. These findings come from a variety of scales in electrophysiological research, functional imaging literature, lesion studies and modeling studies.

Lesion studies were the earliest harbingers of spatial diversity in human language systems. Broca and Wernicke were the first to identify separate cortical areas for speech perception and generation, which were soon followed by Lichtheim's theory of a fronto-temporal network (Demonet, Thierry et al. 2005). Later, functional mapping literature, which generally relies upon virtual lesions caused by electrical cortical stimulation, confirmed the

idea of a cortically diffuse language network with significant subject variability(Burchiel, Clarke et al. 1989; Ojemann, Ojemann et al. 1989).

Microscale recordings have shown that very specific spatial locations encode detailed and complex information about behavior, yet the evidence supports distribution of these neural correlates across time and cortical locations. Because this dissertation studies language tasks, we focus on representations of information related to speech. Several single and multiunit activity studies have shown that specific neurons fire in response to complex auditory stimuli associated with human speech sounds (Barbour and Wang 2003; Steinschneider, Volkov et al. 2005; Mesgarani, David et al. 2008) (Ojemann, Schoenfield-McNeill et al. 2008) as well as birdsongs (Mauk and Buonomano 2004). This evidence appears to show a temporal consolidation of information in the neural code. However, human language is composed of temporal sequences of these complex sounds that are combined hierarchically and eventually give rise to meaning (Doupe and Kuhl 1999). Therefore, in the context of human language, it is the temporal combination of these simplified neural correlates that also give rise to meaning and therefore encode speech information. Spatially, it has been shown that speech generation and perception also have spatially diffuse neural substrates. Birdsongs are generated by rapidly changing assemblies of cells in different nuclei in the avian forebrain (Yu and Margoliash 1996; Leonardo and Fee 2005). Additionally, single unit recordings from awake human subjects have shown that several neurons outside of 'essential' language areas respond to auditory speech stimuli indicating that language networks are spatially diffuse (Engel, Moll et al. 2005). Collectively, the microscale evidence supports the hypothesis of spatially and temporally diverse information encoding in two ways. First, given that human speech consists of temporally sequenced sounds, and that there are single neurons that fire preferentially for

given combinations of complex auditory stimuli and during productive speech, we would expect the neural code to be temporally rich in information. Second, the microscale findings that multiple nuclei are involved in producing speech and that multiple locations outside of core speech areas have single units that respond to human language, both support the hypothesis of spatial diversity in the neural motif.

Macroscale electrophysiological recordings which capture broader cortical areas also support the hypothesis that the neural correlates of language are spatially and temporally diverse. Jacobs et al. have shown that visually presented single letters evoke distinct gamma band power modulations at specific points in time at spatially diffuse yet specific electrodes (Jacobs and Kahana 2009). A study of a single human subject also reported that the representation of spoken consonant-vowel pairs had separable spatial topographies within a 21mm x 21mm array (Blakely, Miller et al. 2008). Temporally, it has been shown that AEPs in human depth electrode recordings from primary auditory cortex correlate with specific voice onset time in parameters that help discriminate phonemes (Steinschneider, Volkov et al. 2005). In scalp recordings, low frequency spectro-temporal representations from multiple electrodes have been used to discriminate imagined articulations of consonant vowel pairs (D'Zmura, Deng et al. 2009) and words (Suppes, Lu et al. 1997). In congruence with the microscale studies, the macroscale electrophysiological evidence also points to diverse representation of language in space, time and frequency.

Using fMRI, which provides the greatest combination of spatial coverage and resolution, researchers have shown language processing and conceptual knowledge representation are spatial diverse as well. BOLD studies of single word repetition paradigms implicate large cortical areas (Petersen and Fiez 1993; Binder, Frost et al. 1997). Although word repetition

tasks incorporate several cognitive functions (auditory perception, short term working memory, speech production) which may recruit larger cortical regions, even auditory processing has been shown to be spatially distributed across the temporal lobe (Binder, Frost et al. 2000). It has also been shown that semantic categories of objects are represented diffusely in overlapping cortical areas (Haxby, Gobbini et al. 2001), yet the spatial patterns of BOLD signal modulation were capable of dissociating semantic categories of visual stimuli (Mitchell, Shinkareva et al. 2008). The functional imaging evidence also supports the spatially diverse element of our hypothesis.

Finally, the speech modeling literature supports the hypothesis that cortical systems are broadly represented as well. Models of human speech production suggest a spatially diverse organization with roles distributed around the Sylvian fissure (Guenther, Ghosh et al. 2006). While competing models of speech processing differ in their organization, all support a broadly distributed system for receptive speech processing. A dual stream model of speech perception has been suggested by Hickok et al. which suggests broadly distributed ventral comprehension and dorsal articulation networks (Hickok and Poeppel 2007). Another model advocates a linkage between speech and motor systems, which further expands the speech network into semantically related motor areas (Pulvermuller 2005).

Based on the research summarized above, we see that there is sufficient evidence that language systems exist across a broad cortical area and that the electrophysiological correlates of language related information have distinct temporal representations over broad windows. This evidence combined with the support for oscillatory activity above 60 Hz is the basis for the second aim of this dissertation. The second aim is to test the

hypothesis that the spatio-temporal dynamics of multiple frequency bands above 60 Hz are part of the neural correlates of phonemic content in speech tasks. We hypothesize that part of the neural code in pial recordings associated with phonemes either spoken or heard can be captured in the spatial, temporal and spectral dynamics of power modulation. Based on this research, we plan to quantitatively analyze the amount of spatial, temporal and spectral diversity in the neural motif that corresponds to phonemic content in ECoG from humans.

2.3.1 Diversity in microarray ECoG

In the review of the literature for the first two aims, a substantial body of evidence was cited from all scales of electrophysiology and functional imaging. The fact that the microscale literature contains evidence of spatial, temporal and spectral diversity has already been addressed. The primary focus of this section is on providing additional evidence for spatial diversity in microscale electrophysiology in areas outside of human language. Several avenues of animal research have shown behaviorally significant spatial patterns of power modulation in microscale pial recordings. These studies have reported somatotopic diversity in rodent whisker barrel cortex (Staba, Bergmann et al. 2004), odor-specific spatial patterns in rabbit olfactory bulb (Freeman and Baird 1987), and visual stimulus related patterns in monkey visual cortex (Freeman and van Dijk 1987). Freeman et al. also studied the spatial diversity in human cortex using the gamma and beta bands and found that the optimal electrode spacing to capture the spatial patterns was 1.25 mm (Freeman, Rogers et al. 2000). Subsequent human studies using microscale pial recordings have shown spatial differences within 1 mm during wrist movements (Leuthardt, Freudenberg et al. 2009) and spoken words (Kellis, Miller et al. 2010). Thus, with regard to

the third aim of this dissertation, we expect that microscale recordings will exhibit both diversity in the frequency bands above 60 Hz that dissociate cognitive task and anatomy, and diversity in the spatio-temporal dynamics of those bands that is correlated with phonemic content.

2.4 Significance

Finally, we ask the question: why is this research relevant? The contributions of this research have the potential to cause a major revision in the view of macroscale high frequency surface cortical potentials. This revised perspective may cause researchers to consider frequencies in the high gamma range as independent entities and open new electrophysiological territory with which to improve clinical practice, BCI applications and scientific research.

2.4.1 Clinical Applications

Epilepsy can be a debilitating disease. It effects an estimated 2.1M people in the United States alone (Kobau, Control et al. 2008) with annual costs of medical treatments and lost income reaching approximately $15.5B (CDC 2010). In its most debilitating form, when seizures cannot be controlled by medication, patients are unable to work or drive. This form of epilepsy affects 31% of patients (Kobau, Control et al. 2008). In epilepsy patients that cannot control seizures through medication, ECoG is used clinically for seizure localization and functional mapping (Goldring and Gregorie 1984).

Functional brain mapping is critical to reducing speech and motor loss of function morbidities after neurosurgical resections for epilepsy and other maladies (Berger, Kincaid et al. 1989; Burchiel, Clarke et al. 1989; Keles, Lundin et al. 2004) because the functional

anatomy of language areas can be quite variable (Ojemann, Ojemann et al. 1989). The clinically accepted method for functional mapping, electrical cortical stimulation (ECS), is prone to after discharges which can reduce mapping accuracies (Blume, Jones et al. 2004), so passive ECoG-based mapping techniques have been studied and show promise as an alternative to ECS (Crone, Miglioretti et al. 1998; Leuthardt, Miller et al. 2007; Sinai, Crone et al. 2009; Wu, Wisneski et al. 2010). Many of these passive mapping techniques rely upon the gamma band (primarily 75-100 Hz, one up to 250 Hz) to identify functional cortex, and while they show promise, the sensitivity and specificity of these techniques are not sufficient to reliably replace ECS mapping. Another promising clinical application of ECoG is seizure forecasting and prediction (Worrell, Parish et al. 2004; Adeli, Ghosh-Dastidar et al. 2007; Mormann, Andrzejak et al. 2007). Although there have been several studies that have attempted prediction and some have used the gamma band (30-60 Hz), again these studies have not yet reached the point of clinical viability. Both mapping and seizure prediction efforts may benefit from exploration of neural signatures in multiple frequency bands above 60 Hz.

2.4.2 Brain Computer Interface Research (BCI)

Brain computer interfaces are a potential application of neural electrophysiology that promise restoring quality of life for those who are cognitively healthy, but physically disabled due to stroke, spinal cord injury, amputation or neuromuscular disorders. Paralysis affects approximately 5.5M people in the United States and over 50% experience "a lot of difficulty" or are completely unable to move (Cahill 2009). The U.S. population is aging and while 13% of the population is now over age 65, this proportion is expected to grow to 19% of the total population by 2030 (Vincent and Velkoff 2010). As the

proportion grows, the incidence of stroke is expected to grow as well (Lloyd-Jones, Adams et al. 2010) as will the 25% of stroke victims over 65 years of age that have difficulty reaching grasping (CDC/NCHS 2008). A more rare type of paralysis is the locked-in state in which patients are unable to move or respond with the exception of eye blinks. The ability to replace motor or speech function using a BCI-based prosthetics could significantly improve the quality of life and autonomy of these patients.

While there are several platforms for providing BCIs, many electrophysiological instantiations use the amplitudes of different cortical rhythms as their signals (Leuthardt, Schalk et al. 2009; Brumberg and Guenther 2010). Many published ECoG-based BCI applications have utilized power modulations as the cortical control signal and several have used gamma band frequencies. While most gamma band control studies have used frequency bands below 150 Hz, subjects have achieved control by modulating frequencies as high as 520 Hz (Leuthardt, Gaona et al. 2011). In addition to modulating bandlimited power levels, there are also scalp methods which use spatial patterns (Guger, Ramoser et al. 2000); however, we are not aware of any attempts to harness neural motif diversity in the in all three dimensions (space, time and frequency), nor any other attempts to use multiple frequency bands in the high gamma range. The finding of neural correlates in the spectro-temporal dynamics of multiple frequency bands above 60 Hz would greatly expand the information available to BCIs and may make multi-modal BCI systems more realizable.

2.4.3 Scientific Research

The proposed research would also challenge the implicit view of gamma portrayed in the much of the macroscale electrophysiological literature. Many studies using ECoG and other modalities have identified gamma band power changes as a reliable and specific

phenomenon that localizes event-related neural activity in anatomy and time. At the macroscale level, localized gamma band power increases have been associated with several cognitive processes [for summaries see (Jerbi, Ossandón et al. 2009) for ECoG, (Herrmann, Fründ et al. 2010) for EEG, and (Kaiser and Lutzenberger 2003; Tallon-Baudry 2009) for MEG]. If successful, this research will show evidence that ECoG is capable of capturing oscillatory behavior well above the 60 Hz mark and show that the dynamics of these high frequency indicators neuronal activity have physiological significance. Given the wide range of current and emerging ECoG research that has relied on gamma band phenomenology, the significance of the proposed research becomes clear. Altering the paradigm that ECoG high-gamma is a uniform phenomena that extends only up to 250 Hz will provide new territory to explore traditional power modulation as well as other techniques such as phase synchrony (Le Van Quyen, Foucher et al. 2001) and cross frequency coupling (Canolty, Edwards et al. 2006) that may reveal cortical networks. In summary, the discovery of frequency diversity in the high-gamma range will provide the opportunity to explore the dynamics of these high-gamma sub-bands and their behavioral and neuronal correlates which may better facilitate the continuing synthesis of cellular, ensemble, and behavioral neuroscience.

2.5 References

Acharya, S., M. Fifer, H. Benz, N. Crone and N. Thakor (2010). "Electrocorticographic amplitude predicts finger positions during slow grasping motions of the hand." Journal of Neural Engineering **7**: 046002.

Ad-Tech, M. I. C. (2008). 2008 product catalog - epilepsy and neurosurgery product guide.

Adeli, H., S. Ghosh-Dastidar and N. Dadmehr (2007). "A wavelet-chaos methodology for analysis of eegs and eeg subbands to detect seizure and epilepsy." Biomedical Engineering, IEEE Transactions on **54**(2): 205-211.

Anderson, K., R. Rajagovindan, G. Ghacibeh, K. Meador and M. Ding (2009). "Theta oscillations mediate interaction between prefrontal cortex and medial temporal lobe in human memory." Cerebral Cortex.

Baker, S., C. Gabriel and R. Lemon (2003). "Eeg oscillations at 600 hz are macroscopic markers for cortical spike bursts." The Journal of Physiology **550**(2): 529.

Barbour, D. L. and X. Wang (2003). "Auditory cortical responses elicited in awake primates by random spectrum stimuli." The Journal of Neuroscience **23**(18): 7194.

Barth, D. S. (2003). "Submillisecond synchronization of fast electrical oscillations in neocortex." The Journal of Neuroscience **23**(6): 2502.

Berger, M. S., J. Kincaid, G. A. Ojemann and E. Lettich (1989). "Brain mapping techniques to maximize resection, safety, and seizure control in children with brain tumors." Neurosurgery **25**(5): 786.

Binder, J., J. Frost, T. Hammeke, P. Bellgowan, J. Springer, J. Kaufman and E. Possing (2000). "Human temporal lobe activation by speech and nonspeech sounds." Cerebral Cortex **10**(5): 512.

Binder, J. R., J. A. Frost, T. A. Hammeke, R. W. Cox, S. M. Rao and T. Prieto (1997). "Human brain language areas identified by functional magnetic resonance imaging." J. Neurosci. **17**(1): 353-362.

Blakely, T., K. Miller, R. Rao, M. Holmes and J. Ojemann (2008). Localization and classification of phonemes using high spatial resolution electrocorticography (ecog) grids, IEEE.

Blum, A. S. and S. B. Rutkove (2007). The clinical neurophysiology primer Totowa, N.J., Humana Press.

Blume, W. T., D. C. Jones and P. Pathak (2004). "Properties of after-discharges from cortical electrical stimulation in focal epilepsies." Clinical Neurophysiology **115**(4): 982-989.

Bragin, A., C. L. Wilson, R. J. Staba, M. Reddick, I. Fried and J. E. Jr. (2002). "Interictal high-frequency oscillations (80-500hz) in the human epileptic brain: Entorhinal cortex." Annals of Neurology **52**(4): 407-415.

Brovelli, A., J.-P. Lachaux, P. Kahane and D. Boussaoud (2005). "High gamma frequency oscillatory activity dissociates attention from intention in the human premotor cortex." Neuroimage **28**(1): 154-164.

Brown, E. C., R. Rothermel, M. Nishida, C. Juhász, O. Muzik, K. Hoechstetter, S. Sood, H. T. Chugani and E. Asano (2008). "In vivo animation of auditory-language-induced gamma-oscillations in children with intractable focal epilepsy." Neuroimage **41**(3): 1120-1131.

Brumberg, J. S. and F. H. Guenther (2010). "Development of speech prostheses: Current status and recent advances." Expert Review of Medical Devices **7**(5): 667-679.

Burchiel, K. J., H. Clarke, G. A. Ojemann, R. G. Dacey and R. H. Winn (1989). "Use of stimulation mapping and corticography in the excision of arteriovenous malformations in sensorimotor and language-related neocortex." Neurosurgery **24**(3): 322.

Buzsáki, G. (2004). "Large-scale recording of neuronal ensembles." Nature Neuroscience **7**(5): 446-451.

Buzsaki, G. and A. Draguhn (2004). "Neuronal oscillations in cortical networks." Science **304**(5679): 1926-1929.

Cahalan, M. and E. Neher (1992). [1] patch clamp techniques: An overview. Methods in enzymology. R. Bernardo, Academic Press. **Volume 207:** 3-14.

Cahill, A. (2009). "One degree of separation: Paralysis and spinal cord injury in the united states." from http://www.christopherreeve.org/atf/cf/%7B3d83418f-b967-4c18-8ada-adc2e5355071%7D/8112REPTFINAL.PDF.

Canolty, R. T., E. Edwards, S. S. Dalal, M. Soltani, S. S. Nagarajan, H. E. Kirsch, M. S. Berger, N. M. Barbaro and R. T. Knight (2006). "High gamma power is phase-locked to theta oscillations in human neocortex." Science **313**(5793): 1626-1628.

Canolty, R. T., M. Soltani, S. S. Dalal, E. Edwards, N. F. Dronkers, S. S. Nagarajan, H. E. Kirsch, N. M. Barbaro and R. T. Knight (2007). "Spatiotemporal dynamics of word processing in the human brain." Frontiers in Neuroscience **1**: 11.

CDC. (2010). "Epilepsy." Retrieved April 29, 2011, from http://www.cdc.gov/epilepsy/index.htm.

CDC/NCHS. (2008). "Table: Difficulty in physical functioning among medicare beneficiaries, ages 65+: Us, 1992-2008 (source: Mcbs)." Centers for Disease Control and Prevention. National Center for Health Statistics. Health Data Interactive. Retrieved April 29, 2011, from http://www.cdc.gov/nchs/hdi.htm.

Chao, Z., Y. Nagasaka and N. Fujii (2010). "Long-term asynchronous decoding of arm motion using electrocorticographic signals in monkeys."

Contreras, D. (2004). "Electrophysiological classes of neocortical neurons." Neural Networks **17**(5-6): 633-646.

Corbetta, M., E. Akbudak, T. E. Conturo, A. Z. Snyder, J. M. Ollinger, H. A. Drury, M. R. Linenweber, S. E. Petersen, M. E. Raichle, D. C. Van Essen and G. L. Shulman (1998). "A common network of functional areas for attention and eye movements." Neuron **21**(4): 761-773.

Crone, N., D. Boatman, B. Gordon and L. Hao (2001). "Induced electrocorticographic gamma activity during auditory perception." Clinical Neurophysiology **112**(4): 565-582.

Crone, N., D. Miglioretti, B. Gordon and R. Lesser (1998). "Functional mapping of human sensorimotor cortex with electrocorticographic spectral analysis. Ii. Event-related synchronization in the gamma band." Brain **121**(12): 2301-2315.

Crone, N. E. (2000). "Functional mapping with ecog spectral analysis." Neocortical Epilepsies **84**: 343-351.

Crone, N. E., D. Boatman, B. Gordon and L. Hao (2001). "Induced electrocorticographic gamma activity during auditory perception." Clinical Neurophysiology **112**(4): 565-582.

Crone, N. E., L. Hao, J. Hart, Jr., D. Boatman, R. P. Lesser, R. Irizarry and B. Gordon (2001). "Electrocorticographic gamma activity during word production in spoken and sign language." Neurology **57**(11): 2045-2053.

Crone, N. E., D. L. Miglioretti, B. Gordon, J. M. Sieracki, M. T. Wilson, S. Uematsu and R. P. Lesser (1998). "Functional mapping of human sensorimotor cortex with electrocorticographic spectral analysis. I. Alpha and beta event-related desynchronization." Brain **121**(12): 2271-2299.

Curio, G. (2000). "Linking 600-hz "spikelike" eeg/meg wavelets ("sigma-bursts") to cellular substrates: Concepts and caveats." J Clin Neurophysiol **17**(4): 377-396.

D'Zmura, M., S. Deng, T. Lappas, S. Thorpe and R. Srinivasan (2009). "Toward eeg sensing of imagined speech." Human-Computer Interaction. New Trends: 40-48.

Demonet, J.-F., G. Thierry and D. Cardebat (2005). "Renewal of the neurophysiology of language: Functional neuroimaging." Physiol. Rev. **85**(1): 49-95.

Dhond, R. P., T. Witzel, A. M. Dale and E. Halgren (2005). "Spatiotemporal brain maps of delayed word repetition and recognition." Neuroimage **28**(2): 293-304.

Doupe, A. J. and P. K. Kuhl (1999). "Birdsong and human speech: Common themes and mechanisms." Annual Review of Neuroscience **22**(1): 567-631.

Edwards, E., M. Soltani, L. Y. Deouell, M. S. Berger and R. T. Knight (2005). "High gamma activity in response to deviant auditory stimuli recorded directly from human cortex." J Neurophysiol **94**(6): 4269-4280.

Edwards, E., M. Soltani, W. Kim, S. S. Dalal, S. S. Nagarajan, M. S. Berger and R. T. Knight (2009). "Comparison of time-frequency responses and the event-related potential to auditory speech stimuli in human cortex." J Neurophysiol **102**(1): 377-386.

Engel, A. K., C. K. Moll, I. Fried and G. A. Ojemann (2005). "Invasive recordings from the human brain: Clinical insights and beyond." Nature reviews. Neuroscience **6**(1): 35-47.

Farwell, L. A. and E. Donchin (1988). "Talking off the top of your head: Toward a mental prosthesis utilizing event-related brain potentials." Electroencephalography and Clinical Neurophysiology **70**(6): 510-523.

Fell, J. r., P. Klaver, K. Lehnertz, T. Grunwald, C. Schaller, C. E. Elger and G. n. FernÃ¡ndez (2001). "Human memory formation is accompanied by rhinal?Hippocampal coupling and decoupling." Nature Neuroscience **4**(12): 1259.

Freeman, W. J. and B. Baird (1987). "Relation of olfactory eeg to behavior: Spatial analysis." Behavioral Neuroscience **101**(3): 393.

Freeman, W. J., L. J. Rogers, M. D. Holmes and D. L. Silbergeld (2000). "Spatial spectral analysis of human electrocorticograms including the alpha and gamma bands." Journal of Neuroscience Methods **95**(2): 111-121.

Freeman, W. J. and B. W. van Dijk (1987). "Spatial patterns of visual cortical fast eeg during conditioned reflex in a rhesus monkey." Brain Research **422**(2): 267-276.

Fries, P., D. Nikolic and W. Singer (2007). "The gamma cycle." Trends in Neurosciences **30**(7): 309-316.

Georgopoulos, A. P., E. Karageorgiou, A. C. Leuthold, S. M. Lewis, J. K. Lynch, A. A. Alonso, Z. Aslam, A. F. Carpenter, A. Georgopoulos and L. S. Hemmy (2007). "Synchronous neural interactions assessed by magnetoencephalography: A functional biomarker for brain disorders." Journal of Neural Engineering **4**: 349.

Georgopoulos, A. P., A. B. Schwartz and R. E. Kettner (1986). "Neuronal population coding of movement direction." Science **233**(4771): 1416.

Gold, J. I. and M. N. Shadlen (2001). "Neural computations that underlie decisions about sensory stimuli." Trends in Cognitive Sciences **5**(1): 10-16.

Goldring, S. and E. M. Gregorie (1984). "Surgical management of epilepsy using epidural recordings to localize the seizure focus." Journal of Neurosurgery **60**(3): 457-466.

Gray, C., P. König, A. Engel and W. Singer (1989). "Oscillatory responses in cat visual cortex exhibit inter-columnar synchronization which reflects global stimulus properties." Nature **338**(6213): 334-337.

Guenther, F. H., S. S. Ghosh and J. A. Tourville (2006). "Neural modeling and imaging of the cortical interactions underlying syllable production." Brain and Language **96**(3): 280-301.

Guger, C., H. Ramoser and G. Pfurtscheller (2000). "Real-time eeg analysis with subject-specific spatial patterns for a brain-computer interface (bci)." Rehabilitation Engineering, IEEE Transactions on **8**(4): 447-456.

Haxby, J. V., M. I. Gobbini, M. L. Furey, A. Ishai, J. L. Schouten and P. Pietrini (2001). "Distributed and overlapping representations of faces and objects in ventral temporal cortex." Science **293**(5539): 2425-2430.

He, B. J., A. Z. Snyder, J. M. Zempel, M. D. Smyth and M. E. Raichle (2008). "Electrophysiological correlates of the brain's intrinsic large-scale functional architecture." Proceedings of the National Academy of Sciences **105**(41): 16039-16044.

Heldman, D. A. (2007). Epidural electrocorticography and intra-cortical local field potentials in motor cortex during volitional arm movements and their applications to neural prosthetic control. Sever Institute School of Engineering and Applied Science Department of Biomedical Engineering. St Louis, MO, Washington University. PhD Dissertation.

Herrmann, C. S., I. Fründ and D. Lenz (2010). "Human gamma-band activity: A review on cognitive and behavioral correlates and network models." Neuroscience & Biobehavioral Reviews **34**(7): 981-992.

Hickok, G. and D. Poeppel (2007). "The cortical organization of speech processing." Nat Rev Neurosci **8**(5): 393-402.

Hochberg, L. R., M. D. Serruya, G. M. Friehs, J. A. Mukand, M. Saleh, A. H. Caplan, A. Branner, D. Chen, R. D. Penn and J. P. Donoghue (2006). "Neuronal ensemble control of prosthetic devices by a human with tetraplegia." Nature **442**(7099): 164-171.

Hodgkin, A. L. and A. F. Huxley (1939). "Action potentials recorded from inside a nerve fibre." Nature **144**(3651): 710-711.

Hubel, D. H. and T. N. Wiesel (1959). "Receptive fields of single neurones in the cat's striate cortex." The Journal of Physiology **148**(3): 574-591.

Jacobs, J. and M. J. Kahana (2009). "Neural representations of individual stimuli in humans revealed by gamma-band electrocorticographic activity." J. Neurosci. **29**(33): 10203-10214.

Jerbi, K., T. Ossandón, C. Hamamé, S. Senova, S. Dalal, J. Jung, L. Minotti, O. Bertrand, A. Berthoz and P. Kahane (2009). "Task-related gamma-band dynamics from an intracerebral perspective: Review and implications for surface eeg and meg." Hum Brain Mapp **30**: 1758-1771.

Jones, M. S., K. D. MacDonald, B. Choi, F. E. Dudek and D. S. Barth (2000). "Intracellular correlates of fast (>200 hz) electrical oscillations in rat somatosensory cortex." J Neurophysiol **84**(3): 1505-1518.

Kaiser, J. and W. Lutzenberger (2003). "Induced gamma-band activity and human brain function." The Neuroscientist **9**(6): 475.

Kandel, E. R., J. H. Schwartz and T. M. Jessell (2000). Principles of neural science. New York, McGraw-Hill, Health Professions Division.

Keles, G. E., D. A. Lundin, K. R. Lamborn, E. F. Chang, G. Ojemann and M. S. Berger (2004). "Intraoperative subcortical stimulation mapping for hemispheric perirolandic gliomas located within or adjacent to the descending motor pathways: Evaluation of morbidity and assessment of functional outcome in 294 patients." Journal of Neurosurgery **100**(3): 369-375.

Kellis, S., K. Miller, K. Thomson, R. Brown, P. House and B. Greger (2010). "Decoding spoken words using local field potentials recorded from the cortical surface." Journal of Neural Engineering **7**: 056007.

Kobau, R., C. f. D. Control and Prevention (2008). Epilepsy surveillance among adults--19 states, behavioral risk factor surveillance system, 2005, US Dept. of Health and Human Services, Centers for Disease Control and Prevention.

Korzeniewska, A., C. M. Crainiceanu, R. Kus, P. J. Franaszczuk and N. E. Crone (2008). "Dynamics of event-related causality in brain electrical activity." Human Brain Mapping **29**(10): 1170-1192.

Lachaux, J.-P., N. George, C. Tallon-Baudry, J. Martinerie, L. Hugueville, L. Minotti, P. Kahane and B. Renault (2005). "The many faces of the gamma band response to complex visual stimuli." Neuroimage **25**(2): 491-501.

Lawrence, B. M., R. L. White and L. H. Snyder (2005). "Delay-period activity in visual, visuomovement, and movement neurons in the frontal eye field." Journal of neurophysiology **94**(2): 1498.

Le Van Quyen, M., J. Foucher, J. Lachaux, E. Rodriguez, A. Lutz, J. Martinerie and F. Varela (2001). "Comparison of hilbert transform and wavelet methods for the analysis of neuronal synchrony." Journal of Neuroscience Methods **111**(2): 83-98.

Leonardo, A. and M. S. Fee (2005). "Ensemble coding of vocal control in birdsong." The Journal of Neuroscience **25**(3): 652.

Leuthardt, E., K. Miller, N. Anderson, G. Schalk, J. Dowling, J. Miller, D. Moran and J. Ojemann (2007). "Electrocorticographic frequency alteration mapping: A clinical technique for mapping the motor cortex." Neurosurgery **60**(4): 260.

Leuthardt, E. C., Z. Freudenberg, D. Bundy and J. Roland (2009). "Microscale recording from human motor cortex: Implications for minimally invasive electrocorticographic brain-computer interfaces." Neurosurgical FOCUS **27**(1): E10.

Leuthardt, E. C., C. Gaona, M. Sharma, N. Szrama, J. Roland, Z. Freudenberg, J. Solis, J. Breshears and G. Schalk (2011). "Using the electrocorticographic speech network to control a brain–computer interface in humans." Journal of Neural Engineering **8**: 036004.

Leuthardt, E. C., K. Miller, N. R. Anderson, G. Schalk, J. Dowling, J. Miller, D. W. Moran and J. G. Ojemann (2007). "Electrocorticographic frequency alteration mapping: A clinical technique for mapping the motor cortex." Neurosurgery **60**(4): 260-271.

Leuthardt, E. C., K. J. Miller, G. Schalk, R. P. N. Rao and J. G. Ojemann (2006). "Electrocorticography-based brain computer interface - the seattle experience." Ieee Transactions on Neural Systems and Rehabilitation Engineering **14**(2): 194-198.

Leuthardt, E. C., G. Schalk, J. Roland, A. Rouse and D. W. Moran (2009). "Evolution of brain-computer interfaces: Going beyond classic motor physiology." Neurosurgical FOCUS **27**(1): E4.

Leuthardt, E. C., G. Schalk, J. R. Wolpaw, J. G. Ojemann and D. W. Moran (2004). "A brain-computer interface using electrocorticographic signals in humans." Journal of Neural Engineering **1**(2): 63-71.

Lloyd-Jones, D., R. J. Adams, T. M. Brown, M. Carnethon, S. Dai, G. De Simone, T. B. Ferguson, E. Ford, K. Furie, C. Gillespie, A. Go, K. Greenlund, N. Haase, S. Hailpern, P. M. Ho, V. Howard, B. Kissela, S. Kittner, D. Lackland, L. Lisabeth, A. Marelli, M. M. McDermott, J. Meigs, D. Mozaffarian, M. Mussolino, G. Nichol, V. L. Roger, W. Rosamond, R. Sacco, P. Sorlie, R. Stafford, T. Thom, S. Wasserthiel-Smoller, N. D. Wong, J. Wylie-Rosett, o. b. o. t. A. H. A. S. Committee and Stroke Statistics Subcommittee (2010). "Heart disease and stroke statistics--2010 update: A report from the american heart association." Circulation **121**(7): e46-215.

Logothetis, N. K., J. Pauls, M. Augath, T. Trinath and A. Oeltermann (2001). "Neurophysiological investigation of the basis of the fmri signal." Nature **412**(6843): 150-157.

Mainy, N., J. Jung, M. Baciu, P. Kahane, B. Schoendorff, L. Minotti, D. Hoffmann, O. Bertrand and J.-P. Lachaux (2008). "Cortical dynamics of word recognition." Human Brain Mapping **29**(11): 1215-1230.

Makeig, S., M. Westerfield, T. P. Jung, S. Enghoff, J. Townsend, E. Courchesne and T. Sejnowski (2002). "Dynamic brain sources of visual evoked responses." Science **295**(5555): 690.

Malmivuo, J. and R. Plonsey (1995). Bioelectromagnetism : Principles and applications of bioelectric and biomagnetic fields. New York, Oxford University Press.

Manning, J. R., J. Jacobs, I. Fried and M. J. Kahana (2009). "Broadband shifts in local field potential power spectra are correlated with single-neuron spiking in humans." J. Neurosci. **29**(43): 13613-13620.

Mauk, M. D. and D. V. Buonomano (2004). "The neural basis of temporal processing." Annu. Rev. Neurosci. **27**: 307-340.

Maunsell, J. H. and D. C. Van Essen (1983). "Functional properties of neurons in middle temporal visual area of the macaque monkey. I. Selectivity for stimulus direction, speed, and orientation." Journal of neurophysiology **49**(5): 1127.

Mesgarani, N., S. David, J. Fritz and S. Shamma (2008). "Phoneme representation and classification in primary auditory cortex." The Journal of the Acoustical Society of America **123**: 899.

Miller, K. J. (2010). "Broadband spectral change: Evidence for a macroscale correlate of population firing rate?" J. Neurosci. **30**(19): 6477-6479.

Miller, K. J., K. E. Weaver and J. G. Ojemann (2009). "Direct electrophysiological measurement of human default network areas." Proceedings of the National Academy of Sciences **106**(29): 12174-12177.

Miller, K. J., S. Zanos, E. E. Fetz, M. den Nijs and J. G. Ojemann (2009). "Decoupling the cortical power spectrum reveals real-time representation of individual finger movements in humans." J. Neurosci. **29**(10): 3132-3137.

Mitchell, T. M., S. V. Shinkareva, A. Carlson, K.-M. Chang, V. L. Malave, R. A. Mason and M. A. Just (2008). "Predicting human brain activity associated with the meanings of nouns." Science **320**(5880): 1191-1195.

Mormann, F., R. Andrzejak, C. Elger and K. Lehnertz (2007). "Seizure prediction: The long and winding road." Brain **130**(2): 314.

Mormann, F., J. Fell, N. Axmacher, B. Weber, K. Lehnertz, C. E. Elger and G. Fernández (2005). "Phase/amplitude reset and theta-gamma interaction in the human medial temporal lobe during a continuous word recognition memory task." Hippocampus **15**(7): 890-900.

Neher, E., B. Sakmann and J. H. Steinbach (1978). "The extracellular patch clamp: A method for resolving currents through individual open channels in biological membranes." Pflügers Archiv European Journal of Physiology **375**(2): 219-228.

Nunez, P. L. and R. Srinivasan (2006). Electric fields of the brain : The neurophysics of eeg. New York, Oxford University Press.

O'Keefe, J. and J. Dostrovsky (1971). "The hippocampus as a spatial map: Preliminary evidence from unit activity in the freely-moving rat." Brain Research.

Ojemann, G., J. Ojemann, E. Lettich and M. Berger (1989). "Cortical language localization in left, dominant hemisphere." Journal of Neurosurgery **71**(3): 316-326.

Ojemann, G. A., J. Schoenfield-McNeill and D. Corina (2008). "The roles of human lateral temporal cortical neuronal activity in recent verbal memory encoding." Cereb. Cortex: bhn071.

Petersen, S. and J. Fiez (1993). "The processing of single words studied with positron emission tomography." Annual Review of Neuroscience **16**(1): 509-530.

Pfurtscheller, G., B. Graimann, J. E. Huggins, S. P. Levine and L. A. Schuh (2003). "Spatiotemporal patterns of beta desynchronization and gamma synchronization in corticographic data during self-paced movement." Clinical Neurophysiology **114**(7): 1226-1236.

Pfurtscheller, G. and F. Lopes da Silva (1999). "Event-related eeg/meg synchronization and desynchronization: Basic principles." Clinical Neurophysiology **110**(11): 1842-1857.

Pfurtscheller, G., C. Neuper and J. Kalcher (1993). "40-hz oscillations during motor behavior in man." Neuroscience Letters **164**(1-2): 179-182.

Pockett, S., G. E. J. Bold and W. J. Freeman (2009). "Eeg synchrony during a perceptual-cognitive task: Widespread phase synchrony at all frequencies." Clinical Neurophysiology **120**(4): 695-708.

Ponomarenko, A., N. Chepurnova, S. Chepurnov and H. Haas (2002). "Hippocampal ripple oscillations (200 hz) in mechanisms of memory consolidation]." Uspekhi fiziologicheskikh nauk **33**(4): 34.

Pulvermuller, F. (2005). "Brain mechanisms linking language and action." Nat Rev Neurosci **6**(7): 576-582.

Ray, S., E. Niebur, S. S. Hsiao, A. Sinai and N. E. Crone (2008). "High-frequency gamma activity (80-150 hz) is increased in human cortex during selective attention." Clinical Neurophysiology **119**(1): 116-133.

Renshaw, B., A. Forbes and B. R. Morison (1940). "Activity of isocortex and hippocampus: Electrical studies with micro-electrodes." Journal of neurophysiology **3**(1): 74-105.

Roest, A., B. van Bets, P. Jorens, I. Baar, J. Weyler and R. Mercelis (2009). "The prognostic value of the eeg in postanoxic coma." Neurocritical Care **10**(3): 318-325.

Rouse, A. and D. Moran (2009). Neural adaptation of epidural electrocorticographic (eecog) signals during closed-loop brain computer interface (bci) tasks, IEEE.

Salmelin, R. (2007). "Clinical neurophysiology of language: The meg approach." Clinical Neurophysiology **118**(2): 237-254.

Schalk, G., J. Kubanek, K. Miller, N. Anderson, E. Leuthardt, J. Ojemann, D. Limbrick, D. Moran, L. Gerhardt and J. Wolpaw (2007). "Decoding two-dimensional movement trajectories using electrocorticographic signals in humans." Journal of Neural Engineering **4**: 264-275.

Schalk, G., K. J. Miller, N. R. Anderson, J. A. Wilson, M. D. Smyth, J. G. Ojemann, D. W. Moran, J. R. Wolpaw and E. C. Leuthardt (2008). "Two-dimensional movement control using electrocorticographic signals in humans." Journal of Neural Engineering **5**(1): 75-84.

Sederberg, P. B., M. J. Kahana, M. W. Howard, E. J. Donner and J. R. Madsen (2003). "Theta and gamma oscillations during encoding predict subsequent recall." J. Neurosci. **23**(34): 10809-10814.

Sinai, A., N. E. Crone, H. M. Wied, P. J. Franaszczuk, D. Miglioretti and D. Boatman-Reich (2009). "Intracranial mapping of auditory perception: Event-related responses and electrocortical stimulation." Clinical Neurophysiology **120**(1): 140-149.

Spydell, J. D., M. R. Ford and D. E. Sheer (1979). "Task dependent cerebral lateralization of the 40 hertz eeg rhythm." Psychophysiology **16**(4): 347-350.

Staba, R. J., T. D. Ard, A. M. Benison and D. S. Barth (2005). "Intracortical pathways mediate nonlinear fast oscillation (>200 hz) interactions within rat barrel cortex." J Neurophysiol **93**(5): 2934-2939.

Staba, R. J., P. C. Bergmann and D. S. Barth (2004). "Dissociation of slow waves and fast oscillations above 200 hz during gaba application in rat somatosensory cortex." The Journal of Physiology **561**(1): 205-214.

Steinschneider, M., I. O. Volkov, Y. I. Fishman, H. Oya, J. C. Arezzo and M. A. Howard (2005). "Intracortical responses in human and monkey primary auditory cortex support a temporal processing mechanism for encoding of the voice onset time phonetic parameter." Cerebral Cortex **15**(2): 170.

Suppes, P., Z. L. Lu and B. Han (1997). "Brain wave recognition of words." Proceedings of the National Academy of Sciences of the United States of America **94**(26): 14965.

Tallon-Baudry, C. (2009). "The roles of gamma-band oscillatory synchrony in human visual cognition." Frontiers in bioscience: a journal and virtual library **14**: 321.

Tallon-Baudry, C., O. Bertrand, M.-A. Henaff, J. Isnard and C. Fischer (2005). "Attention modulates gamma-band oscillations differently in the human lateral occipital cortex and fusiform gyrus." Cereb. Cortex **15**(5): 654-662.

Taylor, D. M., S. I. H. Tillery and A. B. Schwartz (2002). "Direct cortical control of 3d neuroprosthetic devices." Science **296**(5574): 1829.

Towle, V. L., H.-A. Yoon, M. Castelle, J. C. Edgar, N. M. Biassou, D. M. Frim, J.-P. Spire and M. H. Kohrman (2008). "Ecog gamma activity during a language task: Differentiating expressive and receptive speech areas." Brain **131**(8): 2013-2027.

Trautner, P., T. Rosburg, T. Dietl, J. Fell, O. A. Korzyukov, M. Kurthen, C. Schaller, C. E. Elger and N. N. Boutros (2006). "Sensory gating of auditory evoked and induced gamma band activity in intracranial recordings." Neuroimage **32**(2): 790-798.

Uhlhaas, P. J., G. Pipa, B. Lima, L. Melloni, S. Neuenschwander, D. Nikoli and W. Singer (2009). "Neural synchrony in cortical networks: History, concept and current status." Frontiers in Integrative Neuroscience **3**.

Velliste, M., S. Perel, M. C. Spalding, A. S. Whitford and A. B. Schwartz (2008). "Cortical control of a prosthetic arm for self-feeding." Nature **453**(7198): 1098-1101.

Vincent, G. K. and V. A. Velkoff (2010). The next four decades the older population in the united states: 2010 to 2050, U.S. Census Bureau.

Whittingstall, K. and N. K. Logothetis (2009). "Frequency-band coupling in surface eeg reflects spiking activity in monkey visual cortex." **64**(2): 281-289.

Wijdicks, E. F. M. (2010). "The case against confirmatory tests for determining brain death in adults." Neurology **75**(1): 77.

Wisneski, K. J., N. Anderson, G. Schalk, M. Smyth, D. Moran and E. C. Leuthardt (2008). "Unique cortical physiology associated with ipsilateral hand movements and neuroprosthetic implications." Stroke **39**(12): 3351-3359.

Wolpaw, J. R., D. J. McFarland, G. W. Neat and C. A. Forneris (1991). "An eeg-based brain-computer interface for cursor control." Electroencephalography and Clinical Neurophysiology **78**(3): 252-259.

Worrell, G., L. Parish, S. Cranstoun, R. Jonas, G. Baltuch and B. Litt (2004). "High-frequency oscillations and seizure generation in neocortical epilepsy." Brain **127**(7): 1496.

Wu, M., K. Wisneski, G. Schalk, M. Sharma, J. Roland, J. Breshears, C. Gaona and E. Leuthardt (2010). "Electrocorticographic frequency alteration mapping for extraoperative localization of speech cortex." Neurosurgery **66**(2): E407.

Ylinen, A., A. Bragin, Z. Nádasdy, G. Jandó, I. Szabo, A. Sik and G. Buzsáki (1995). "Sharp wave-associated high-frequency oscillation (200 hz) in the intact hippocampus: Network and intracellular mechanisms." The Journal of Neuroscience **15**(1): 30.

Yu, A. C. and D. Margoliash (1996). "Temporal hierarchical control of singing in birds." Science **273**(5283): 1871.

3 Methods

The methods chapter is organized into four major sections. The first describes the general practices applied for all subjects, including the data recording techniques and experimental paradigms. The second section describes the data processing and analysis techniques used to test the hypothesis of Aim 1, that nonuniform power modulation above 60 Hz can dissociate cognitive tasks and anatomic locations. The third section describes processing and analyses used to test Aim 2's hypothesis, that information represented diversely in the spatio-temporal dynamics of the high gamma band improve the ability to identify specific phonemes. The final section briefly describes modifications to the processing and analysis techniques from Aims 1 and 2, that were applied to the microarray ECoG data in pursuit of the third aim.

3.1 General Methods

The following methods apply to all three aims of this dissertation. Subsequent sections describe in detail the specific analyses techniques and any deviations from the general methods described here.

3.1.1 Subjects

The subjects in this study underwent temporary placement of intracranial electrode arrays to identify epileptic seizure foci. 13 subjects (10 female) provided informed consent for the study, which had been reviewed and approved by the Washington University School of Medicine Institutional Review Board. Subjects 1-6 were selected for the dissociation band

analysis because they were right-handed, had no indications of bilateral speech representation and received left hemisphere grid implants. Table 3.1 summarizes the subject data.

Table 3.1 Subjects
Hand Abbreviations: R=Right, L=Left, Am=Ambidextrous, BL Sp=Bilateral Speech. Cognitive capacity abbreviations: FSIQ=Full Scale IQ, VIQ=Verbal IQ, PIQ=Performance IQ. Grid Location Notes: All grids were left-sided. Grid Location Abbreviations: F=Frontal, P=Parietal, T=Temporal, ST=Sub-Temporal. Task Abbreviations: H-S=Hearing-Speaking (Auditory Repetition), R-S=Reading-Speaking (Visual Repetition), HR-NW=Hear and Repeat Non-words, Verb=Verb Generation, Concept=Concept Generation

Subject	Age/ Sex	Hand	Cognitive Capacity	Grid Location	Epileptic Focus	Number of Trials Per Task
1-FOTE55	15/F	R	Normal	Left-F/P	Left Temporal	72 H-S 72 R-S
2 – NTES60	44/M	R	Avg to High Avg	Left-F	Left Orbito-Frontal	72 H-S 72 R-S
3 – SZNE71	27/M	R	Low Average (FSIQ 89, VIQ=86, PIQ=96)	Left-F/P	Right Mesial Parietal	180 H-S 180 R-S
4 – TOFE76	58/F	R	High Avg (FSIQ 116)	Left-F/P	Superior Frontal Gyrus	216 H-S 216 R-S
5 – TTSE78	49/F	R	Avg (FSIQ 100)	Left-F/T	Anterior Temporal	216 H-S 216 R-S
6 – OOTN79	42/F	R	Low Avg (FSIQ 81)	Left-F/T/P	Anterior Temporal/Amygdala/ Hippocampus	109 H-S 109 R-S
7 – TZSE75	48/F	R BL Sp	Low Avg (FSIQ 86)	Left – F/P	Left Frontal Temporal	72 H-S 72 R-S
8 – TZTN81	36/M	L BL Sp	Below Avg (FSIQ 71)	L-F/T/P	Anterior Temporal	72 H-S 72 R-S
9 – TTTE77	46/F	Am BL Sp	Low Avg (FSIQ 81)	R-F/T/P	Inferior Temporal	72 H-S 72 R-S
10 – TOSE65	44/F	L BL Sp	VIQ 94 / PIQ 96	L-F/T	Mesial Temporal	72 H-S 72 R-S
11 – FOST99	36/F	R	FSIQ 116 (PIQ:125, VIQ :106)	L-F + microgrid	Anterior Superior Frontal	108 H-S
12 – Pt101	34 F	R	High Avg Verbal (VCI = 118)	L-T/F/ST + microgrid	Anterior Temporal	264 H-S 111 Verb 89 Concept
13 – Pt110	45/F	R	FSIQ = 89 (23rd pctl), VIQ=88, PIQ=94 (21/34 pctl)	L-F/T + microgrid	Left Temporal Tip	240 H-S 260 HR-NW

3.1.2 Data Acquisition

Macroscale ECoG electrodes, manufactured by either the Ad-Tech Medical Instrument Corporation (Racine, WI) or PMT Corporation (Chanhassen, MN), were implanted below the dura in 8 x 8 or 6 x 8 grid configurations as shown in Figure 3.1. Individual electrodes were 4mm diameter (2.3mm exposed) platinum iridium discs spaced 1 cm apart (center to center) and encapsulated in silastic sheets (Ad-Tech 2008). Separate four-electrode strips were implanted epidurally and facing the skull (away from the cortical surface) for biosignal amplifier ground and reference.

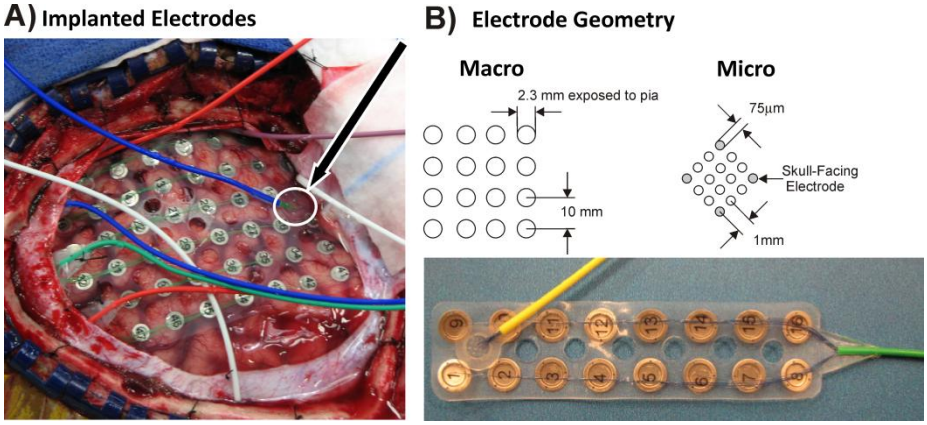

Figure 3.1 Implanted electrode and geometries
A) A photograph of a typical implant configuration. This example shows both the clinical macro electrodes and the microgrid placement with the Leuthardt Grid as placed on the pia mater of a human subject. The arrow shows the location of the microgrid. B) The geometries shown in schematic form and pictorially illustrate the difference in spatial scale between the macro and micro ECoG electrodes. The gray electrodes in the corners of the microarrays face away from the cortex (toward the skull) and provide impedance matched amplifier ground and reference.

ECoG microarrays manufactured by PMT Corporation (Chanhassen, MN) have twelve (12), 75um electrodes spaced 1mm apart in a 4 x 4 grid as shown in Figure 3.1B. The four corner electrodes face away from the cortical surface (toward the skull), are 2mm in length and are used as impedance matched ground and reference electrodes for the 12 electrodes facing the cortex. Since the microarray electrodes have different impedances, they are electrically isolated from the amplifiers recording from the macrogrid electrodes.

Additionally, subjects with ECoG microarrays had a cutaneous ground electrode to use the epidermis as a quasi-Faraday cage around the electrodes.

Biosignal amplifiers manufactured by g.tec (Graz, Austria) will record ECoG and microphone signals using 24-bit resolution analog-to-digital converters. Microphone signal recordings will use ground and references electrically isolated from the ECoG channels to prevent interference. Signals will be captured using one of two sampling schemes. Data was either sampled at 1.2 kHz and filtered between 0.1 and 500 Hz, or sampled at 9.6 kHz with no filtering.

3.1.3 Electrode Localization and Labeling

Researchers estimated electrode coordinates in Montreal Neurological Institute (MNI) atlas space using radiographs and the 'Get Location on Cortex' technique (Miller, Makeig et al. 2007). Brodmann area labels were acquired using the estimated Talairach coordinates from an on-line Talairach Atlas (Jack L. Lancaster 2000). For subjects which had both pre-operative MRI scans and post-operative computed tomography radiographs, the electrodes locations were co-registered to a reconstruction of the subject's gyral anatomy using techniques described by Hermes et al. {Hermes, 2010 #601}.

3.1.4 Experimental Setup

The BCI2000 software package synchronized the experimental tasks with ECoG and microphone signal recordings (Schalk, McFarland et al. 2004). Stimulus periods of 4s were interleaved between 533ms intertrial intervals (ITI) as shown in Figure 3.2B. Visual stimuli appeared for the whole stimulus period on an LCD monitor approximately 60cm from the subject. Auditory stimuli were presented through headphones and had an average duration

of 531ms (SD=89ms). Stimuli for single word repetition tasks came from the same list of 36 monosyllabic English language words shown in Table 3.2. Once subject performed a nonword repetition experiment. During single-word repetition experiments, subjects were instructed to say each stimulus word aloud into a microphone. Certain subjects performed verb generation experiments and were instead instructed to say a verb that is appropriately associated with a stimulus noun. Voice onset times (VOT) were determined by thresholding the rectified and low pass filtered (3rd order Butterworth filter, cutoff frequency of 10Hz) microphone signal by the mean.

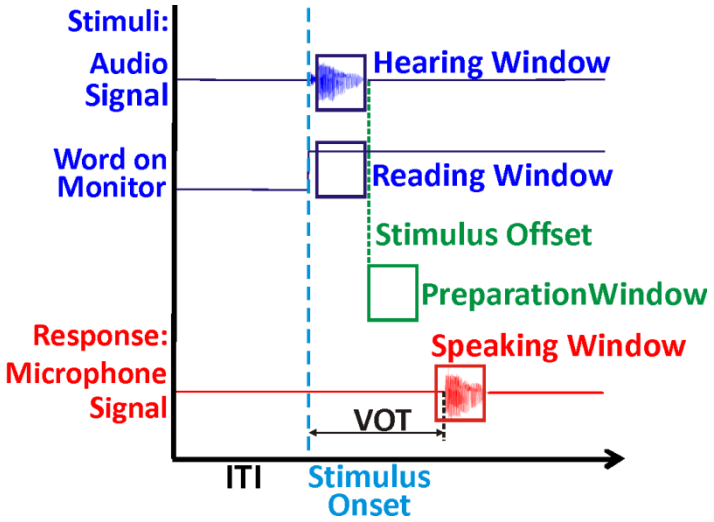

Figure 3.2 Experimental paradigm timing
The stimulus and response timing of the single word repetition and verb generation paradigms. Stimuli are presented either visually on a computer screen, or audibly through headphones. The subject speaks the appropriate response into a microphone. The dissociation band analysis windows for specific cognitive tasks are outlined in the colored rectangles.

Table 3.2 Experimental paradigm - Word Stimuli

CVC Word	B _ T	C _ N	H _ D	L _ D	M _ N	P _ P	R _ D	S _ T	T _ N
EH-/ɛ/	Bet	Ken	Head	Led	Men	Pep	Red	Set	Ten
AH-/æ/	Bat	Can	Had	Lad	Man	Pap	Rad	Sat	Tan
EE-/i/	Beet	Keen	Heed	Lead	Mean	Peep	Read	Seat	Teen
OO-/u/	Boot	Coon	Hood	Lewd	Moon	Poop	Rude	Soot	Tune

Table 3.3 Experimental paradigm – Nonword Stimuli

CVC Word	B _ P	CH_M	D _V	F _ P	G _ D	N _ M	R _ S	S _ B	T _ V	V_D
AH-/æ/	Bap	Cham	Dav	Fap	Gad	Nam	Ras	Sab	Tav	Vad

EH - /ɛ/	Bep	Chem	Dev	Fep	Ged	Nem	Res	Seb	Tev	Ved
IH-/I/	Bip	Chim	Div	Fip	Gid	Nim	Ris	Sib	Eiv	Vid
OO-/u/	Boop	Choom	Doov	Foop	Gud	Num	Roos	Soob	Toov	Vood

3.2 Dissociation Band Analysis

To test the hypothesis that the high-gamma band exhibits nonuniform power changes we evaluated ECoG signals from six subjects (1-6) undergoing treatment for intractable epilepsy. All subjects performed both auditory and visual single-word repetition tasks. Power changes between 60-500Hz were studied in a variety of ways to determine whether power changes at different frequencies could distinguish phases of each task or anatomic locations. Results were consolidated across the subject population by evaluating consistency of power change in three focal anatomic areas.

3.2.1 Preprocessing

Researchers screened all signals for excessive noise prior to any analysis. Channels with excessive noise were dropped from the entire analysis. Trials with excessive environmental noise across all channels, or where speech occurred during stimulus or ITI periods, were also excluded from analysis. After dropping noisy channels and trials, all signals were re-referenced to a common average reference.

3.2.2 Subjects

Subjects 1-6 (four female) from Table 3.1 participated in this portion of the study. All subjects were right-handed, had no indications of bilateral speech representation and received left hemisphere grid implants.

3.2.3 Power Spectral Densities

Discrete estimates of spectral power for cognitive tasks used autoregressive methods. The estimated power spectral densities (PSD), $\boldsymbol{P(f, C, Tr, w)}$, where $\boldsymbol{f}$ is the frequency bin, $\boldsymbol{C}$ is the channel, $\boldsymbol{Tr}$ is the trial, and $\boldsymbol{w}$ is the temporal window), were calculated using the Yule-Walker method and a model order of 50 (Kay and Marple 1981). The model order was selected to subjectively balance PSD smoothness with the ability to precisely detect known sinusoidal noise peaks (environmental noise). Comparison of normalized PSD estimates across cognitive tasks between the autoregressive method and the Fast Fourier Transform are shown in Figures A.1 and A.2 and demonstrate qualitative and quantitative agreement in the spectral estimates. Individual frequency bin spectral estimates were evaluated at 2Hz centers, between 2 and 500Hz by averaging the response of the autoregressive model transfer function at 10 samples spaced 0.2Hz apart and centered on each frequency bin. Cognitive task and corresponding ITI PSDs in each trial are the mean of five spectral estimates using 250ms windows with 75% overlap covering a 500ms block of samples as described in Equation (3.1). Each block of samples was time-cued to the stimulus onset, stimulus offset or VOT in each trial. Blocks of samples for stimuli started 100ms after onset. Preparatory period blocks commence at auditory stimulus offset and productive speech blocks begin 100ms prior to the VOT. The block timing parameters were selected empirically after reviewing time-frequency analyses.

$$\boldsymbol{P_{Activity}(f, C, Tr)} = \frac{\mathbf{1}}{\mathbf{5}} \sum_{\boldsymbol{w=1}}^{\mathbf{5}} \boldsymbol{P(f, C, Tr, w)} \qquad \textbf{(3.1)}$$

Time courses of power in specific frequency bands that span multiple cognitive tasks were calculated using the complex Gabor wavelet transform with time-domain standard deviations of either $4/f_c$ (f<120Hz) or $16/f_c$ (f> 120Hz), where f_c is the center frequency of the wavelet (Bruns 2004). The transform magnitude was down-sampled by computing the mean in non-overlapping windows of 8 samples. The 8-sample window size was selected to synchronize the time course of power in the ECoG signal with the stimulus timing from the BCI2000 software. The down-sampled time-course data is referred to using the symbol, $\boldsymbol{P_{DS}(t, f, C, Tr)}$ where t is the time sample in the down-sampled series, and the other variables are as stated previously.

3.2.4 Dissociation Bands

Sets of frequency bands that dissociated either cognitive task or anatomy were analyzed in several ways. These bands were first detected using normalized spectra, $\boldsymbol{P_{N,Activity1}(f, C, Tr)}$ described in Figure 4.2B and Equation (3.2).

$$\boldsymbol{P_{N,Activity1}(f, C, Tr) = \log_{10}\left[\frac{P_{Activity1}(f, C, Tr)}{P_{ITI}(f, C, Tr)}\right]} \quad \textbf{(3.2)}$$

This normalization technique helps remove the non-stationary changes in the ECoG signal and environmental noise that occur on short (~4s) time scales, equalizes the scales for power increases and decreases, and provides a basis to compare power changes to the schematic illustrations in Figure 2.1. An artifact in the normalization method is the presence of downward pointing spikes in the normalized power spectrum (see Figure 4.1 and Figure 4.2 for examples). Since the power of the environmental noise was relatively constant and in general greater than the cortical power in the signal, the difference between

cognitive task and rest was negligible at the noise frequencies; therefore, a narrow slice of the normalized spectra is not significantly different than zero (ITI power level).

The next step in identifying dissociation bands was to identify specific frequency bands with statistically significant differences in normalized power. The normalized spectra for each channel and frequency bin between 60-500 Hz were first screened by cognitive task to identify channels and frequency bins with power changes that were significantly different than the intertrial interval. These tests were performed on the normalized spectra from all trials using the nonparametric Wilcoxon signed-rank test. For each subject and channel, the p-values for all tests (240 frequency bins x 6 cognitive tasks) were corrected for multiple comparisons using the false discovery rate (FDR) technique (Benjamini and Hochberg 1995). This correction reduces the probability that spurious power fluctuations are detected as task-induced power changes. Channels with significant power change (3-33 channels per subject) were then examined to identify any dissociation bands between pairs of cognitive tasks or channels. For each comparison, all frequency bins between 60-500 Hz were tested to determine whether the medians of the pair of normalized spectra were statistically different. These tests used the nonparametric Wilcoxon rank-sum test. The p-values from these pairwise comparisons were FDR corrected for 240 frequency bin comparisons. To further reject spurious power increases, only bands consisting of at least three contiguous 2 Hz frequency bins having statistically distinct medians were further examined. Those comparisons having at least two qualifying frequency bands were further tested for the presence of a magnitude reversal between two frequency bands. It is also important to clarify that each single channel or pair of channels was only counted once in the consolidation of data across patients. Specifically, even if a single electrode exhibited the dissociation band phenomenon for multiple pairwise cognitive task comparisons, it was

only counted once. The combination of nonparametric statistical tests, FDR correction for multiple comparisons and the requirement for two bands with multiple contiguous frequency bins to have statistically different medians and magnitude reversals greatly reduce the likelihood that the dissociation bands we report reflect statistical sampling error.

To further ensure that the familywise Type I error rate (false positive rate) remained at an acceptable level, we performed a Monte Carlo analysis to determine the actual chance occurrence rate of dissociation bands. We selected the data from Subject 1's exemplar shown in Supplemental Figure 3 since this subject had the greatest quantity of dissociation bands. Then, the labels for all of the hearing and speaking after visual cue normalized spectra were randomly permuted 100,000 times into surrogate groups A and B. For each permutation, the surrogate group medians in each frequency bin were tested at the $p=0.05$, 0.01 and 0.001 levels (with FDR correction) using the Wilcoxon rank-sum test. We counted the number of permutations containing both of the following conditions:

At least three contiguous 2 Hz bins where surrogate group A's median was significantly greater than surrogate group B,

At least three contiguous 2 Hz bins where surrogate group B's median was significantly greater than surrogate group A.

These conditions are identical to those used to detect dissociation bands. We computed the familywise Type I error rate by multiplying the proportion of positive permutations in the Monte Carlo simulation by the number of comparisons performed in the study. Only the results for which the familywise error remains below 0.05 are shown in the results.

After identifying the dissociation bands, single-trial and time course data were also evaluated to further confirm the consistency of the power changes. To show the

consistency of the power changes across the course of the experiments, the normalized spectra, $\boldsymbol{P_{N,Activity}(f,C,Tr)}$, from 30-500Hz for every individual trial were plotted. The boundaries of the dissociation bands are indicated to show the spectral regions that dissociated the cognitive tasks (or locations) of interest. In order to visualize the temporal dynamics of power change in the dissociation bands, the time courses of normalized power change for each cognitive task are shown. In a manner similar to that described for the normalized spectra, time courses were normalized by dividing each time sample by the mean power in the preceding ITI and taking the logarithm as shown in Equations (3.3) and (3.4). One second windows of the normalized, down-sampled power in each frequency band $\boldsymbol{P_{N,DS}(t,f,C,Tr)}$ were aligned to either stimulus onset (hearing or reading), stimulus offset (preparation) or voice onset (speaking). Time course plots show the mean across all trials of the normalized, down-sampled power with 95% confidence intervals to illustrate the statistical significance of the difference in power over time.

$$\bar{\boldsymbol{P}}_{\boldsymbol{DS,ITI}}(\boldsymbol{f},\boldsymbol{C},\boldsymbol{Tr}) = \frac{\mathbf{1}}{\boldsymbol{N_{ITI}}} \sum_{\boldsymbol{t=0}}^{\boldsymbol{N_{ITI}-1}} \boldsymbol{P_{DS,ITI}}(\boldsymbol{t},\boldsymbol{f},\boldsymbol{C},\boldsymbol{Tr}) \tag{3.3}$$

$$\boldsymbol{P_{N,DS,Activity1}}(\boldsymbol{t},\boldsymbol{f},\boldsymbol{C},\boldsymbol{Tr}) = \mathbf{log_{10}}\left[\frac{\boldsymbol{P_{DS,Activity1}}(\boldsymbol{t},\boldsymbol{f},\boldsymbol{C},\boldsymbol{Tr})}{\bar{\boldsymbol{P}}_{\boldsymbol{DS,ITI}}(\boldsymbol{f},\boldsymbol{C},\boldsymbol{Tr})}\right] \tag{3.4}$$

3.2.5 Cortical Activation Plots

Summaries of power change across the population of six subjects show consistency of power change over a wide range of frequencies. These figures show the proportion of channels within three focal anatomic areas (Broca's area, sensorimotor cortex and STG), that had statistically significant power changes in each specified cognitive task by

frequency. These plots show trends in consistency of power change by frequency bin across subjects without allowing the actual magnitude of the power change to influence the shape of the plots. Consistency of power change was evaluated using the coefficient of determination (R^2) which quantifies the percentage of variance in each frequency bin attributed to the difference between a cognitive task and rest. The statistical significance of each R^2 was determined using the p-value of a one-way, balanced analysis of variance. To correct for multiple comparisons in each plot a False Discovery Rate (FDR) correction was applied as follows (Benjamini and Hochberg 1995). In each bar plot, the p-values for all frequency bins between 60-500Hz from the electrodes in the anatomic area of interest and the cognitive task under study are collectively corrected for multiple comparisons using a FDR level of 0.001. After correction, significant p-values were counted by frequency bin for each electrode in the anatomic area of interest and cognitive task. These counts were converted to a percentage by dividing by the total number of electrodes within the corresponding anatomic area, and then shown as bar plots. Cortical activation bar plots show the percentage of electrodes with statistically significant power changes in each frequency bin for each combination of anatomic area and cognitive task.

The shape of the bar plots helped evaluate the difference in the proportion of frequency bins with significant power changes between anatomic locations and cognitive tasks. These differences were quantified using two-sample Kolmogorov-Smirnov (K-S) tests. For each plot, the counts of electrodes with significant p-values (after FDR correction) at each frequency bin were converted to actual data samples. For example, if three electrodes within a region were significant at 72Hz, three 72's were added to the set of data samples. The sets of samples from two cortical activation bar plots were then tested to determine if

they came from the same distribution ($p<0.05$). The difference in shape provides a means to evaluate the differences in power change in focal anatomic locations across the population of subjects.

3.3 Diversity Analysis

3.3.1 Subjects

Subjects 1, 2, 4-11 from Table 3.1 were selected to participate in this portion of the study. Subjects with significant perisylvian grid coverage were selected for this portion of the research. Although four of these subjects had either right hemisphere grids or evidence of bilateral speech organization (7-10), these subjects were only excluded from portions of this analysis which study anatomic organization of information.

3.3.2 Preprocessing

Researchers screened all signals for excessive noise prior to any analysis. Channels with excessive noise were dropped from the entire analysis. Trials with excessive environmental noise across all channels, or where speech occurred during stimulus or ITI periods, were also excluded from analysis. No common average referencing was performed on this data because of the data normalization technique described below. For data sampled at 9600 Hz, all signals were low pass filtered at 545 Hz (9^{th} order Butterworth filter), then downsampled by a factor of 8, so the effective sampling rate of all ECoG and microphone signals was 1200 Hz.

3.3.3 Power Spectral Density Estimation

Because this portion of the research was focused on the temporal dynamics of power modulation, PSD estimates used the complex Gabor wavelet transform with time-domain standard deviations of either $4/f_c$ (f<120Hz) or $16/f_c$ (f> 120Hz), where f_c is the center frequency of the wavelet (Bruns 2004). For each subject, ECoG power estimates were first calculated for the entire duration of the experiment. These PSD estimates are referred to as $\boldsymbol{P_G(\tau, f_c, C)}$, where τ is the absolute sample time in the context of the entire experiment, f_c is the center frequency of the wavelet, and C is the channel of interest. The center frequency parameters for the Gabor wavelets were selected between 5 Hz and 560 Hz with associated time-domain standard deviations to balance the time and frequency resolutions and avoid environmental noise frequencies. The bandwidth of each wavelet is inversely proportional to time-domain standard deviations. The specific center frequencies and time-domain standard deviations used in this analysis are listed in Table 3.4.

Table 3.4 Gabor wavelet center frequencies and associated time-domain standard deviations

f_c (Hz)	σ_t (s)
5 7.5 10 12.5 15 17.5 20 22.5 25 27.5 30 33 36 40 45 50 70 80 90 100	$4/f_c$
110 130 140 150 160 170 190 200 210 230 250 260 270 290 310 340 380 400 440 500 520 540 560	$16/f_c$

3.3.4 Downsampling

To reduce the amount of data, the Gabor PSD estimates (P_G) were down-sampled by computing the mean in non-overlapping windows of 32 samples. The 32-sample window size was selected because 1) it synchronized the PSD estimates with the stimulus timing from the BCI2000 software and 2) the majority of the power in the individual traces of

$\boldsymbol{P_G(\tau, f_c, C)}$ existed below approximately 15 Hz. The down-sampled PSD estimates are referred to as $\boldsymbol{P_{DS}(t, f_c, C)}$ where $\boldsymbol{t}$ is the time sample in the downsampled series, $\boldsymbol{f_c}$ is the center frequency of the wavelet, $\boldsymbol{C}$ is the channel.

3.3.5 Data Normalization

For this analysis, it was desirable to allow features in all frequencies to have equal weightings regardless of their absolute power levels. Since power in cortical signals decreases geometrically with frequency, a normalization was necessary (Nunez and Srinivasan 2006). After downsampling, by the central limit theorem, the PSD estimate distributions become more normally distributed. Therefore, the downsampled power spectral densities were z-scored as shown in Equation (3.7). In the data driven analysis, to ensure that the machine learning computations were carried out agnostically on the testing data sets, the mean and standard deviation from the training data set were used to z-score the testing data. In all Receiver Operating Characteristic (ROC) analyses, the downsampled PSDs were z-scored prior to division into training and testing datasets.

$$\boldsymbol{P_{DSZ}(t, f_c, C)} = \frac{\boldsymbol{P_{DS}(t, f_c, C)} - \boldsymbol{\mu(f_c, C)}}{\boldsymbol{\sigma(f_c, C)}} \tag{3.5}$$

Where

$$\boldsymbol{\mu(f_c, C)} = \frac{1}{N}\sum_{t=1}^{N} \boldsymbol{P_{DS}(t, f_c, C)}$$

$$\boldsymbol{\sigma(f_c, C)} = \sqrt{\frac{\boldsymbol{1}}{\boldsymbol{N}}\sum_{\boldsymbol{t=1}}^{\boldsymbol{N}} \left(\boldsymbol{P_{DS}(t, f_c, C)} - \boldsymbol{\mu(f_c, C)}\right)^{\boldsymbol{2}}}$$

3.3.6 Data Driven Evaluation of Information Content

To determine whether the ECoG signals contained sufficient information to identify phonemic content, we applied machine learning techniques to classify phonemes within cognitive tasks. The data driven approach consists of six steps: partitioning, normalization, task and category selection, dimensionality reduction, whitening, parameter selection and classification.

The downsampled PSD estimates $\boldsymbol{P_{DS}}$ are first partitioned by trials into training and testing data. To ensure that there are approximately equal numbers of stimuli or utterances for each phoneme, the training and testing data were segregated by runs. A run consists of 36 trials in which all of the stimuli were presented once. Each subjected completed $\boldsymbol{N}$ = 2-6 runs of the experiment, therefore $\boldsymbol{N}$-way crossfold validation was performed on the data. In each crossfold, one run was set aside for testing, while the other N-1 runs were used for training and validation. Of the N-1 training runs, 20% of the trials were set aside for validating classification parameters.

Once partitioned, the downsampled data was normalized. The training data was z-scored using the mean and standard deviation as shown in Equation (3.7). The testing data was z-scored using the mean and standard deviation from the training data. The z-scored training set is referred to as $\boldsymbol{P_{DSZ,Tr}}$, while the testing set is referred to as $\boldsymbol{P_{DSZ,Tx}}$.

The next step was to select the data during a single cognitive task and label the signals using the specific category (vowels or consonants). Within each partition, for a given cognitive task (hearing or speaking), windows of samples surrounding the appropriate behavioral cue were captured. Hearing windows corresponded to samples from 100 ms

before stimulus onset through 700 ms afterward. Speaking windows captured samples 400 ms prior through 600 ms after voice onset. For each trial, the windowed samples of $\boldsymbol{P_{DSZ,Tr}}$ and $\boldsymbol{P_{DSZ,Tx}}$ for all channels and frequency bands were reshaped into a single vector representing that trial's data. The matrices of the training and testing data for the data driven approach, $\boldsymbol{X_{Tr}}$ and $\boldsymbol{X_{Tx}}$ respectively, were labeled with the specific phoneme within the category being classified (e.g., one of EE, OO, EH, or AH for the vowel category).

The vectors representing each trial contained many tens of thousands of features. The downsampled, z-scored PSDs were composed of 43 frequency bands and 48-80 channels. The task windows were 31 – 39 time samples long. Therefore, the total number of features per trial (64k-134k) far exceeded the total number of trials for any subject as shown in Table 3.1 and would result in overfitting problems during classification. Therefore, the dimensionality of the trial data was reduced. As an initial step, the features were constrained to an optimal set of channels. The procedure for selecting the optimal set of channels is described in Section 3.3.12.1. Once the optimal set of electrodes was identified, the non-optimal electrodes were removed from the data and the dimensionality was further reduced using principal component analysis (PCA). First, the mean for each feature (a single channel, frequency and time sample) across the training trials was removed from both training and test data. The zero-mean training data matrix, $\boldsymbol{X_{Tr0}}$, has dimensions $\boldsymbol{N_T}$ x $\boldsymbol{N_f}$ where $\boldsymbol{N_f \gg N_T}$, the PCA resulted in the eigenvector matrix $\boldsymbol{W_{Tr}}$, and a set of eigenvalues $\boldsymbol{\lambda_{Tr}}$. The eigenvectors were $\boldsymbol{N_T}$ column vectors ($\boldsymbol{w_{Tr}}$) with length $\boldsymbol{N_f}$. The $\boldsymbol{N_T}$ eigenvalues indicated the percentage of variance accounted for by the principal components associated with each eigenvector. The number of principal components used

after the dimensionality reduction, $\boldsymbol{b}$, was treated as a parameter and calculated based on the total percentage of variance in the training data accounted for by the $\boldsymbol{b}$ eigenvectors. To transform the zero-mean training and test data ($\boldsymbol{X_{Tr0}}$ and $\boldsymbol{X_{Tr0}}$) into the principal component space, the matrices were multiplied by the first $\boldsymbol{b}$ eigenvectors as shown by Equation (3.6). The transformed training data, $\boldsymbol{Y_{Tr}}$, had reduced dimensionality $\boldsymbol{N_T}$ x $\boldsymbol{b}$, where $\boldsymbol{b \ll N_f}$. The zero-mean testing data was also transformed into the reduced dimensionality PCA space using the same eigenvectors as shown by Equation (3.7).

$$\boldsymbol{Y_{Tr} = X_{Tr0} W_{Tr}^{1:b}} \tag{3.6}$$

$$\boldsymbol{Y_{Tx} = X_{Tx0} W_{Tr}^{1:b}} \tag{3.7}$$

Prior to training the classifiers, each of the $\boldsymbol{b}$ features in the dimensionally reduced data were whitened. Each feature was scaled and shifted to have a zero mean and range on the interval $[-1, 1]$. Whitening the data accomplished two goals. First, it ensured that all features met the expectation of support vector machine (SVM) classifiers that features are scaled between (-1, 1). Second, it ensured that each feature had equal weighting in the classifier regardless of the amount of variance accounted for. This is important because the differences between the cognitive behaviors (specific phonemes) classified were relatively subtle and may not have accounted for a large amount of variance in the data.

Several classification algorithms were tested on the data including: linear discriminant analysis, a Naïve Bayes classifier, two variants of the large margin nearest neighbor algorithm, multi-class SVMs and random forests. The optimal parameter set for each classification algorithm was selected in each crossfold using the validation data (20% of the

training data). The parameters with the best classification accuracy on the validation data were applied to retrain the classifier on both training and validation samples prior to classifying the test data. Table 3.5 enumerates the specific parameters and associated ranges swept for each classification algorithm. The number of features used by each classifier was also treated as a parameter and varied according to the percentage of variance accounted for by the principle components used in the dimensionality reduction step. The variance accounted included 50, 60, 70, 80, 90 and 99 percent.

Table 3.5 Classifier parameters swept

Classifier	Parameters Examined
Linear Discriminant	**PCA Percentage of Variance (POV) (Number of Features)**
Naïve Bayes	**PCA POV, Number of Features**
Large Margin Nearest Neighbor	**PCA POV, Number of Features Number of Nearest Neighbors (1-10)**
Random Forest	**PCA POV, Number of Features Number of features per tree (1/4, 1/3, 1/2 of all features)**
Support Vector Machines	**PCA POV, Number of Features Kernel (linear, radial, sigmoidal) Regularization $\log_{10}(C) = -6 - 6$ Gamma(kernel parameter) $\log2(\gamma) = -6 - 6$**

During testing, the classifier that was optimized on the training and validation data was applied to the test data. It is important to restate that the test data was preprocessed using the parameters calculated from the training data. First, the test data was z-scored using the means and standard deviations from the training set data. After partitioning, the training feature means were removed from the test partition. Next, the zero-mean test data was transformed into the PCA feature space using the eigenvectors from the training data. Finally, the reduced dimensionality test data features were whitened using the means and ranges from the training data.

Classification accuracy for each algorithm was summarized over all crossfolds in two ways. First, the overall percentage accuracy was computed along with an associated p-value based on the total number of trials, the number of trials classified correctly and the chance probability. The p-value was calculated by determining the probability that random draws of the labels would produce the classifier accuracy or better as shown in Equation (3.8).

$$\mathbf{p-value} = \sum_{\mathbf{n=N_{correct}}}^{\mathbf{N_T}} \binom{\mathbf{N_T}}{\mathbf{n}} \mathbf{p^n (1-p)^{N_T - n}} \tag{3.8}$$

Where

$$\binom{N_T}{n} = \frac{N_T!}{n!\,(N_T - n)!}$$

And, N_T is the total number of trials,

n is the number of trials classified correctly,

and p is the probability of randomly drawing the labels

from the phonemic category (i.e., $1/4^{th}$ for vowels,

$1/9^{th}$ for consonants)

Since it is possible to have classification accuracies that exceed the random probability p that are not statistically significant, the results were thresholded for statistical significance at $p<0.05$.

3.3.7 Matched Filter Overview

The matched filter receiver was introduced in the communications world nearly 50 years ago as an optimal receiver for pulse modulated carrier signals in the presence of white noise (North 1963) and has since been applied to many different digital modulation

schemes (Scholtz 1982). If the transmitted amplitude modulated waveform is known by the receiver a priori, and the only interfering factor in the communications channel is additive white Gaussian noise, it can be shown that the matched filter has the optimal receiver performance when the output is sampled at intervals of the waveform period. Figure 3.3 and Equation (3.9) show the block diagram and analytical equation for the output of a simple matched filter.

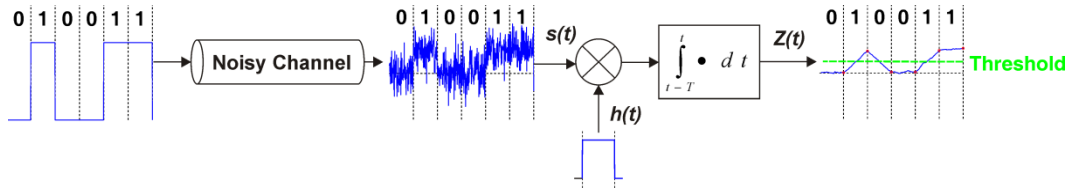

Figure 3.3 Matched filter correlator block diagram
This block diagram illustrates the signal flow through a noisy channel and recovery using the matched filter correlator. If the reference waveform, ***h(t)***, is known a priori, the correlator illustrated above recovers the maximum likelihood estimate of the symbol using the optimal threshold.

$$\mathbf{Z(T)} = \int_0^{\mathbf{T}} \mathbf{s(\tau)h(\tau)d\tau} \qquad \mathbf{(3.9)}$$

Where, *s(t)* is the received signal and *h(t)* is the reference waveform and *T* is the duration of the symbol

When the reference waveform is received at the receiver input, (i.e., $s(t) = h(t)$), Equation (3.9) is simply the autocorrelation of the reference waveform and $Z(T)$ is an estimate of the energy in the reference waveform. When $s(t)$ represents another waveform, Equation (3.9) is the cross-correlation between the two waveforms. Assuming that the two waveforms have equal total energies, then $Z(T)$ will be an estimate of the similarity between $s(t)$ and $h(t)$. For example, if the two waveforms are orthogonal (e.g., sine and cosine), then $Z(T)$ will be zero. If the two waveforms are opposites, (i.e. $s(t) = -h(t)$), then $Z(T)$ will be the negative of the autocorrelation.

The continuous output of the integrator in Figure 3.3 is a sliding correlation between the reference waveform and the received signal and is defined analytically in Equation (3.10).

The output score, $Z(t)$, at any point in time provides an estimate of the similarity of the previous T seconds of the received signal compared to the reference waveform.

$$\mathbf{Z(t) = \int_{t-T}^{t} s(\tau)h(\tau)d\tau} \tag{3.10}$$

An example illustrating graphically how the matched filter correlator provides a similarity score between different received waveforms and the reference is shown in Figure 3.4 below.

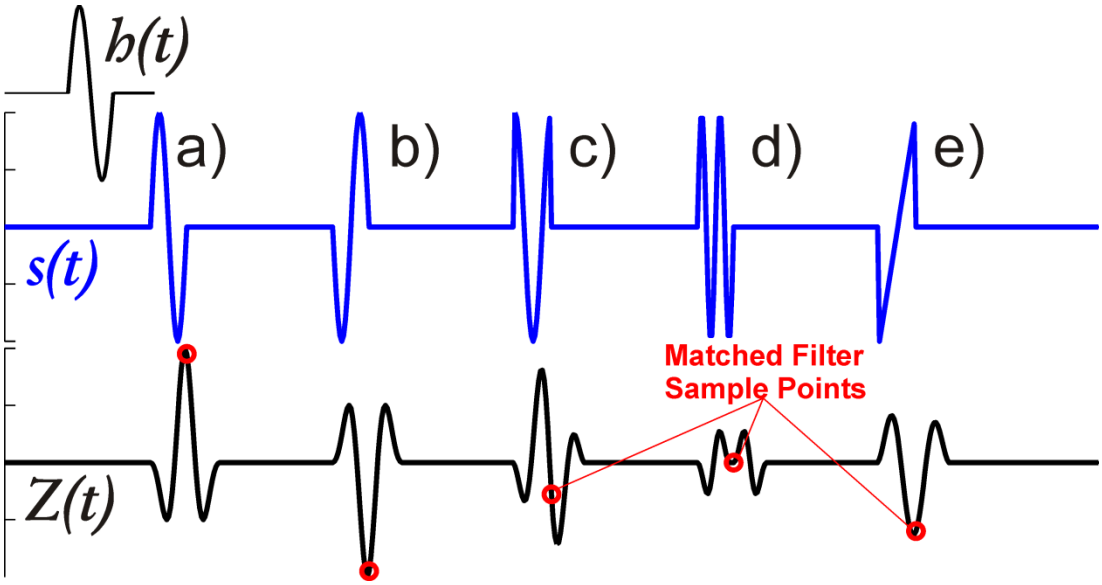

Figure 3.4 Matched filter score comparison
Illustrative example representing the difference in matched filter score for different signals. The reference waveform is a single period of a sine wave($h(t) = sin(2\pi ft)$). The received waveform, $s(t)$, when correlated with the reference waveform yields the score $Z(t)$ which is sampled at the end of each reference waveform period. For each signal waveform (a. through e.), note the change in the both the raw score and the score matched filter sample points indicated by the red circles. The equations for each waveform in $s(t)$ are: a) $h(t)$; b) $-h(t)$; c) $h(t + \pi/2)$; d) $h(2t)$; e) sawtooth wave with same frequency as $h(t)$.

3.3.8 Multi-Dimensional Matched Filters for Neural Motifs

Since neural signals exhibit amplitude modulations in specific bands, the patterns of power modulation in several channels and frequency bands could be considered multi-carrier, multi-site waveforms. These properties lend themselves to the application of a matched filter. The multi-dimensional matched filter also captures a diverse snapshot of the neural

motif associated with a specific cognitive behavior. Since the ECoG signals are nonstationary and the noise characteristics may not be white (indeed in many situations it is not clear which waveforms should be considered "signal" and which should be considered "noise"), performance may be imperfect. However, the matched filter does offer a mechanism through which the structure of the neural motif correlated with specific behaviors may be evaluated. In the following paragraphs, we describe how the matched filter concept is applied to ECoG data. First, we define the discrete multi-dimensional matched filter. Next, we define how the multi-dimensional matched filter reference waveforms are calculated. Finally, we examine how the matched filter will be modified to modulate the information content in various dimensions.

3.3.8.1 Discrete Multi-Dimensional Matched Filter

Since all of the ECoG signals have been digitally sampled, the remainder of the equations will use discrete summations instead of integrals. After the ECoG PSDs were preprocessed, downsampled and z-scored ($\boldsymbol{P_{DSZ}}$), they had dimensions of time samples, channels and frequencies. The matched filter correlator score equation (3.10) was therefore modified to consolidate all three dimensions as shown in Equation (3.11).

$$\mathbf{Z[t]} = \sum_{\mathbf{i=1}}^{\mathbf{N}} \sum_{\mathbf{f \in f_c}} \sum_{\mathbf{c \in C}} \mathbf{s(t - N + i, f, c)h(i, f, c)} \qquad \textbf{(3.11)}$$

Where,
***N* is the number of time samples in the reference waveform h**
f_c is the set of Gabor wavelet center frequencies
and C is the set of channels that were recorded

This version of the matched filter correlator combines all of the dimensions into a single score at each time sample, yet it maintains the properties of the original matched filter

receiver. If the input signal and reference waveform are similar, $Z[t]$ will be high, if they are dissimilar, $Z[t]$ will be low.

3.3.8.2 Matched Filter Reference Waveforms

Matched filter waveforms were computed for combinations of single cognitive tasks (hearing or speaking) and single phonemes (one of 13 shown in Table 3.2). To compute the multi-dimensional reference waveforms, the downsampled and z-scored power estimates, P_{DSZ}, are first organized into trials, then subdivided into training and testing trials. A fourth index ($\boldsymbol{Tr}$) is now included with $P_{DSZ}(t, f_c, C, Tr)$ to reference a specific trial. The time-sample index ($\boldsymbol{t}$) is now understood to be within the context of a single trial. After trial parcellation, training trials with the appropriate phoneme label were identified. Windows of time samples during the cognitive task of interest (either hearing or speaking) were saved for the reference waveform computation. The reference waveform for that specific task and phoneme combination was the average for each time sample, channel and frequency tuple over the training trials. The process is described graphically in Figure 3.5 and in Equation (3.12).

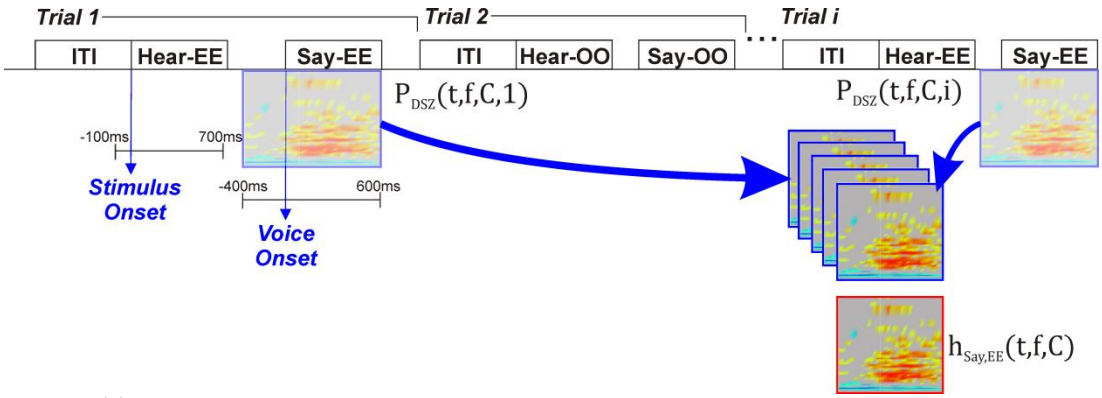

Figure 3.5 Trial structure, timing and matched filter reference waveform construction
The basic structure of the auditory single word repetition experiment shows that each trial consists of ITI, stimulus and response. The horizontal bars below Trial 1 show the relationships of the reference waveform time windows for hearing and speaking to the stimulus or voice onset. To determine the reference waveform for a particular cognitive task and phoneme (speaking the phoneme EE in this example), the downsampled

and z-scored PSDs (P_{DSZ}) from each trial with the relevant phoneme, during the temporal window corresponding to the specific task are first collected (blue boxed time-frequency plots). The reference waveform h_{SayEE} (red boxed time-frequency plot) is the average across trials.

$$\mathbf{h_{Task,m}[t, f_c, C] = \frac{1}{N_{Tr}} \sum_{Tr=1}^{N_{Tr}} P_{DSZ}(t, f_c, C, Tr)} \quad \textbf{(3.12)}$$

Where,

N_{Tr} is the number of training trials with the phoneme m, t is the set of all time samples in the temporal window of interest for the specific $Task$, f_c is the set of Gabor wavelet center frequencies and C is the set of channels that were recorded

A set of reference waveforms $h_{Task,m}$ were generated for each cognitive task and phoneme combination. Reference waveforms for general cognitive tasks (e.g., speaking all phonemes) were generated by averaging P_{DSZ} for a specific cognitive task over all phonemes. Likewise, by applying each reference waveform in the matched filter sliding correlator, a family of matched filter scores $Z_{Task,m}[t]$ was generated for all cognitive tasks and phonemes, and general cognitive tasks.

3.3.8.3 Matched Filter Reference Waveform Dot Product Matrices

To compare the distinctiveness of the reference waveforms for different phonemes within the same cognitive task, we computed the dot products between reference waveforms and summated the results across subjects. Comparisons were divided by cognitive task (hearing or speaking) and phonemic category (vowels or consonants). For each subject, task and category, dot products between reference waveforms for different phonemes were computed, and then normalized by dividing each dot product by the largest single dot product for that subject, task and category. Finally, data for each task and category was combined by taking the average of the normalized dot products across subjects. The data were visualized by plotting the mean dot product scores in a format similar to a confusion matrix.

3.3.8.4 Modulating Information Content

The matched filter concept also provided a structure with which to modify the amount of information in the three dimensions of the reference waveform. Two approaches to modulating information content in the matched filter were used: truncation and smoothing. Truncation removed information from the matched filter. By limiting the range of the summations in Equation (3.11), a range of time samples, frequencies or channels were removed from the reference waveform. In addition to removing information, this approach reduced the total energy in the reference waveform and therefore reduced the signal to noise ratio. The second approach to modifying the matched filter was smoothing. This method modified the reference waveform by adding additional summations. Prior to averaging the response over the training trials, one or more dimensions were averaged as shown in Equations (3.13) and (3.14).

$$\mathbf{h_{Task,m,TimeAvg}[t, f_c, C]} = \frac{\mathbf{1}}{\mathbf{N_{Tr}}} \sum_{\mathbf{Tr=1}}^{\mathbf{N_{Tr}}} \frac{\mathbf{1}}{\mathbf{N_w}} \sum_{\mathbf{t_i=1}}^{\mathbf{N_w}} \mathbf{P_{DSZ}(t_i, f_c, C, Tr)} \tag{3.13}$$

Where, N_{Tr} is the training trials that had phoneme m, N_w is the number of time samples in the temporal window for the specific *Task*; t is the set of all time samples in the temporal window for the *Task*, $\boldsymbol{f_c}$ is the set of Gabor wavelet center frequencies and C is the set of channels that were recorded

$$\mathbf{h_{Task,m,FreqAvg}[t, f_c, C]} = \frac{\mathbf{1}}{\mathbf{N_{Tr}}} \sum_{\mathbf{Tr=1}}^{\mathbf{N_{Tr}}} \frac{\mathbf{1}}{\mathbf{N_f}} \sum_{\mathbf{f_i=f_{c,l}}}^{\mathbf{f_{c,h}}} \mathbf{P_{DSZ}(t, f_i, C, Tr)} \tag{3.14}$$

Where, N_f is the number of center frequencies being averaged between $f_{c,l}$ and $f_{c,h}$, the lower and upper bounds of a band of center frequencies being averaged. All other symbols are as stated above.

The smoothing approach was applied to the time and/or frequency domains and reduced the amount of information without necessarily decreasing the total energy in the reference waveform. Examples illustrating the smoothing concept in the time and frequency domains are shown in Figure 3.6.

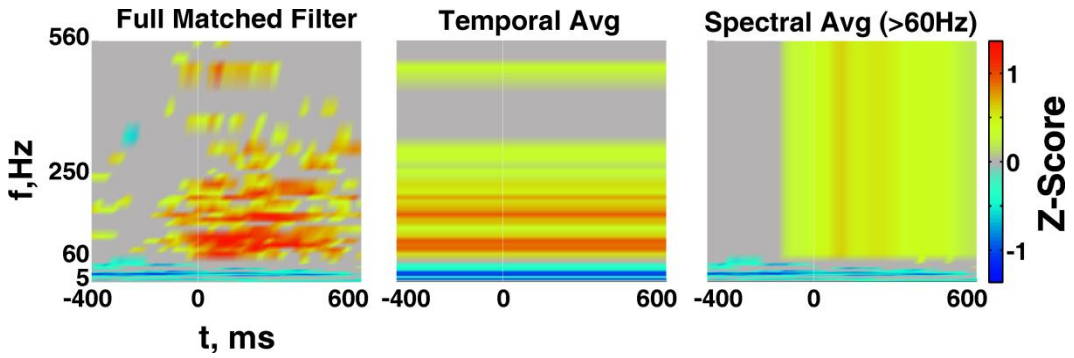

Figure 3.6 Example matched filter and smoothing techniques
The three matched filters excerpts demonstrate the effects of smoothing in the time and frequency domains. The full matched filter (left) reveals several distinct temporal and spectral power modulation patterns before smoothing. The temporal average (center) replaces the temporal dynamics at each center frequency with the average power level across the time window at that frequency. Note that the spectral diversity is retained. The spectral average smoothing technique (right) replaces the spectral dynamics in frequency bands above 60 Hz with the average power across all bands from 70-560 Hz for each time sample in each trial. In this case, temporal diversity is retained.

The truncation and smoothing reference waveform variants which modulated the information contribution from each dimension of space, time and frequency each produced matched filter scores that were compared quantitatively using the Receiver Operating Characteristic (ROC) curve.

3.3.9 Receiver Operating Characteristic Analysis

The ROC curve characterized the sensitivity and specificity of a matched filter reference waveform quantitatively (Peterson, Birdsall et al. 1954). The ROC curve was developed by sweeping a threshold over the range of the matched filter score for a specific reference waveform to determine whether the task and phoneme represented was detected. Scores above the threshold indicated a detection of the task and phoneme at that threshold level. The detections were then compared to the labels. The number of true positives and false positives were counted and plotted as a single point on the ROC curve. As the threshold was raised from the lowest to the highest matched filter score, the ROC curve trace moved from the lower right corner (0% false positives, 0% true positives) to the upper right

corner (100% false positives, 100% true positives). The area under the ROC curve (AUC) was an indicator of the reference waveform's ability to distinguish the specific cognitive task and phoneme pair from all other tasks and phonemes and was therefore the quantitative metric used to evaluate the reference waveform. This process is illustrated graphically in Figure 3.7.

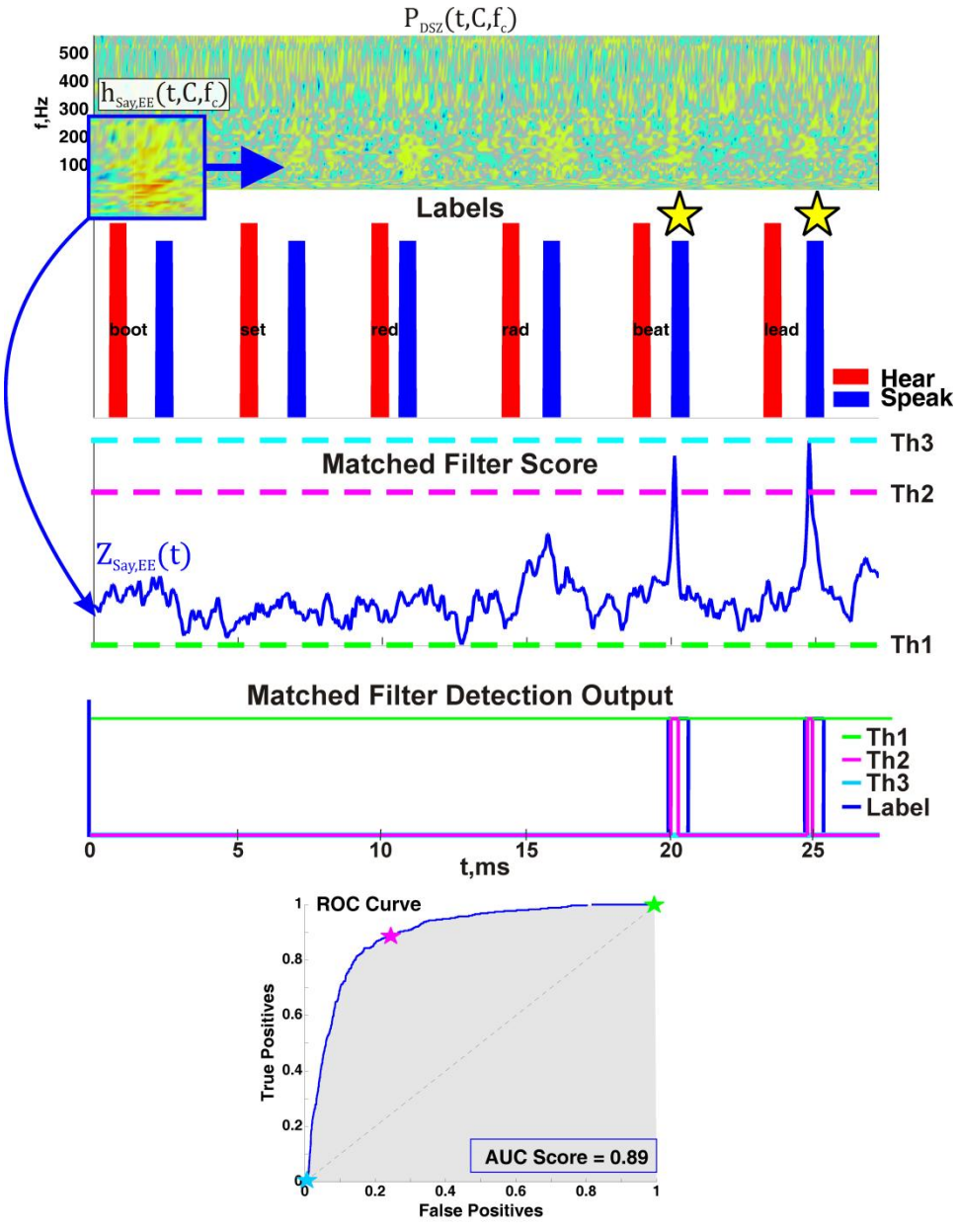

Figure 3.7 ROC Curve development from matched filter score

Exemplar data illustrates how the matched filter reference waveform ($\boldsymbol{h}_{Say,EE}$) is correlated with the downsampled and z-scored PSD estimates ($\boldsymbol{P}_{DSZ}$) to compute the matched filter score ($\boldsymbol{Z}_{SayEE}$). The task and phoneme labels are shown on the same time scale as $\boldsymbol{P}_{DSZ}$ and $\boldsymbol{Z}_{Say,EE}$. The two yellow stars highlight specific times when the phoneme 'EE' was spoken. Thresolding the matched filter score at different levels produces different detection outputs. By counting the percentage of true and false positive detections compared to the label, the ROC curve is developed. The area under the ROC curve in gray yields the score which quantifies the information content in the reference waveform.

As in the data driven analysis, we used a multiple crossfold validation approach in which the reference waveforms were calculated on the training trials and then evaluated on a separate set of testing trials. Crossfolds are separated by runs of 36 trials (each stimulus {Kruskal, 1952 #603}presented once) as described in Section 3.3.6. To evaluate the performance of the reference waveforms, ROC curves were generated for the entire time course of the training data (classification) and the testing data (prediction). To quantify the contribution of high-gamma band dynamics we systematically varied the contributions of spatial (channels), temporal and spectral diversity using different matched filter variants.

3.3.10 Area Under the Curve Analysis of Variance

The AUC metric for several reference waveform variants formed the basis of a full-factorial, N-way Analysis of Variance (ANOVA) experiment with replications. Table 3.6 contains the different factors involved in the ANOVA. The results of the ANOVA were the amount of variance accounted for by each individual factor in the experiment and the significance of each factor in predicting AUC in the model. Pairwise interactions between factors were also considered. The ANOVA technique assumes that errors are distributed normally. Examination of the errors revealed a non-Gaussian distribution, therefore, tests for significance between AUC scores generated by different reference waveform variants used the nonparametric Kruskal-Wallis test {Kruskal, 1952 #603}.

Table 3.6 N-Way ANOVA Factors and Levels

Factor	Levels	Degrees of Freedom
Subjects	**10**	**9**

Cognitive Tasks	**2 (Hearing, Speaking)**	**1**
Phonemes	**13**	**12**
Spatial Variants	**3 (Single Best Electrode, Optimal Set of Electrodes, Whole Grid)**	**2**
Temporal Variants	**3 (Single Best Time Sample, Time Average, Time Varying)**	**2**
Low Frequency (<60 Hz) Spectral Variants	**3 (Not Included, Spectral Average, Discrete Bands)**	**2**
High Frequency (<60 Hz) Spectral Variants	**3 (Not Included, Spectral Average, Discrete Bands)**	**2**

This experiment requires (10 x 2 x 13 x 3 x 3 x 3 x 3) 21,060 experimental configurations with 2-6 replications per configuration based on the number of crossfolds performed by each particular subject. Additionally, the experiments were repeated with the matched filters for general cognitive tasks (hearing or speaking all phonemes). To complete these experiments in a reasonable amount of time, computations were performed using the facilities of the Washington University Center for High Performance Computing, which were partially provided through grant NCRR 1S10RR022984-01A1.

Although the ANOVA factors for subjects, cognitive tasks and phonemes were not of primary concern in this analysis, they were a significant source of variance and were therefore included in the model. The variants exploring the spatial, temporal and spectral diversity bear further discussion. The temporal and spectral dimensions each had three levels which correspond to matched filter variants which: 1) truncated the information in that dimension, 2) smooth the information 3) include the full amount of information from that dimension. Consider the temporal variants of the matched filter as an example. The truncated version used only the best single time sample from the reference waveform (the methodology for choosing the best sample will be described in the following sections). The smoothed variant used all time samples, but averages the power for each channel and frequency tuple over the entire matched filter window as described in Section 3.3.8.4. The

full-diversity variant used all time samples in the reference waveform as originally computed. The three levels of spatial variants were the best single channel, optimal number of channels and all channels. Two sets of spectral variants were used to allow analysis of the high gamma bands (>60 Hz) and lower frequencies separately. Each set of spectral variants (<60 Hz and >60 Hz) also had three variants. The truncated spectral variant removed all of the relevant frequency bands. The smoothed spectral variant averaged the power across the relevant bands, and the full diversity spectral variant used the reference waveform as originally computed. In order to complete the full factorial experimental design, each of these reference waveform variants were also combined.

The results of the ANOVA determined the significance of individual factors and multi-factor interactions in accounting for variance in the model. Additionally, each of the dimensional variants (space, time and frequency) will be examined to determine if the populations for each level are significantly different. This analysis helped test the hypothesis that information is diversely encoded in the neural motif, and helped quantify the extent of diversity in each dimension.

3.3.11 Monte Carlo Analysis

Because of the regular temporal structure of the experimental paradigm, which had a deterministic ITI, there was a significant rhythmic component in the ECoG signal correlated with the time scale of specific cognitive tasks. In order to determine the true random level of performance on this data set, a Monte Carlo analysis was performed. The downsampled, z-scored PSD estimates were kept intact while, on a trial-wise basis, the stimulus labels, ITI duration and voice onset timing were randomly jittered 1000 times. For each random iteration, trial boundaries were reestablished, trials were partitioned into

training and testing sets, a reference waveform was generated on the training data set, then the matched filter scores were computed for the training and testing data. Different percentile AUC scores from the testing data during the Monte Carlo simulation were used as the threshold for statistical significance. For example, if results with a p-value of less than were desired, the 95th percentile AUC score from the Monte Carlo simulation was selected as the significance threshold.

3.3.12 Dimensional Contribution to Diversity Analysis

Beyond the ANOVA, additional studies quantified the information contribution of each dimension (space, time and frequency) of the neural motif.

3.3.12.1 Spatial Diversity Analysis

To determine the extent of cortical areas that provide significant information within the matched filter reference waveform, two additional analyses were performed. As a preliminary step, matched filter scores using reference waveforms from all channels individually were calculated. The single channel matched filter score was then correlated with the label of interest. Channels were rank ordered by decreasing correlation r^2 with the labels for each pair of tasks and phonemes. Then AUC scores were calculated by adding single channels in order of decreasing r^2. The result was a trace that showed matched filter score versus the number of channels included in the reference waveform.

The second spatial analysis again used reference waveforms from single electrodes. The goal of this analysis was to determine how many single channel reference waveforms produced matched filter scores above chance for each cognitive task. This analysis was completed for hearing and speaking individual phonemes, then for general cognitive tasks.

Chance level AUC scores for the single channel analysis were established by randomly shuffling the time and frequency and channel indices of the matched filter 10 times for each phoneme, task and crossfold (520-1560 simulations per subject). On a per subject basis, the average AUC score over crossfolds for each pair of cognitive tasks and phonemes was compared to the 95th percentile chance AUC score to determine the statistical significance of the score. The number of phonemes with above chance AUC scores for each single channel and cognitive task were plotted on the MNI atlas brain as a heat map. To consolidate the results across patients with grids in different yet overlapping locations, the total number of phonemes with above chance scores in each single location was normalized by the total number of electrodes across patients at that location.

3.3.12.2Temporal Diversity Analysis

Two additional analysis of temporal diversity in the neural motif were performed as well. First, for each cognitive task and phoneme, the matched filter scores from reference waveforms using a single time sample were computed. Using the correlation scores between the matched filter scores and the labels, the time steps were rank ordered by decreasing r^2. After ranking, AUC scores were computed by adding single time samples to the reference waveform in decreasing r^2 order. A plot of AUC score versus the number of time samples included in the reference waveform was then plotted by cognitive task for each class of phonemes (consonants/vowels) as well as the general cognitive tasks.

Secondly, to determine if there were trends across the subject population in the relative importance of the different time samples in the hearing and speaking windows, the median rank of each time sample across subjects, phonemes and crossfolds was compared to those for the generic cognitive tasks. To visualize the trends, the rank (1 is best, higher is worse)

was converted to a quality score by subtracting the rank from the total number of time samples in the behavioral time window (31 time samples for hearing, 39 time samples for speaking). The conversion from rank to quality makes the plots more intuitive since higher ranks are qualitatively better.

3.3.12.3Spectral Diversity Analysis

The spectral diversity analysis was very similar to that of the temporal diversity analysis. The only difference was the substitution of individual frequency bands for time samples. Instead of rank ordering correlations from single time samples, the r^2 values from reference waveforms using single frequency bands were used. The AUC scores from matched filters adding single frequency bands in order of decreasing r^2 were computed. Then the ranks of each frequency band were computed and converted to quality scores as described in the previous section as well.

3.3.13 Exemplar Feature Comparisons

Exemplar data illustrating differences between features of reference waveforms for various phonemes and cognitive tasks were analyzed using nonparametric methods. Although the PSDs were z-scored, quantitative analysis of different features revealed that the distributions were non-Gaussian. To determine when a feature was statistically significant across trials, we used the Wilcoxon signed-rank test (Wilcoxon 1945). This nonparametric test quantifies the probability that the median of a specific sample set is different than zero. To determine when a feature was statistically distinct between two sets of trials, we used the Wilcoxon rank-sum test (Wilcoxon 1945). This non-parametric test quantifies the probability that the median of the differences between the populations is nonzero.

3.4 Microarray Methods

As discussed in Chapter 1, the third aim of this dissertation is to examine microarray ECoG signals and determine if the spectral diversity discovered in Aim 1 and the spatio-temporal dynamics examined in Aim 2 exist at a spatial scale one order of magnitude smaller. The data from these experiments comes from three subjects (11-13) that received ECoG microarray implants simultaneously with the clinical macrogrids. In general, the analysis techniques for this aim were identical to those described above, with the exception that for the third aim, they were applied only to microarray ECoG signals. Minor differences in preprocessing and experimental tasks are described below.

3.4.1 Microarray Data Preprocessing

Because the microarray electrode impedances were one order of magnitude higher than the macrogrid electrodes, additional preprocessing steps were required. All microarray data was captured at 9600 Hz with no filtering. To remove excessive environmental noise, the raw signals were filtered using a comb filter with notches at harmonics of 60 Hz (zero-phase, infinite impulse response comb, Q=35) prior to the rest of the preprocessing described in Section 3.3.2.

3.4.2 Experimental Setup

Two of the subjects for this study performed different experiments. Subject 12 was congenitally blind and therefore did not perform the visual single word repetition paradigm. Instead, for the dissociation band analysis, ECoG data from the auditory single word repetition task and verb generation tasks were used. Because of faulty microphone connections, none of the speaking data from Subject 12 was usable. An additional auditory

task used for the dissociation band analysis was an auditory motion detection paradigm. The subject listened to stereo auditory stimuli that either moved from left to right, right to left, or remained stationary. The subject was required to click a mouse button if the sound moved. Subject 13 used a different set of stimuli for the auditory single word repetition experiment studied for the dissociation band analysis. These stimuli were not phonemically matched, therefore a second experiment was used for the diversity analysis. For the diversity study, Subject 13 heard and repeated the phonemically matched nonwords shown in Table 3.3.

3.5 References

Ad-Tech, M. I. C. (2008). 2008 product catalog - epilepsy and neurosurgery product guide.

Benjamini, Y. and Y. Hochberg (1995). "Controlling the false discovery rate: A practical and powerful approach to multiple testing." Journal of the Royal Statistical Society. Series B (Methodological) **57**(1): 289-300.

Bruns, A. (2004). "Fourier-, hilbert- and wavelet-based signal analysis: Are they really different approaches?" Journal of Neuroscience Methods **137**(2): 321-332.

Jack L. Lancaster, M. G. W., Lawrence M. Parsons, Mario Liotti, Catarina S. Freitas, Lacy Rainey, Peter V. Kochunov, Dan Nickerson, Shawn A. Mikiten, Peter T. Fox, (2000). "Automated talairach atlas labels for functional brain mapping." Human Brain Mapping **10**(3): 120-131.

Kay, S. M. and S. L. Marple, Jr. (1981). "Spectrum analysis: A modern perspective." Proceedings of the IEEE **69**(11): 1380-1419.

Miller, K. J., S. Makeig, A. O. Hebb, R. P. N. Rao, M. denNijs and J. G. Ojemann (2007). "Cortical electrode localization from x-rays and simple mapping for electrocorticographic research: The "location on cortex" (loc) package for matlab." Journal of Neuroscience Methods **162**(1-2): 303-308.

North, D. O. (1963). "An analysis of the factors which determine signal/noise discrimination in pulsed-carrier systems." Proceedings of the IEEE **51**(7): 1016-1027.

Nunez, P. L. and R. Srinivasan (2006). Electric fields of the brain : The neurophysics of eeg. New York, Oxford University Press.

Peterson, W., T. Birdsall and W. Fox (1954). "The theory of signal detectability." Information Theory, IRE Professional Group on **4**(4): 171-212.

Schalk, G., D. J. McFarland, T. Hinterberger, N. Birbaumer and J. R. Wolpaw (2004). "Bci2000: A general-purpose, brain-computer interface (bci) system." IEEE Transactions on Biomedical Engineering **51**(6): 1034-1043.

Scholtz, R. (1982). "The origins of spread-spectrum communications." Communications, IEEE Transactions on **30**(5): 822-854.

Wilcoxon, F. (1945). "Individual comparisons by ranking methods." Biometrics Bulletin **1**(6): 80-83.

4 High Frequency Nonuniformities

We tested the first hypothesis of this dissertation, that different cognitive tasks can evoke distinct patterns of spectral power modulation in bands above 60 Hz, using two analyses. First we examine the nonuniformity of power modulation across cognitive tasks. Second, we quantify the nonuniformity by counting dissociation bands. Finally, we present a consolidated view across subjects.

4.1 Behavioral Data

Each of the six subjects performed both the auditory and visual versions of the single-word verbal repetition paradigm. The mean voice onset time (VOT) across subjects for the auditory task was 998 ms (SD=453 ms), and for the visual task was 825 ms (SD=463 ms). These statistics are on the same order of magnitude as those from studies using similar tasks (Church, Coalson et al. 2008) and indicate that the subjects did not have difficulty performing the experimental tasks.

4.2 High-Gamma Band Power Changes are Nonuniform and Extend up to 500 Hz

Each of the six subjects in this study had electrodes with behaviorally-induced power changes that were nonuniform, but were instead concentrated in specific frequency bands. These nonuniform power changes are most visible in the normalized log magnitude spectra as shown for an exemplar subject and single electrode in Figure 4.1. In this example, there are marked differences between the spectra for the six different cognitive tasks especially in the frequency bands between 60-120, 122-400 and 480-500Hz. This electrode responded

strongly to the auditory stimulus between 60-160Hz, however, the visual stimulus response had a much smaller magnitude and was statistically different than rest primarily between 140-160Hz & 200-230Hz. The two speaking tasks had similar responses across a wide range of frequencies between 90-400Hz with notable differences in the 80-130Hz and 480-500Hz bands. The two preparatory periods appear to be a blend between the spectral patterns of the stimuli and vocal response. All subjects had electrodes that exhibited nonuniform power changes in the normalized spectra across various cognitive tasks. In many cases, the nonuniformities in the high-gamma band were specific enough to dissociate different cognitive tasks and anatomic locations.

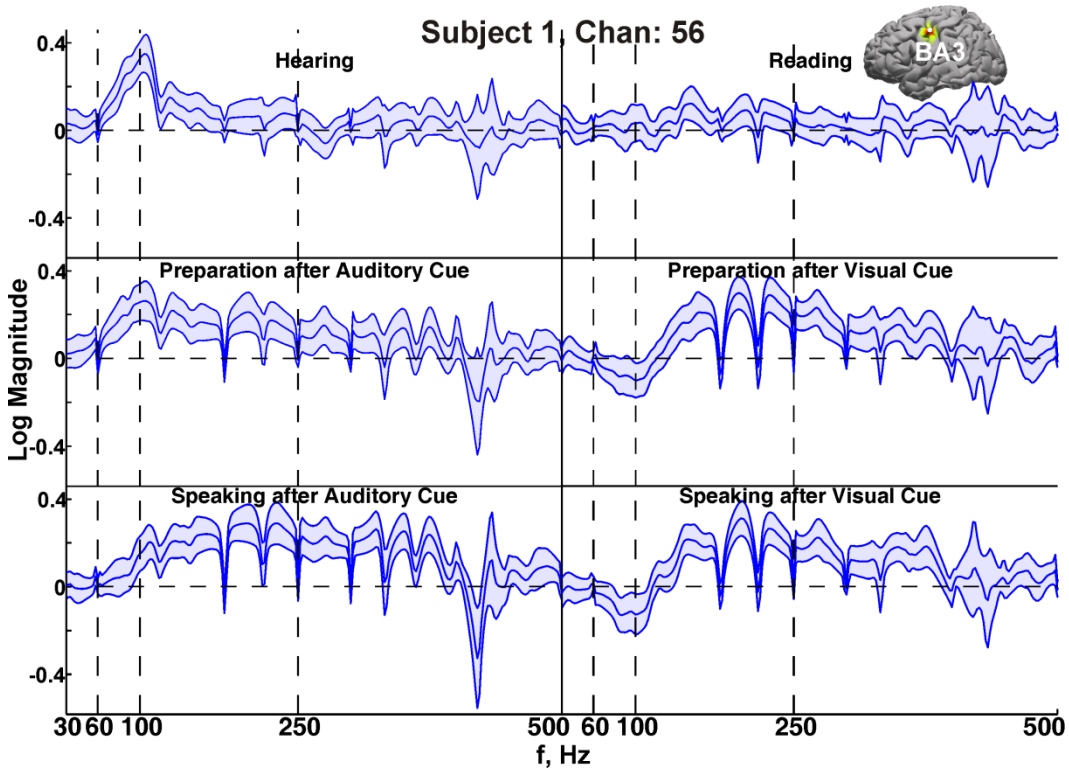

Figure 4.1 Single subject normalized spectra for all cognitive tasks
Exemplar normalized spectra illustrate that high-gamma band power changes are nonuniform and distinct between tasks. The blue center line is the mean normalized spectra across 71 trials. The shaded area encapsulates the 95% confidence intervals. Vertical dashed lines at 60, 100 and 250Hz outline typical gamma band analysis boundaries. Frequencies with normalized spectra greater than zero indicate behavior-induced power increases, while values less than zero reflect power decreases. Note that for all six cognitive tasks, the patterns of spectral power change are unique across a wide range of frequencies. Each cognitive tasks has different bandwidths of frequencies that are statistically different than rest, and in some bands the direction (sign) of power change between cognitive task reverses (e.g., 60-120Hz Hearing vs. Speaking after Visual

Cue). The sharp downward spikes are the result of environmental noise components that do not change in magnitude between cognitive task and ITI.

4.3 High-Gamma Dissociation Bands Quantify Nonuniformity in Spectral Power Change

We quantified the nonuniformity of power change in high-gamma frequencies by identifying dissociation bands. When the independence of power change in two different high-gamma frequency bands can dissociate cognitive tasks or anatomic locations, they are identified as "dissociation bands" as illustrated in Figure 4.2B and C and as follows. It is important to clarify here that a dissociation band is broader than the individually highlighted zones in the figures. We define a single band as the conjunction of several contiguous frequencies that have statistically significant power modulation in the same direction. The definition of dissociation bands requires power modulations in opposite directions in contrasting cognitive tasks or separable anatomic locations. Thus, for example in Figure 4.2B, the frequency bands between 54-92 Hz and 284-324 Hz show preferential power modulation correlated with either hearing words or saying a word that has been heard. The band between 54-92 Hz is interrupted by artifact and similarly the band between 284-324 Hz. For clarity, the single frequency bin in each frequency band is used to illustrate the reversal in power magnitude. In the lower frequency band (54-92 Hz) the 80Hz bin illustrates the confidence intervals on normalized power change are nonoverlapping and Speaking after Auditory Cue has a greater normalized power than Hearing. In the second highlighted frequency band (284-324 Hz) the 288 Hz bin illustrates again the confidence intervals are nonoverlapping, but Hearing induces a greater power change than Speaking after Auditory Cue. Additionally, because the independence of low-gamma (30-60 Hz) and high-gamma (>60 Hz) has been previously reported, we also

constrained our search for dissociation bands to the frequency range between 60-500 Hz (Crone, Boatman et al. 2001; Edwards, Soltani et al. 2005). The single-trial normalized spectra in Figure 4.2D illustrate the consistency of the dissociation band phenomena. Over 216 trials, the normalized spectra show that for Hearing, the 284-324 Hz band has a consistently higher magnitude of power change (warmer colors) than Speaking after the Auditory Cue. Likewise, in the 54-92 Hz band, the Speaking after Auditory Cue normalized spectra have consistently larger magnitudes of power change (warmer colors) than Hearing. The reversal in normalized power is also evident in the time-course of power in the two dissociation bands. Figure 4.2E shows the mean and 95% confidence intervals of the normalized, down-sampled spectra for the frequency bands centered at 80Hz and 288Hz. Over the course of the three cognitive tasks in the auditory repetition paradigm, the power levels reverse toward the end of the preparatory task and just prior to voice onset. From these three views of the spectral power, it is evident the power levels at this electrode are independent enough to dissociate the different tasks in these two high-gamma sub-bands.

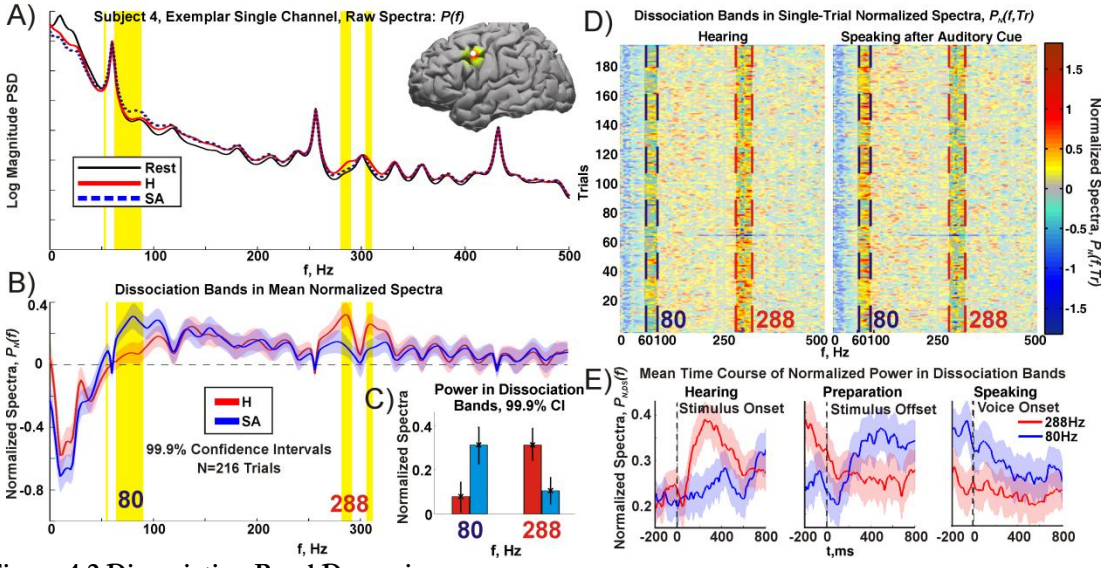

Figure 4.2 Dissociation Band Dynamics

The dynamics of power in dissociation bands. A) Exemplar mean raw PSDs for rest and two cognitive tasks (H=Hearing, SA=Speaking after Auditory Cue) for N=216 trials. Yellow bands around 80Hz and 288Hz highlight high-gamma frequency bands that dissociate the two tasks. B) Mean normalized spectra (solid lines) with 99.9% confidence intervals (shaded areas) show differences in the spectral power change patterns as averaged over all trials. Nonoverlapping confidence intervals and a reversal in the relationship between power levels in the two highlighted frequency bands illustrate a pair of dissociation bands. Note also that behaviorally induced power change is significantly different than rest as high as 500Hz. C) Bar plot with 99.9% confidence intervals illustrates the statistical significance of the difference in normalized power between the two cognitive tasks for the dissociation bands in B. This format is used for other subjects in Figure 4.3. D) Single-trial normalized spectra for the single electrode and two cognitive tasks in A, B and C illustrate the consistency of power change in the dissociation bands across trials. These plots show that normalized spectra in the dissociation bands are not dominated by outliers in any single trial. The color intensity outside of the dissociation bands is subdued to highlight activity in the bands under study. E) Time courses of power in the dissociation bands from A, B and C. The mean down-sampled and normalized power level for each frequency with 95% confidence intervals shows that during over the course of the experiment, power levels in the two dissociation bands reverse.

It is important at this point to address the affect of the system noise floor on this analysis. It is generally accepted that electrophysiological spectra demonstrate power law behavior, dropping off geometrically ($P(f) \propto {}^{1}/_{f}$) {Nunez, 2006 #15}. In the raw spectra shown in Figure 4.2A, the effect of the noise floor causes the power spectral density to stop decaying geometrically once the noise power overwhelms the physiological signal. All of the quantified analyses use the normalized spectra described by equation (3.2) which account for the system noise floor. The system noise floor does not change on the time scale of a single trial (4.533s in this research). Therefore the normalized spectral magnitude in bands obscured by the noise floor should not be statistically different than zero. However it is possible for behavior-induced power changes to rise above the system noise floor, while falling below the level of noise during the intertrial interval. In this situation, the activity spectra will be normalized by the noise floor thereby reducing the detected magnitude of the change compared to the actual physiologic modulation. With this effect in mind, it is clear that the system noise floor artifact has no ability to create spurious dissociation bands at high frequencies, it can only obscure them.

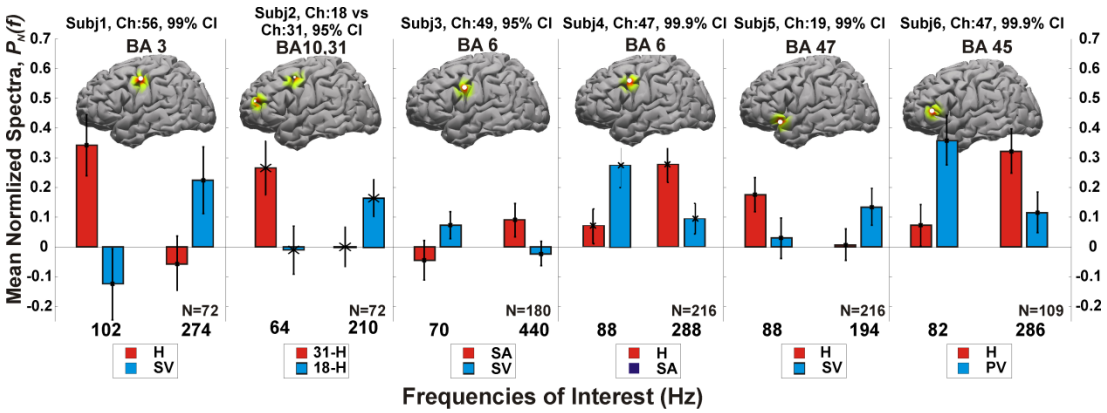

Figure 4.3 Dissociation Band Exemplars

Exemplar dissociation bands for all six subjects. See **Error! Reference source not found.** for the derivation f individual bar plots. The electrode(s) of interest, confidence intervals, associated Brodmann Area (BA) labels, and cortical location on the MNI model brain are shown above each bar plot for reference. Subject 2 did not have single electrodes with dissociation bands and therefore the exemplar shows power change reversals between two electrodes during the same cognitive task. Cognitive Task Key: H=Hearing, R=Reading, PA=Preparation after Auditory Cue, PV=Preparation after Visual Cue, SA=Speaking after Auditory Cue, SV=Speaking after Visual Cue.

We identified several pairs of dissociation bands for each subject. The single electrode dissociation bands represent single anatomic locations where different high-gamma bands distinguish cognitive tasks. We also tested for pairs of electrodes that had different high-gamma bands that dissociated anatomic locations during the same cognitive task. Figure 4.3 contains exemplar single or multi-electrode dissociation bands for all six subjects. Five of the six subjects had single-electrode dissociation bands that distinguished strictly cognitive task. The second subject's exemplar comes from a pair of electrodes that dissociated solely anatomic locations. Figure A.3 contains the normalized spectra associated with each subject's exemplar dissociation bands. While many of the dissociations were caused by differences in the magnitude of normalized power increases, there were dissociation bands that were caused by significant power decreases. Figure A.4 summarizes the percentages of single electrode dissociation bands in which at least one of the dissociating frequency bands had a significant power decrease.

Figure 4.4 contains a quantitative summary of the electrodes and electrode pairs with dissociation bands by individual subject and statistical strength. To ensure that the familywise Type I error rate (false positive rate) in this figure remained at an acceptable level, we performed a Monte Carlo analysis to determine the actual chance occurrence rate of dissociation bands. We selected the data from Subject 1's exemplar shown in Figure A.3 since this subject had the greatest quantity of dissociation bands. Then, the labels for all of the hearing and speaking after visual cue normalized spectra were randomly permuted 100,000 times into surrogate groups A and B. For each permutation, the surrogate group medians in each frequency bin were tested at the p=0.05, 0.01 and 0.001 levels (with FDR correction) using the Wilcoxon rank-sum test. We counted the number of permutations containing both of the following conditions:

At least three contiguous 2 Hz bins where surrogate group A's median was significantly greater than surrogate group B,

At least three contiguous 2 Hz bins where surrogate group B's median was significantly greater than surrogate group A.

These conditions are identical to those used to detect dissociation bands. We computed the familywise Type I error rate by multiplying the proportion of positive permutations in the Monte Carlo simulation by the number of comparisons performed in the study. The table below records the factors contributing to the total number of comparisons as well as overall familywise Type I error rate.

Table 4.1 Familywise Type I Error Rate Computations

Dissociation Band Test p-value	0.05	0.01	0.001

Permutations with dissociation bands	**58**	**4**	**0***
Single Channel Activity Comparisons	**15**	**15**	**15**
Channels with Significant Power	**33 + 4 + 3 + 16 + 9 + 28 = 93**	**19 + 11 + 3 + 20 = 53**	**8 + 9 + 2 + 9 = 28**
Single Channel Type I Error Rate	**15 x 93 x 58/100,000 = 0.8091**	**15 x 53 x4/100,000 = 0.0318**	**15 x 28 x 1/100,000 = 0.0042**
Channel Pair Activity Comparisons	**6**	**6**	**6**
Channel Pairs with Significant Power	**33 x 32 + 1 x 3 + 3 x 2 + 16 x 15 + 9 x 8 + 28 x 27 = 2,133**	**19 x 18 + 11 x 10 + 3 x 2 + 20 x 19 = 838**	**8 x 7 + 9 x 8 + 2 x 1 + 9 x 8 = 202**
Channel Pair Type I Error Rate	**6 x 2,133 x58/100000 = 7.4228**	**6 x 838 x 4/100,000 = 0.1526**	**6 x 202 x 1/100,000 = 0.0121**

*** There were no random occurrences after 100,000 permutations, therefore we used a 1/100,000 rate for the rest of the calculations.**

The tests highlighted in yellow all maintained familywise Type I error rates below 0.05, and therefore prove that our results are significant, even after the most conservative correction for multiple comparisons. These corrections may be so stringent, that they increase the number of Type II errors (false negatives) in our analysis; however, to show that the data support our hypothesis under the most stringent of corrections, only these results are shown below. The results in Figure 4.4 strongly support our hypothesis that nonuniform power modulations between 60-500 Hz can be specific to cognitive task and location. The majority of subjects continue to exhibit both single channels and channel pairs that dissociate either cognitive tasks or anatomic locations even after correction for multiple comparisons.

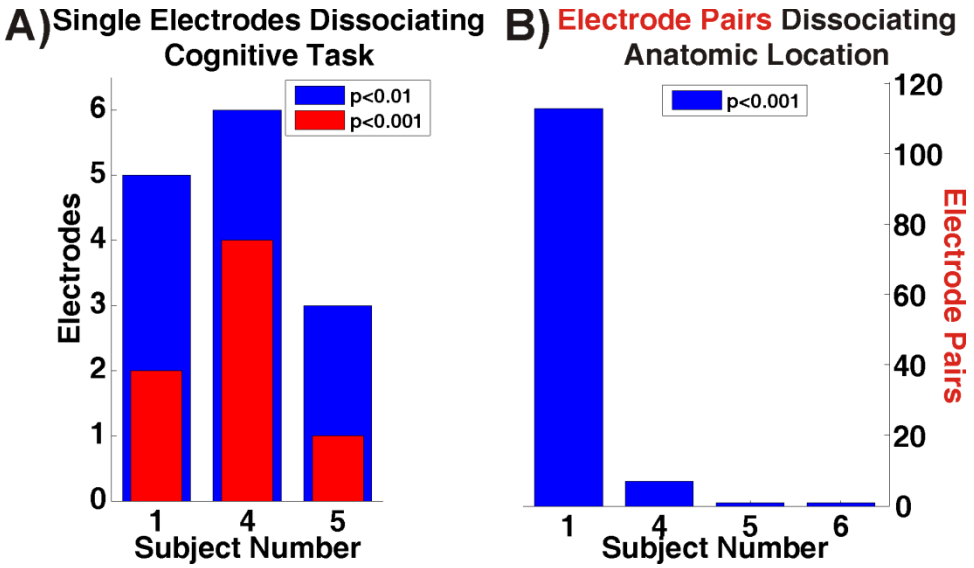

Figure 4.4 Quantitative Summary of dissociation bands across the subject population
Each bar shows the number of single electrodes (A) or electrode pairs (B) with dissociation bands for each subject by p-value. A) This chart quantifies the number of single electrodes with significant power changes in different high-gamma frequencies that dissociated two or more cognitive tasks. B) This chart quantifies the number of electrode pairs in which different high-gamma frequencies dissociated anatomic locations during the same cognitive task.

The numbers of single electrodes with high-gamma bands dissociating cognitive task are plotted in **Error! Reference source not found.**A, while Figure 4.4B summarizes the umber of electrode pairs that dissociate anatomic location. All of the statistics shown have a familywise error rate below 0.05. The statistics across this group of subjects show that the independence of power change in sub-bands across the range of high-gamma frequencies is not an anomaly. The pervasive occurrence of dissociation bands especially within data from single electrodes across this population of subjects indicates that ECoG signals can capture population dynamics that produce nonuniform power changes across the high-gamma band up to 500Hz.

4.4 Cross-Subject Analysis by Anatomy and Cognitive Task

Evaluating spectral power modulation across subjects shows that power changes occur nonuniformly even within small anatomic regions. Three cortical regions: left sensorimotor cortex (Brodmann Areas (BA) 1-4), Broca's area (BA 44-45), and left superior temporal gyrus (STG, BA 22, 42), have all been implicated in functional imaging studies using similar language tasks and were therefore selected for more detailed analysis (Church, Coalson et al. 2008). In Figure 4.5, for each combination of cortical region and cognitive task, bar plots show the percentage of electrodes within that region from all six subjects that had statistically significant R^2 values (FDR correction level of 0.001) at each frequency. These plots provide a means to evaluate the significance and consistency of spectral power change across the subject population and have the appearance of a pseudo-spectrum, but allow an evaluation across the subject population without permitting individual differences in the magnitude of power change to affect the shape of the plot. By confining the scope to three anatomical areas and four cognitive tasks, we can visualize trends in high-gamma band power change across the entire population of subjects. In these plots, high numbers at a given frequency indicate that a high percentage of electrodes within a specific cortical region had consistent power changes across subjects during a specific cognitive task. Because of variation in individual channel power levels caused by differences in electrode impedances and cortical population characteristics, power changes will be masked at different high frequencies as they are obscured by the system noise floor. If uniform and broadband high frequency power increases as in Figure 2.1 were the only motif present, the histograms in Figure 4.5 would decrease monotonically. Any channel with significant induced power increases for a given task should remain significant from 60 Hz until the power levels fall below the system noise floor. The only exception would be environmental noise frequencies where there is no significant power change. On the other

hand, if power changes are confined to specific bands then the shape of the activation plots should have variation due to band specific power changes from different electrodes within the anatomic area or from individual differences between subjects that result in non-monotonically decreasing trends. The results show that power changes occur nonuniformly even within small cortical regions.

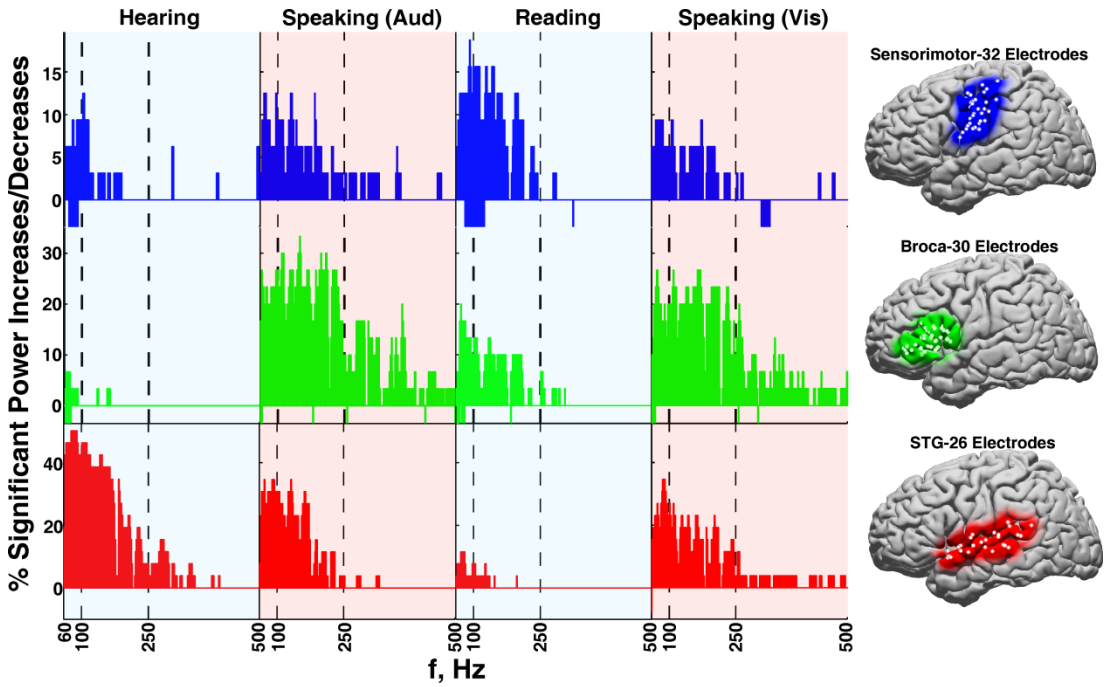

Figure 4.5 Consolidated cortical activation plot for the population of 6 subjects
Positive numbers indicate percentage of electrodes with statistically significant ($p<0.001$, FDR corrected for multiple comparisons) power increases. Negative numbers correspond to power decreases. Rows of activation plots correspond to cortical regions, columns to cognitive tasks. Markers at 60Hz, 100Hz and 250Hz are typical gamma or high-gamma analysis boundaries. All subject electrodes for each cortical region of interest are plotted on the MNI model brain for reference. Multiple peaks per plot, shifts in percentage of cortex with significant power changes across frequency bands, and changes in bandwidths with significant power changes within cortical populations are all evidence of nonuniform power modulation in high-gamma bands (60-500Hz).

The histograms in Figure 4.5 contain trends that are not monotonically decreasing. As an example, consider the histogram for speaking after auditory cue in Broca's area. Approximately 22% of the channels have significant power changes between 60-100 Hz, while 30% of the channels have significant power changes between 144-154 Hz. Both of

these bands are between 60 Hz noise harmonics. This illustrates that some channels did not have significant power increases between 60-100 Hz, but did have significant power increases in the higher band between 144-154 Hz. This example is in clear contrast to the uniform power change hypothesis which predicts monotonic decreases in the histograms as frequency increases.

Additionally, there are three trends in the consolidated cortical activation plots in Figure 4.5 that support the hypothesis that high-gamma power change occurs nonuniformly across a wide range of frequencies. First, many single activation plots exhibit multiple peaks (e.g., sensorimotor cortex while Speaking after Auditory Cue, Broca's area while Speaking after Visual Cue, STG while Speaking after Auditory Cue). These peaks indicate the presence of statistically significant power changes in different frequency bands during the same cognitive task and within the same cortical region across the population of subjects. Second, within cortical regions (single rows in Figure 4.5), cognitive tasks have either distinct active bandwidths or shifts in frequency band representations within similar active bandwidths. As an example, within Broca's area, Reading is distinguished from the other three tasks by active frequency range (60-300Hz vs. 60-500Hz). In contrast, Hearing and Speaking after Visual Cue have similar active bandwidths (60-500Hz), but are separable by the different proportions of cortex engaged across the range of active frequencies. For example, during Speaking after the Auditory Cue, there are peaks in the histograms around 112, 150, 200, 286, 380 and 450Hz, while during Speaking after the Visual Cue, the peaks in the histograms appear at 70, 110, 170, 290 and 338Hz. This second trend explicitly shows that the cortical region activates at different frequencies in a behavior-dependent manner. If power change occurred uniformly, and the only variable within these plots was the number of electrodes within the population that were active, all histograms would be

flat with differing heights according to the percentage of electrodes with significant power change. The third trend is that for any given cognitive task, there is variation in the active bandwidths between the three cortical regions. In other words, there does not appear to be a unified activation bandwidth across cortical regions for a specific cognitive task. As a quantitative measure of the differences identified by the second and third trends, we evaluated the statistical significance of the differences in bar plot shape using two-sample Kolmogorov-Smirnoff tests (see Table A.1 for detailed results). Overall, these tests indicate that 83% of cortical activation plot comparisons (55/66 comparisons) are statistically distinct ($p<0.05$). These three trends were also present in individual subjects. Figure A.5 shows cortical activation plots for a single subject exemplar that illustrates these same three trends.

4.5 Dissociation Band Summary

This study demonstrates in a population of six subjects, that ECoG surface cortical potentials have nonuniform induced power changes in high-gamma sub-bands. Dissociation bands showed that sub-band power modulations were independent enough to dissociate cognitive tasks and anatomic locations. Moreover, when power modulations were summated across subjects there were persistent behaviorally and anatomically dependent trends. Neither the dissociation bands nor the peaks in the cortical activation plots can be caused by uniform power increases.

4.6 References

Church, J. A., R. S. Coalson, H. M. Lugar, S. E. Petersen and B. L. Schlaggar (2008). "A developmental fmri study of reading and repetition reveals changes in phonological and visual mechanisms over age." Cereb. Cortex **18**(9): 2054-2065.

Crone, N., D. Boatman, B. Gordon and L. Hao (2001). "Induced electrocorticographic gamma activity during auditory perception." Clinical Neurophysiology **112**(4): 565-582.

Edwards, E., M. Soltani, L. Y. Deouell, M. S. Berger and R. T. Knight (2005). "High gamma activity in response to deviant auditory stimuli recorded directly from human cortex." J Neurophysiol **94**(6): 4269-4280.

5 Spatio-Temporal Dynamics of High Frequency ECoG

In the previous chapter, we showed that there is sufficient diversity in frequencies above 60Hz to discriminate between two different cognitive tasks or anatomic locations. We next set out to determine whether the specific spatio-temporal dynamics of these frequency bands contain signals correlated with the phonemic content of either hearing or speaking single words. We begin with a data driven analysis to determine whether band-specific power modulations in ECoG signals contain sufficient information to discern phonemes within single cognitive tasks. Then, we study the separability of the matched filter representations of phonemes within cognitive tasks. Afterward the diversity of information content in the spatial, temporal and spectral domains is quantified using the matched filter construct.

5.1 Behavioral Data

Each of the ten subjects performed the auditory single-word repetition paradigm. The mean voice onset time (VOT) across subjects was 1,212 ms (SD=468 ms). These statistics are on the same order of magnitude as those from studies using similar tasks (Church, Coalson et al. 2008) and indicate that the subjects did not have difficulty performing the experiment.

5.2 Data Driven Analysis

To determine whether there was sufficient information content in the ECoG signals to distinguish phonemes during a single cognitive task, we first attempted to discriminate phonemes using data driven classification techniques. Various dimensionality reduction

techniques and classification algorithms were applied in an attempt to extract the maximum amount of information from the ECoG signal. Phonemes were classified within a single cognitive activity (hearing or speaking) and phonemic category (vowels or consonants). Specifically, within the category, words were classified into either one of four vowel classes or one of nine consonant classes. The specific classes are identified in Table 3.1 and Table 3.2. Since all phonemes were equally probable, chance classification levels were 25% for the vowels and 11.1% for consonants. Four classification algorithms were used including: linear discriminant analysis, a Naïve Bayes classifier, Random Forests and Support Vector Machines. Because of variability in each subjects' cortical anatomic organization, spectral features and temporal rate of articulation, a variety of parameters were sampled within each classification approach to find the best possible prediction performance on 20% of the training data set aside for validation. Overall the algorithm that yielded the best results consistently across the subject population was the Naïve Bayes classifier. Figure B.1 shows the results for individual subjects by classification algorithm, cognitive task and phonemic category.

The summary data below comes from the Naïve Bayes classifier only. Only p-values below the thresholded for statistical significance ($p < 0.05$) were consolidated. Regardless of the accuracies, subjects with p-values greater than 0.05 were dropped from the results. Figure 5.1 summarizes the data driven classification results by negative log probabilities and classification accuracies. Figure 5.1A shows that the range of significant p-values spans several orders of magnitude; however, the p-value confounds both the accuracy and the number of trials. The statistics in Figure 5.1B show the range and median accuracies for the subjects with significant p-values. These results indicate that there is a significant

amount of information in the ECoG signal to related to the identity of spoken phonemes in 5-6 subjects and heard phonemes in 2 subjects.

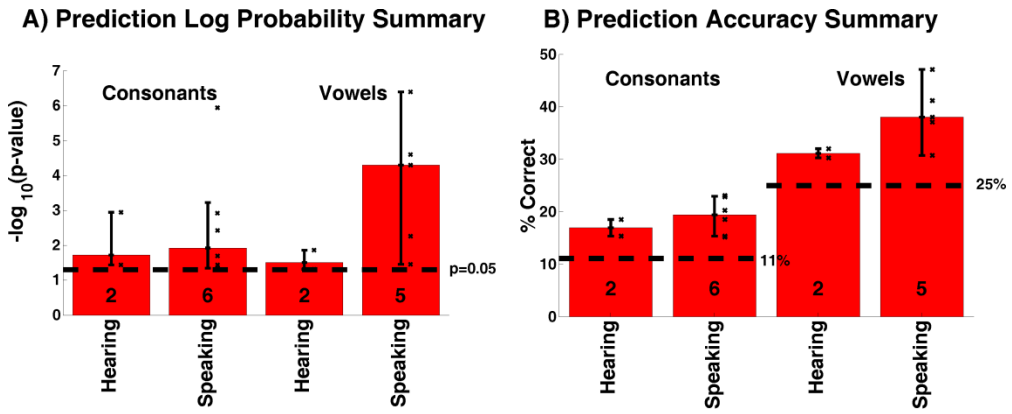

Figure 5.1 Summary of phoneme classification
Bars plotting the median prediction log probabilities and accuracies for those subjects with performance above chance. Error bars illustrate the 95% confidence intervals on the median generated by 100 bootstraps. Digits in each bar indicate the number of subjects (out of 10) that were above chance ($p<0.05$). Individual data points are plotted as a scatter plot with 'x' marks. A) Bars indicate the median negative log probabilities for subjects with p-values < 0.05 for each cognitive task and phonemic category (consonants / vowels). The dashed line shows the threshold at $-\log_{10}(0.05)$. B) Bars show the median accuracy for subjects with p-values < 0.05 for each cognitive activity and phonemic category. Chance accuracies are shown by the dotted lines for each phonemic category. These results show that when using a data driven classification approach, there is sufficient information in the power modulation dynamics of ECoG signals to predict phonemic content within a specific cognitive task above chance.

Exemplar confusion matrices from the best subject for each combination of cognitive task and phonemic category in Figure 5.2 illustrate the distribution of classification accuracies by phoneme.

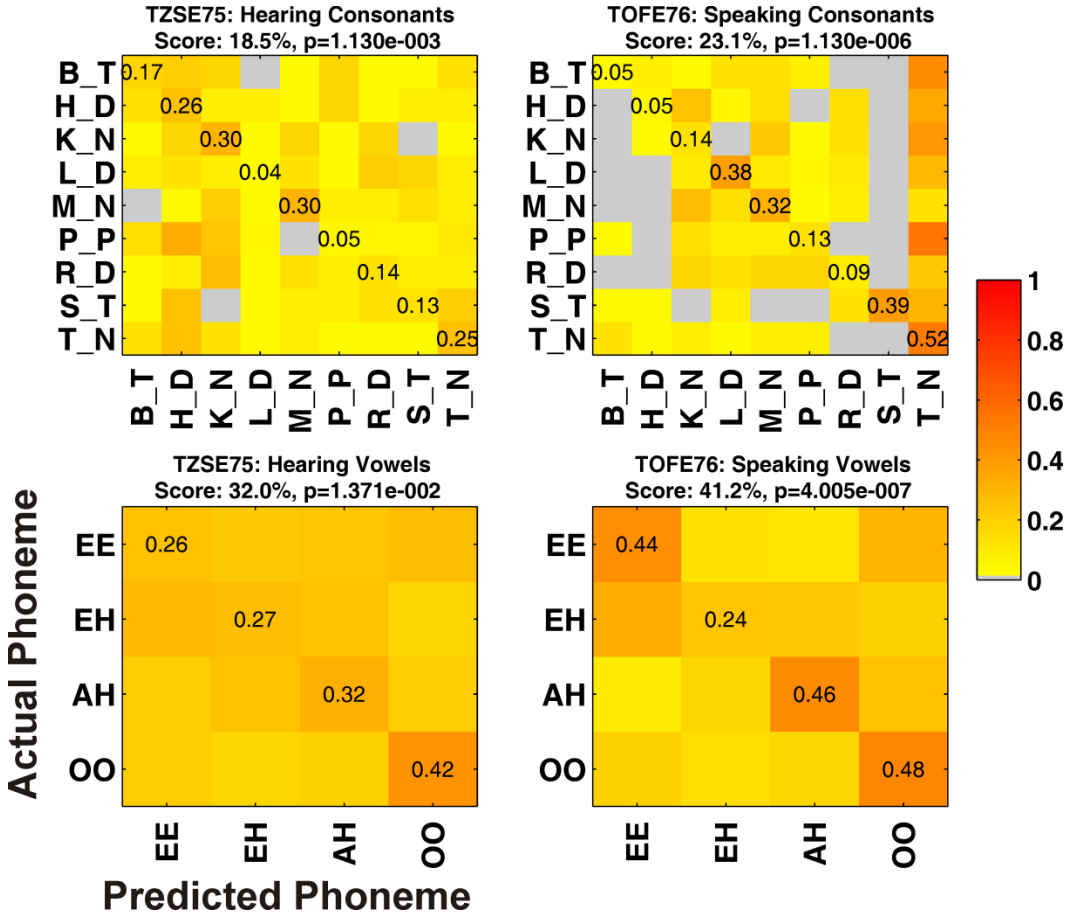

Figure 5.2 Exemplar confusion matrices by cognitive task and phonemic category
These confusion matrices show the distribution of predicted versus actual phoneme labels. ECoG from each of these subjects contained enough information to predict several phonemes from each category above chance levels (11.1% for consonants, 25% for vowels). Each exemplar indicates the accuracy over all crossfolds and the associated p-value.

While these results are not perfect, there are factors that may explain some of the misclassifications. First, the brain is a stochastic system. Neural responses to the auditory stimuli are modulated by changes in attentiveness and alertness (Woldorff, Gallen et al. 1993; Jäncke, Mirzazade et al. 1999), and adaptation that takes place over time (Ulanovsky, Las et al. 2004). Second there is a significant amount of variability in the stimuli. Since each word belongs to both a vowel and consonant category, there are nine different consonant pair variants within each vowel class, and four different vowel variants within each consonant class. It is possible that the overlap and variation within each phoneme

class obscures some of differences that would enable higher prediction scores. Third, there is variation in the cortical areas covered by ECoG electrodes for each subject. Since there are specific areas of the cortex associated with receptive and productive speech, coverage of these areas (or lack thereof) will impact the amount of information captured by the ECoG recordings. Fourth, the ECoG signals are non-stationary in nature. Changes in the ECoG signal characteristics may occur between runs (several minutes up to 24 hours depending on the subject) which form the boundaries for dividing the data into crossfolds. These differences are not accounted for by the classifier and will decrease accuracy. Finally, there are several behavioral variables that are not controlled in this task and that may affect the neural representation. These include the volume of speech, rate of speech, and specific formant frequencies. In spite of these factors, the results remain above chance for several subjects and therefore provide a basis for analyzing the diversity of information content in ECoG signals.

5.3 Matched Filter Receiver Operating Characteristic

Based on the knowledge that the ECoG signals contained evidence of a neural motif correlated with phonemic content, we set out to capture as much diversity in power modulation as possible in a construct that would allow quantification of the amount of information content in each dimension. We chose the matched filter since it provides a straightforward way to modulate the information contributions in each dimension of the ECoG signal separately. As discussed in the methods, the matched filter is a template of the average ECoG signal correlated with a specific phoneme and cognitive task. In order for the matched filter to effectively decode phonemes, it is essential that the

representations for each phoneme are separable. We measure this separability by taking pairwise dot products between matched filters for individual phonemes as shown in Figure 5.3. High dot product scores indicate a high degree of commonality between two matched filters, similar in concept to a correlation. Low dot products indicate that the two matched filters are dissimilar. The mean normalized scores for each pairwise dot product across all 10 subjects provide a generalized measure of the specificity of the matched filters to individual phonemes. The hot colors that span the diagonal in contrast to the cooler surrounding colors indicate that there is a high specificity in the matched filter responses. These dot product matrices reveal that on average, over this subject population, the matched filter representations are sufficiently different to distinguish individual phonemes within each category and cognitive task.

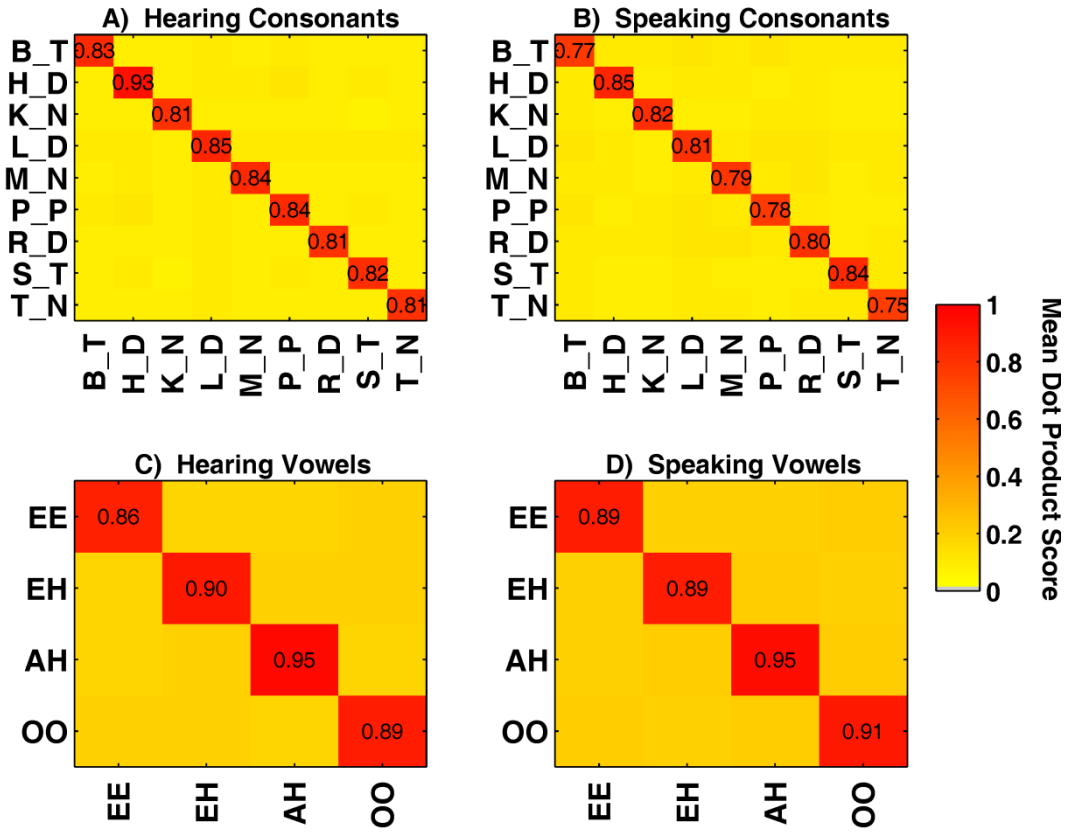

Figure 5.3 Summary matched filter reference waveform dot product matrices
The dot products between matched filters representing different phonemes within specific cognitive tasks and phonemic categories reveal specificity in the neural motifs. For each subject, task and category, matched filters from the training data were created for each phoneme. Pairwise dot products between matched filters for all phonemes were normalized by dividing by the greatest dot product score within a cognitive task and phonemic category. Each panel shows the average normalized dot product score across 10 subjects for each cognitive task and phonemic category.

Having established that individual matched filters within a specific cognitive task and phonemic category are sufficiently distinct to separate phonemes, we next illustrate that matched filters can predict the exact phoneme and task within the context of the entire training and testing data sets which contain all cognitive tasks (rest, hearing and speaking) and phonemes within a category. We evaluated the information content in the individual matched filters, using a Receiver Operating Characteristic (ROC) curve analysis which determined the sensitivity and specificity of the matched filter. Figure 5.4 shows exemplar data from the ROC curve analysis for a single subject, cognitive task and phoneme. As described in the methods section, each subject's data is divided into training and testing sets separately for each crossfold. The matched filter for a specific cognitive task and phoneme in the training set is generated for a given crossfold. The sliding correlation of the matched filter with the ECoG yields a score for each time sample. Figure 5.4A shows the normalized matched filter score and the label from the training data. There is a clear correlation between the two traces which results in the ROC curve shown in Figure 5.4B. The curve is above the dashed line across the diagonal, indicating better than chance performance. The total area under the curve (AUC) is indicated in the legend at 90.3%. Figure 5.4 C and D parallel A and B in format, but are computed using the matched filter constructed from the training data to score the testing data. The AUC statistic for the testing data is comparable to the training data (89.2%), indicating that the matched filter for this task has a reasonable amount of specificity for this particular cognitive task and

phoneme on both the training and testing datasets. These analyses indicate that the matched filter construct is a valid way to quantitatively evaluate the extent of diversity within the ECoG neural motifs for specific phonemes.

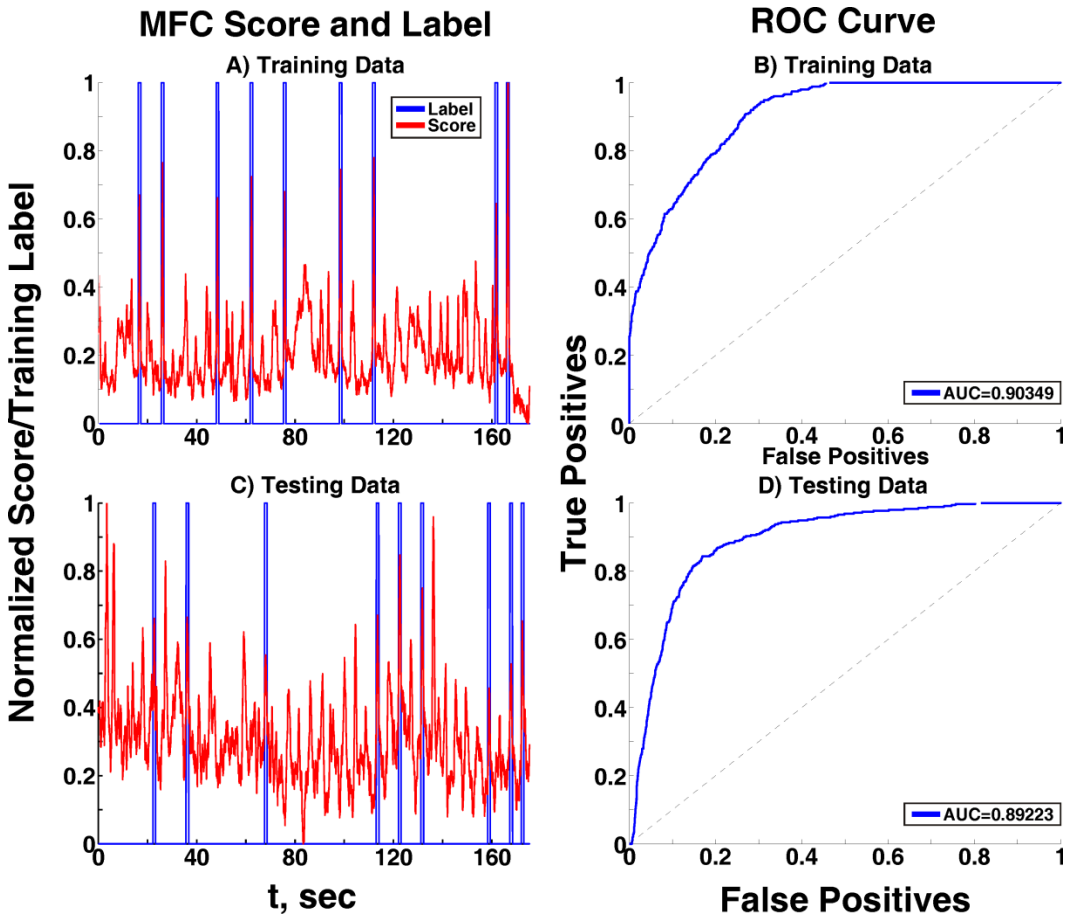

Figure 5.4 Exemplar receiver operating curve analysis
Exemplar data illustrates that the matched filter for saying the vowel 'EE' has above chance accuracies both the training and testing data. This subject performed the experiment twice; therefore one run was used for training and the other for testing. A) The time course of training scores (**red**) and labels (**blue**) demonstrates the matched filter can localize instances of saying EE phonemes in the midst of hearing and saying all different phonemes. B) ROC for saying EE phonemes on the training data set has an AUC of 90.3%, (above the chance level of 50%). C) Time course of testing scores (**red**) and labels (**blue**) shows that the matched filter continues to localize saying EE phonemes well even on the test data. D) ROC for saying EE words on the testing data has an AUC of 89.2%.

It is clear from the score traces in Figure 5.4 that there is a rhythmic component in the signal. There are two putative sources to this rhythm. First, there is a regular structure to the two cognitive tasks (hearing and speaking) in this experiment. Therefore, it is possible

that the matched filters are only discriminating cognitive tasks, but not phonemic content. Second, because the ITI during these experiments was constant, we propose that there was a temporal expectation in the ECoG therefore the subject associated with preparatory attention (Gómez, Marco-Pallarés et al. 2006). To determine whether the matched filter reference waveforms were capable of discriminating specific phonemic content during a single cognitive task, we performed a classification experiment similar in structure to the data driven analysis. First, the reference waveforms for all phonemes during a specific cognitive task were computed on the training data. Then the downsampled, z-scored PSD estimates from the test data during the temporal window corresponding to the cognitive task under studied were scored. We used a single trial out crossfold validation approach to account for inter-run nonstationarities, so the test data came from one trial at a time. The test data was classified using the phoneme reference waveform with the largest matched filter score. While there are differences from the data driven classification results, these show that the matched filter construct is capable of discriminating phonemes above chance levels in several of the subjects.

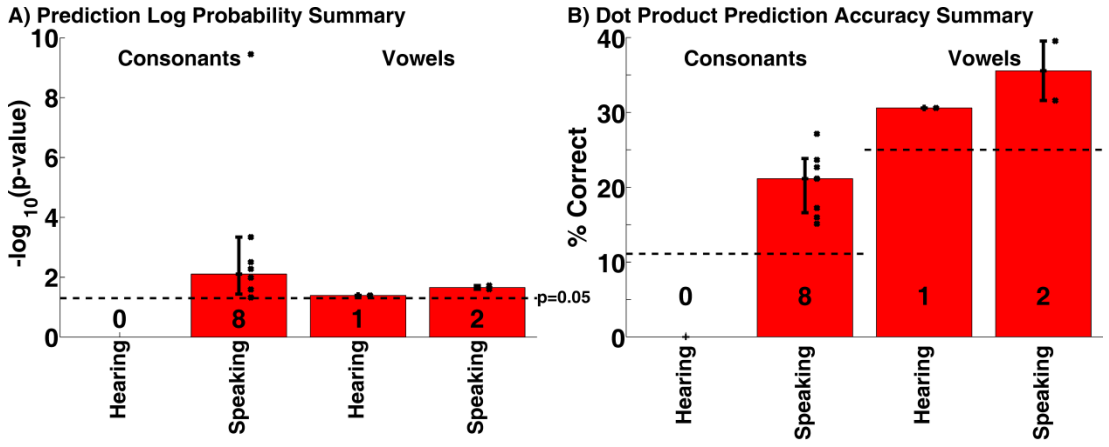

Figure 5.5 Single trial matched filter classification summary
Results from classification using only matched filter scores show that the matched filters can discriminate phonemic content. Bars plot the median prediction log probabilities and accuracies for those subjects with performance above chance. Error bars illustrate the 95% confidence intervals on the median generated by

100 bootstraps. Digits in each bar indicate the number of subjects (out of 10) that were above chance ($p<0.05$). Individual data points are plotted as a scatter plot with 'x' marks. A) Bars indicate the median negative log probabilities for subjects with p-values < 0.05 for each cognitive task and phonemic category (consonants / vowels). The dashed line shows the threshold at $-\log_{10}(0.05)$. B) Bars show the median accuracy for subjects with p-values < 0.05 for each cognitive activity and phonemic category. Chance accuracies are shown by the dotted lines for each phonemic category. These results show that the neural motif captured by the matched filter can discern phonemic content within a single cognitive task.

5.4 Analysis of Variance

The full ANOVA on the matched filter AUC scores provides insight into the specific factors of the matched filter analysis that affected the scores most. Table 5.1 contains the results. All single factors were significant ($p<5e-5$), with the notable exception of the variants affecting diversity in the frequency bands below 60 Hz. The greatest single factor in affecting the matched filter scores was the specific subject; however, the sum of squares for error had a magnitude nearly three times greater than that for the subject factor. The large error term indicates that there are significant variations in crossfolds (which represent repeated measurements), and other factors not accounted for by the model. Collectively the two single *behavioral* factors (Task and Phoneme) accounted for a significant portion of the variance, as did the interactions between subject and behavioral factors. This indicates that subject had preferential AUC score levels for specific cognitive tasks and phonemes. The single *diversity* factors (Channel, Time, <60 Hz, >60 Hz) with the largest impact on the model were time and channel, consistent with previous findings of spatial and temporal diversity. While the single factor representing diversity in the frequency bands above 60 Hz was significant, it is notable that the paired interactions between high frequency diversity and subject, and high frequencies and channel accounted for more variance than high frequency diversity as a single factor. These results seem to indicate that there is both subject and anatomic specificity affecting high frequency spectral diversity. Based on the results of the dissociation band analysis in the previous chapter, this is likely because some

subjects in this portion of the study did not have significant power modulations in the high frequency bands. Each of the diversity factors was examined more closely on an individual basis using additional analyses.

Table 5.1 Analysis of variance results
Abbreviations: <60: frequency bands below 60 Hz, >60: frequency bands above 60 Hz

	Source	Sum Squares	Degrees of Freedom	Mean Squared Error	F Statistic	Prob>F
Single Factors	Subject	222.8322	9	24.7591	2988.9028	0
	Task	4.2945	1	4.2945	518.4284	2.2895e-114
	Phoneme	19.4416	12	1.6201	195.581	0
	Channel	9.3817	2	4.6909	566.2777	8.2945e-245
	Time	14.642	2	7.321	883.7864	0
	# <60	0.00029677	1	0.00029677	0.035826	0.84988
	# >60	1.9546	1	1.9546	235.9547	3.6176e-053
Interactions	Subject*<60	30.6676	18	1.7038	205.6758	0
	Subject*>60	23.6244	18	1.3125	158.4398	0
	Subject*Task	39.5704	9	4.3967	530.7674	0
	Subject*Phoneme	54.881	108	0.50816	61.3444	0
	Subject*Time	9.4528	18	0.52515	63.3962	3.0414e-229
	Subject*Channel	11.0123	18	0.61179	73.8551	6.1741e-269
	# <60*>60	3.4456	3	1.1485	138.6496	1.3813e-089
	<60*Task	1.0109	2	0.50547	61.0201	3.3187e-027
	<60*Phoneme	0.79468	24	0.033112	3.9972	1.4979e-010
	<60*Time	3.5993	4	0.89982	108.6254	1.818e-092
	<60*Channel	0.57437	4	0.14359	17.3344	3.1802e-014
	>60*Task	0.35294	2	0.17647	21.3034	5.6324e-010
	>60*Phoneme	2.0839	24	0.08683	10.4821	9.6193e-040
	>60*Time	1.7537	4	0.43843	52.9264	1.3227e-044
	>60*Channel	16.0329	4	4.0082	483.8694	0
	Task*Phoneme	2.6454	12	0.22045	26.6121	5.5577e-061
	Task*Time	6.5477	2	3.2739	395.2174	1.833e-171
	Task*Channel	0.56444	2	0.28222	34.0696	1.6238e-015
	Phoneme*Time	0.74777	24	0.031157	3.7613	1.3209e-009
	Phoneme*Channel	2.8374	24	0.11823	14.2722	5.8482e-058
	Time*Channel	0.79144	4	0.19786	23.8854	9.0019e-020
	Error	617.3087	74521	0.0082837		
	Total	1205.5619	74879			

5.5 Spatial Diversity

Because of the importance of showing results anatomically, in this section only the set of subjects that had left speech lateralization and left hemisphere grids are studied. Figure 5.6 contains exemplar time-frequency plots from matched filters showing two different spatial locations and two different phonemes. This exemplar illustrates that several anatomic areas with distinct spectral and temporal responses have statistically significant activity for single phonemes. The locations of the two electrodes of interest are indicated by the red and green stars overlaid on this subject's gyral anatomy. Each phoneme has several time-frequency tuples (pair of specific time sample and frequency band) that are statistically distinct across the training data set between the two electrodes. To simplify the figure, selected statistically different tuples are highlighted by the contours overlaid on the plots.

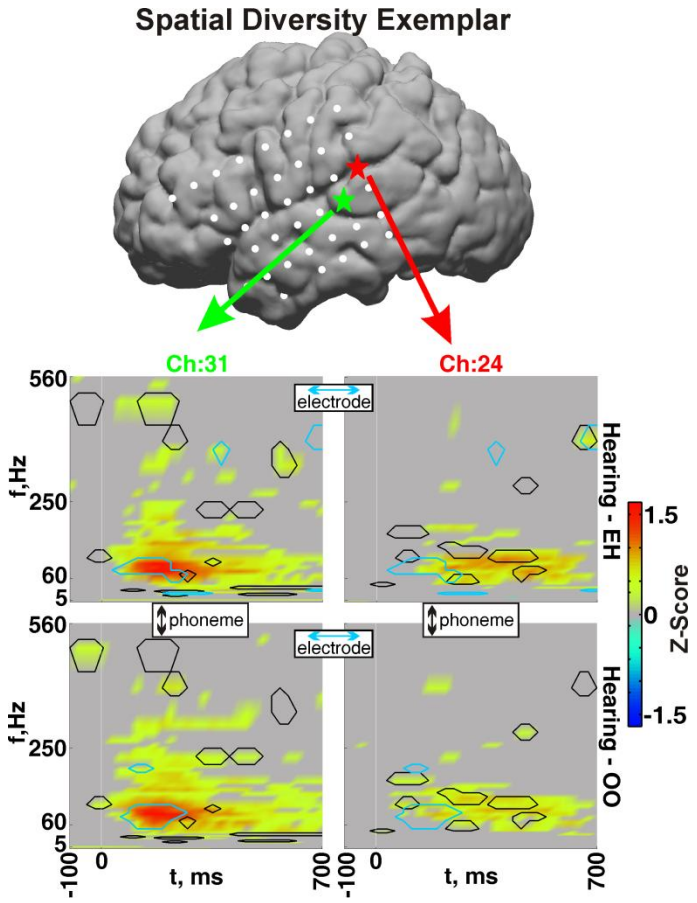

Figure 5.6 Exemplar matched filter comparison showing spatial diversity
Four individual time-frequency plots from two different matched filters in a single subject. Heat maps indicate the z-score of power modulation over the first cross fold ($p<0.015$ after FDR correction). There were 52 trials of EH words and 53 trials of OO words in the training data. Electrodes 24 and 31 both show significant yet distinct patterns of temporal and spectral power change for these two phonemes. Contours overlaid on the time-frequency plots highlight selected regions of the plots that are statistically distinct, blue contours contrast differences between anatomic locations ($p<0.0011$ after FDR correction). Black contours contrast difference between phonemes at the same anatomic location ($p<0.05$). These differences are used to classify and predict whether the subject said an EH word or an OO word.

The first analysis of diversity focuses on the three matched filter variants that contrasted differing levels of spatial diversity. The three reference waveform variants included the single best channel, the optimal number of channels based on the training data and the whole macrogrid array. The best and optimal channel variants were selected for each cognitive task, phoneme and crossfold in the subset of subjects with left hemisphere grids and left lateralized speech. The results of the ANOVA contrasting these three variants are contained in Table 5.2. While all of the single factors were significant, it was notable that

the channel factor (representing the spatial variants) accounted for the least amount of variance in the model. The only nonsignificant paired interaction was between cognitive activity and channel. It was interesting that the paired interactions for subject and channel and phoneme and channel also accounted for significant amounts of variance in the model. These results require further analyses.

Table 5.2 ANOVA for spatial variants only

	Source	Sum Squares	Degrees of Freedom	Mean Squared Error	F Statistic	Prob>F
Single Factors	Subject	21.497	5	4.2994	569.9575	0
	Task	2.0079	1	2.0079	266.1848	2.3972e-058
	Phoneme	1.6697	12	0.13915	18.4461	1.0821e-039
	Channel	0.86615	2	0.43308	57.4116	2.2268e-025
Interactions	Subject*Task	1.5378	5	0.30756	40.7728	3.0012e-041
	Subject*Phoneme	6.3754	60	0.10626	14.0861	5.575e-127
	Subject*Channel	1.8809	10	0.18809	24.9343	1.2398e-046
	Task*Phoneme	0.4675	12	0.038958	5.1646	1.1245e-008
	Task*Channel	0.033084	2	0.016542	2.1929	0.1117
	Phoneme*Channel	0.66619	24	0.027758	3.6798	3.4031e-009
	Error	37.8224	5014	0.0075434		
	Total	74.3189	5147			

Several different analyses were carried out to contrast AUC score performance for matched filter variants with different amounts of spatial information. Figure 5.7 summarizes the results of the spatial diversity analysis. All data for this figure came from the set of subjects with left lateralized speech organization and left-hemisphere grids. Figure 5.7A contains the results of the nonparametric Kruskal-Wallis test comparing the AUC scores from this set of subjects across all cognitive tasks and phonemes. The contrasted populations were generated from matched filters that either used the single electrode with the highest classification score (***Best Location***), the set of electrodes with the best overall classification score (***Optimal Area***), or all possible electrodes (***Whole Grid***). The inset to panel A shows that the optimal set of electrodes has a statistically higher ($p<0.05$) median AUC score than the other two variants. This means that the optimal set of electrodes has more

information than either the single best electrode or the whole grid. This trend is clarified in Figure 5.7B. Here the two plots show the median AUC score across subjects and phonemes for each cognitive task, as single electrodes are added to the matched filter in order of decreasing correlation with the training label. It is clear from these two plots that there is a point in these curves showing that in these subjects there is a set of electrodes that maximizes the AUC score. It appears that on average, approximately 18-24 cm^2 of cortex is optimal for predicting phonemes which are heard, while approximately 9-12 cm^2 of cortex is the optimal amount of cortex for predicting spoken phonemes[2] (Bullock, McClune et al. 1995). While it may seem counter-intuitive that adding information to the matched filter would decrease performance, it is important to remember that the brain is carrying on a variety of functions within the context of these experiments, and it is likely that there is activity on some electrodes that is uncorrelated with the phonemic content. The uncorrelated activity in these electrodes is likely causing the decrease in AUC score beyond the optimal set of electrodes.

In order to quantify the spatial extent of the information encoding in the ECoG signal, we present two additional analyses. First we contrast the AUC scores in the optimal set of electrodes with AUC scores generated by using a subtractive approach. In the subtraction analysis, we contrast AUC scores from two different variants. First, we show scores generated using the optimal set of electrode after removing the best single electrode (O***ptimal Minus 1 Best***). Second, we show scores generated using the whole grid after removing the optimal set of electrodes (***Whole Minus Optimal***). The results are shown

---

[2] These areas are based on findings from Bullock, et al. that correlation in ECoG signals falls to 0.2 at 2 cm and 0 at 3 cm, and therefore assume that individual electrodes capture significant electrophysiological activity from a 1 cm radius or less, approximately 3 cm^2 of cortex.

in Panel C. These scores are the summation across six subjects. While there is a drop in the interquartile range and median scores for the ***Optimal Minus 1 Best*** scores, they are still above the chance line. This indicates that there is a statistically significant amount of information encoded in the optimal set of electrodes even after excluding the single best electrode and that the electrophysiological activity in the surrounding areas is still highly correlated with the specific phoneme either spoken or heard. In contrast, when the whole clinical grid is used without the optimal set of electrodes the interquartile range falls below the chance level. These results reveal that phonemic information is diffusely represented within the optimal set of electrodes and that no single electrode dominates the phonemic representation in the matched filter. However, phonemic information is specifically confined to the areas within this optimal set, as the result of the whole grid minus the optimal set represents a quantitatively larger set of electrodes (44-60), which does not have predictive AUC scores above chance.

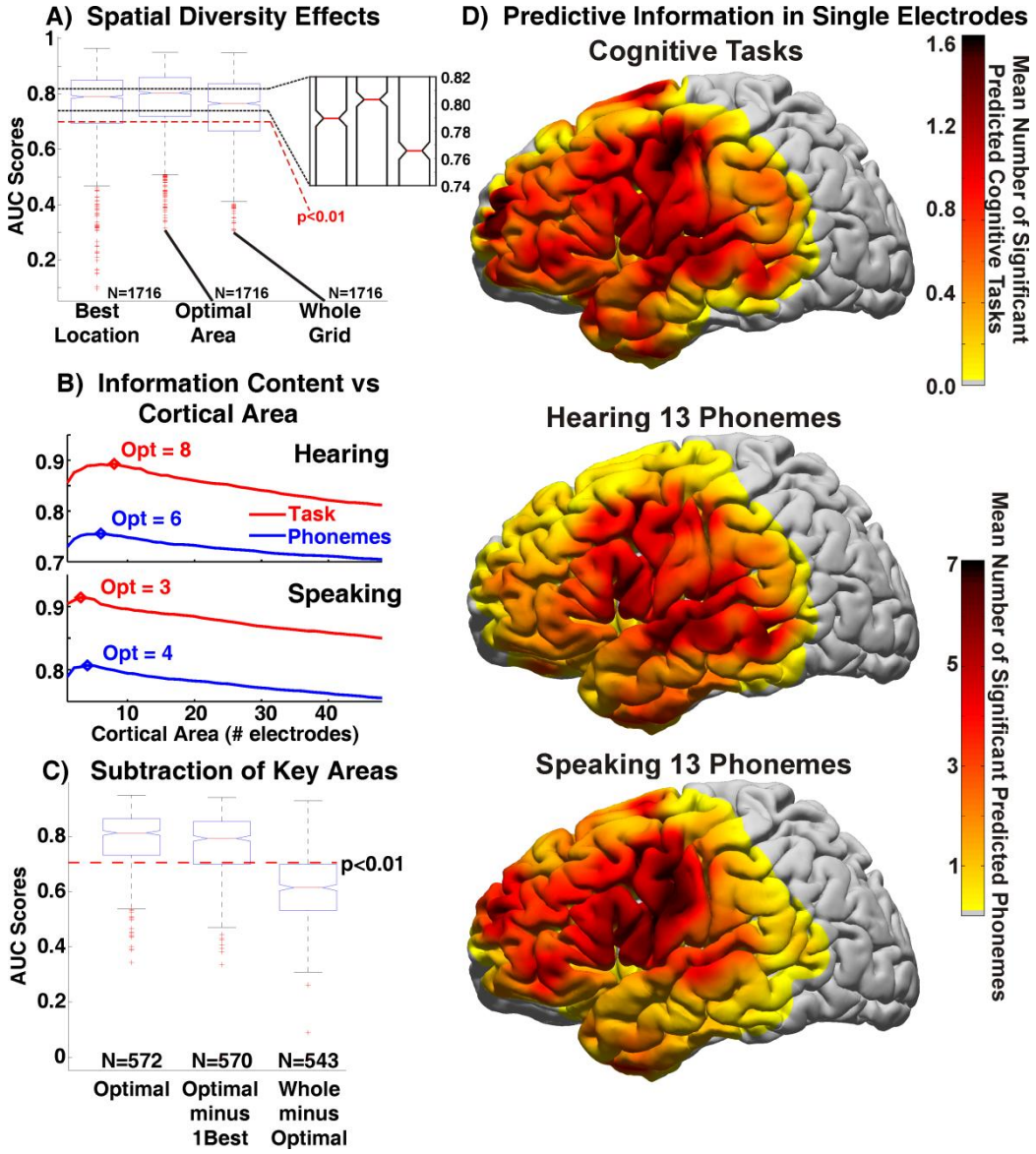

Figure 5.7 Spatial diversity summary

Summary of spatial diversity in neural motifs shown in four different analyses. A) The results of nonparametric ANOVA tests (Kruskal-Wallis) showing the range of the data (whiskers), interquartile range (boxes), median (red line) and 95% confidence intervals on the median (notches around red line) for six subjects and all cognitive tasks, phonemes and crossfolds on the test data. The three different data series contrast the AUC scores for the matched filters which used only the ***Best Location***, the ***Optimal*** cortical area or the ***Whole*** clinical ECoG grid. All three populations were above the $p<0.01$ line for chance based on the Monte Carlo simulations. The inset shows that the 95% confidence intervals on the medians were nonoverlapping between these populations and that the optimal cortical area had a significantly higher median AUC score. B). Analysis of the information content in the matched filter as a function of cortical area included. Curves are plotted for matched filters predicting cognitive tasks in general (***Task***) as well as specific phonemes within a specific cognitive task (***Phonemes***). When added in decreasing order of correlation (best electrode first), the mean AUC scores for both the hearing and speaking tasks increase up to a certain point. For both sets there is an optimal cortical area for predicting phonemic content using the matched filter approach that appears to be approximately 18-24 cm^2 for hearing and 9-12 cm^2 for speaking (see text for discussion). C) The subtraction analysis contrasts the AUC scores from the ***Optimal*** set of

electrodes with scores from the ***Optimal Minus 1 Best*** electrode removed, and the ***Whole*** grid ***Minus Optimal*** set removed. These figures show that information is represented in a spatially diffuse manner within the ***Optimal*** set of electrodes, but that outside the ***Optimal*** set, prediction performance is not significantly above chance. D) The results of the single electrode analyses show the anatomic distribution of phonemic information. The heat map shows the average number of cognitive tasks (out of 2) or phonemes (out of 13), that single electrodes could predict above chance, averaged across six subjects. Areas predicting the greatest number of cognitive tasks are located in perisylvian cortex, motor cortex, supplemental motor area and prefrontal areas. Areas predicting up to 7 different phonemes were located in typical speech areas yet show distinct representations between hearing and speaking phonemes.

Figure 5.7D reveals the anatomic extent of information encoding using a single electrode analysis. The data for these plots used matched filters with single electrodes only. For every each location in the grid, single electrode AUC scores for each cognitive task in general and then for hearing and saying individual phonemes were generated. The number of cognitive tasks and phonemes with average AUC scores above chance ($p<0.05$, Monte Carlo shuffling simulation) over all crossfolds were counted, and then summed across subjects by anatomic location. Since the anatomic coverage varied by subject, these plots are normalized by dividing by the number of electrodes covering each location. The heat maps plotted on the MNI model brain reveal a broad cortical region that can predict several cognitive tasks or phonemes. While most of these are located in perisylvian and motor areas, the areas are cortically diffuse. Areas predicting the greatest number of general cognitive tasks (hearing or speaking) are located in perisylvian cortex, motor cortex, supplemental motor area and prefrontal cortex. These subjectively show that even in subjects with normal speech organization, phonemic information is encoded in a spatially diffuse manner. Although there is variation between subjects in the cortical organization of speech (Ojemann, Ojemann et al. 1989), Figures B.2-B.4 showing the results of this analysis on individual subjects reveal the same trends of diffuse representation across the set of phonemes. The areas implicated in saying or hearing individual phonemes are typical compared with those implicated by functional imaging studies (Petersen, Fox et al. 1989; Binder, Frost et al. 1997; Church, Coalson et al. 2008).

Collectively, the spatial diversity analyses of the neural motifs in ECoG reveal three notable findings. First, there is an optimal cortical area of approximately 9-24 cm^2 that appears to encode predictive information regarding phonemic content depending on the specific cognitive task. Second, within this optimal cortical area, there is a diffuse representation of that phonemic information. Finally, the anatomic locations which encode the highest amounts of phonemic information are consistent with those from functional imaging studies and implicate a relatively large cortical area including perisylvian cortex, middle and superior temporal gyrus, motor cortex, supplemental motor area and prefrontal areas.

5.6 Temporal Diversity

Time is the second dimension we analyze to study diversity in neural motifs encoding phonemic information. The exemplar in Figure 5.8 identifies the cortical location of a single electrode with significant activity across several phonemes. The figure shows the time-frequency plot from the matched filter for a single channel and phoneme of interest. There is significant activity in several time samples and frequency bands; however, the blue rectangle highlights the band of interest at 150 Hz. Within this single anatomic location and frequency of interest, the time courses of power modulation for different phonemes exhibit distinct patterns. This exemplar represents the type of diversity we sought to quantify with the following analyses.

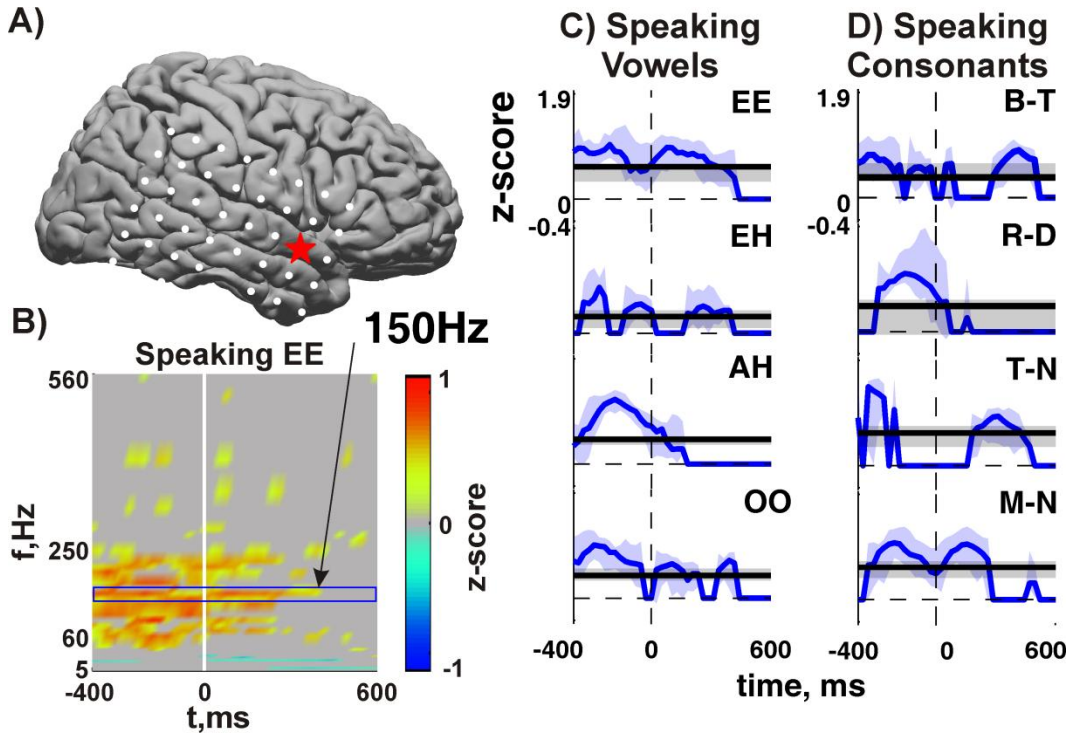

Figure 5.8 Temporal diversity exemplar
A) The anatomic location of the ECoG electrodes on the MNI model brain as determined using the Get Location on Cortex Method (see Methods). The red star represents the approximate location of the electrode of interest. B) The exemplar matched filter for this electrode of interest shows significant (Wilcoxon sign-rank test, $p<0.010237$, after FDR correction) power modulation in several time-frequency tuples. The blue box highlights the frequency of interest, 150 Hz. C) and D) The individual time course plots show two traces. The blue traces plot the statistically significant (Wilcoxon sign-rank test, $p<0.05$) median power z-scores for this channel and frequency band over the training trials in the first crossfold (N = 13-18 consonants, N=35-39 vowels). The blue shaded areas indicate the 95% confidence intervals on the median (100 bootstraps with resampling). The black traces plot the median and 95% confidence intervals of the time-average 150 Hz power across trials. Note that the blue traces within the vowel and consonant categories are each distinct, while the black traces are not. These indicate that information correlated with phonemic class is encoded in the temporal pattern of power modulation.

The first analysis of diversity focuses on the three matched filter variants that contrasted differing levels of temporal diversity. The three reference waveform variants included the truncated version with the best single time sample, the smoothed version which used the temporal average and the time varying version with full temporal diversity. The best time sample was selected for each cognitive task, phoneme and crossfold for all 10 subjects. The results of the ANOVA contrasting these three variants are contained in Table 5.3. Again all of the single factors were significant. In this analysis, the time factor accounted

for more variance in the model than either cognitive task or phoneme. Additionally, the paired interactions that include time were accounted for less variance than time as a single factor. These results seem to indicate that temporal diversity is more universal in the neural motif. The following analyses help illustrate the sources and distribution of the temporal diversity in the neural motif.

Table 5.3 ANOVA for temporal variants

	Source	Sum Squares	Degrees of Freedom	Mean Squared Error	F Statistic	Prob>F
Single Factors	Subject	10.389	9	1.1543	177.3086	8.8441e-269
	Task	0.3448	1	0.3448	52.9614	4.3505e-013
	Phoneme	1.6563	12	0.13803	21.2015	2.0501e-045
	Time	1.6766	2	0.83829	128.7623	2.5565e-054
Interactions	Subject*Task	1.5272	9	0.16969	26.0649	1.1939e-043
	Subject*Phoneme	3.8769	108	0.035897	5.5139	1.0691e-060
	Subject*Time	0.81857	18	0.045476	6.9852	9.3834e-018
	Task*Phoneme	0.2274	12	0.01895	2.9108	0.00050725
	Task*Time	0.34668	2	0.17334	26.6254	3.4739e-012
	Phoneme*Time	0.12713	24	0.0052969	0.81362	0.72288
	Error	19.0232	2922	0.0065103		
	Total	39.9259	3119			

Figure 5.9 reports the results of the temporal diversity summary analyses. The box and whisker plots in Figure 5.9A reveal a statistically significant difference between the three matched filter variants which contrasted different amounts of temporal information. Across 10 subjects, two cognitive tasks and 13 phonemes, there were statistically significant differences between the three variant populations indicating that the ***Time Varying*** matched filters had the best scores. While the 95% confidence intervals on the median for each variant were all above the chance threshold, only the interquartile range for the time varying population was completely above the chance line. The difference between the ***Best 1-Sample*** population and the two other populations may be explained by an increase in the signal to noise ratio. This does not explain the difference between the ***Temporal Mean***

and ***Time Varying*** populations since both used the full complement of time-samples from the matched filter. The difference between these two populations can only be explained by the significance of the time-varying pattern in the neural motifs.

To determine whether there was an optimal number of time samples to include in the matched filter, Figure 5.9B plots the cumulative AUC score as time samples are added to the matched filter in decreasing order of correlation starting with the single best time sample. In contrast to the results in the spatial summary, any plateau in these curves occurs toward the right side of the plots indicating that the highest matched filter scores occur when nearly all the time samples are included. Only 20% or less of the time samples which have the lowest correlations result in AUC score decreases. This indicates that the majority of the time windows are well scoped to capture ECoG signals relevant to decoding phonemes and general cognitive tasks.

To gain insight on the specific time samples in the matched filter that provide the greatest information content, Figure 5.9C plots the median rank (best r^2 highest) for each specific time sample across the subject population, all phonemes and crossfolds for each cognitive task. This plot reveals two interesting trends. First, the highest ranking time samples are in line with what we intuitively expect from the auditory single word repetition paradigm. The rank of the hearing time samples increases with time. This is due to the steadily increasing post-stimulus neural activity associated with: receptive speech processes, auditory working memory and pre-articulatory processing that occur prior to voice onset (Salmelin 2007). The analysis in Figure 5.9B indicated that 20% of time samples with the lowest ranks did not improve the AUC score. In the hearing traces in panel C, the rank rises above the 20^{th} percentile at approximately 53 ms. While this is earlier than the onset

of gamma responses to auditory stimuli reported in the literature (Crone, Boatman et al. 2001; Canolty, Soltani et al. 2007), it does correlate with ERP responses to auditory stimuli (Edwards, Soltani et al. 2009). Additionally, because the temporal structure of the experiment was deterministic, it is also likely there are correlates of expectation appearing at early stages after stimulus onset (Gómez, Marco-Pallarés et al. 2006). The time samples with the highest rankings during speaking are centered on the voice onset time, with approximately equal amounts of information before and after voice onset until the end of the speaking window. The results in panel B show that only 13% of the time samples with the lowest ranks failed to improve the AUC score. In panel C, the ranks fall below the 13th percentile only beyond 560 ms after voice onset indicating that the majority of the matched filter window for speaking captures signal correlated with phonemic content.

The second notable trend is that there are only slight significant differences between the rankings for the general cognitive tasks and those for specific phonemes. The differences occur in the brief window immediately surrounding voice onset and the end of the speaking period. At voice onset, the rank of the task time samples exceeds those for phonemes even though they both have their peaks immediately preceding voice onset. This indicates that the time samples surrounding voice onset have consistently higher ranks when detecting general cognitive tasks, while the matched filters encoding different phonemes have a slightly more dispersed temporal distribution. Likewise, at the end of the speaking window, time samples for phoneme-specific matched filters have consistently higher rankings, indicating that these time samples are more important for deciphering phonemic class than for determining task identity. However, most of the time samples at the end of the speaking window are below the percentile level which improves AUC scores. The broader temporal representation for phonemes makes intuitive sense, as each

phoneme consists of sounds and motor articulatory movements that occur either in the center of the vocal response (vowels), or at both the beginning and the end of the response (consonants). Category specific rankings for consonants and vowels were compared, but there were no significant differences between rankings.

Overall, these analyses show that phonemic information is encoded both specifically and diversely in the time domain. The statistically significant difference between the matched filter variants definitively shows that temporal dynamics are a significant factor in representing the neural motifs correlated with specific phonemes. The window size and distribution analysis, however, indicate that the information is diffusely spread across temporal windows 650 - 1150 ms wide. Specifically the optimal hearing window seems to span the time from 50 – 700 ms post-stimulus and the optimal speaking window is 400 ms before through 560 ms after voice onset.

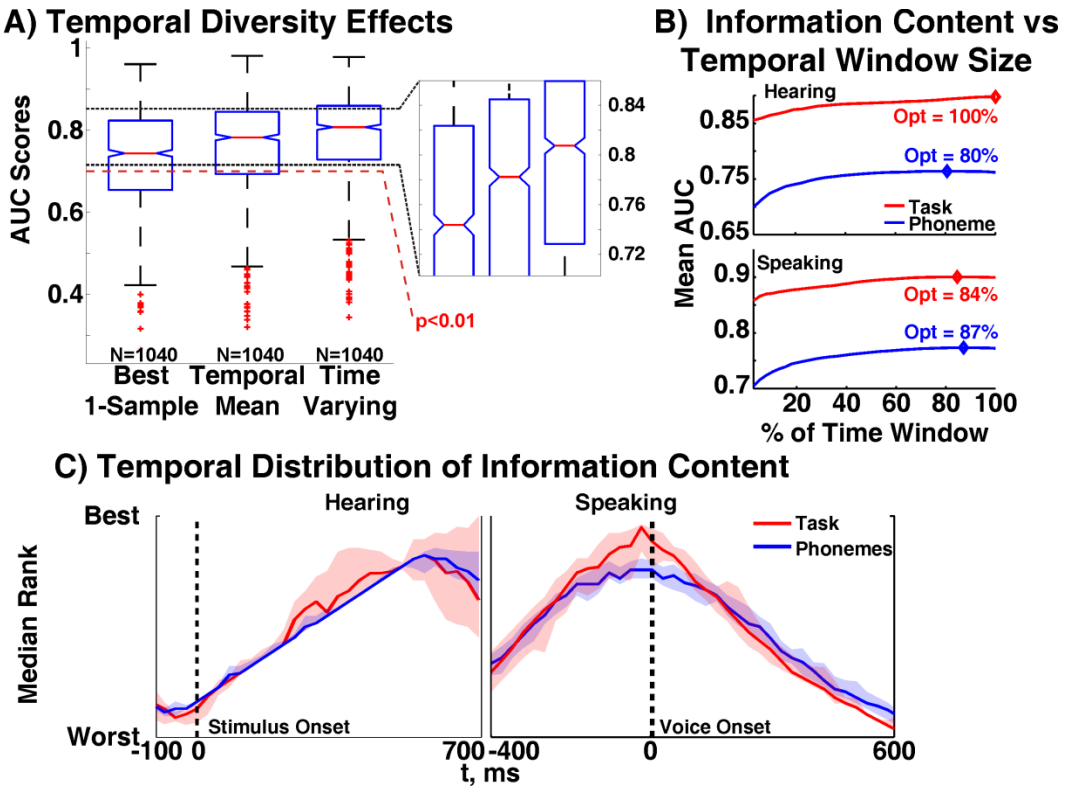

Figure 5.9 Temporal diversity summary
Results of analyses defining the temporal diversity in ECoG signals. A) The results of nonparametric ANOVA tests (Kruskal-Wallis) showing the range of the data (whiskers), interquartile range (boxes), median (red line) and 95% confidence intervals on the median (notches around red line) for 10 subjects and all cognitive tasks, phonemes and crossfolds on the test data. The three different data series contrast the AUC scores for the matched filters which used only the ***Best Time Sample***, the ***Temporal Mean*** of all time samples, or the ***Time Varying*** information from all time samples. The confidence intervals on the medians for all three populations were above the $p<0.01$ line for chance based on the Monte Carlo simulations, however only the ***Time Varying*** population had an interquartile range above the chance line. The inset shows that the 95% confidence intervals on the medians between these populations were nonoverlapping and that the ***Time Varying*** population had the highest median AUC score. B). Analysis of the information content in the matched filter as a function of the percentage of time samples used to predict phonemic content. When added in decreasing order of correlation (best time sample first), the mean AUC scores for all subjects and phonemes increases through the majority of the time window for each task. This indicates that 80% or more of the time samples for each cognitive task encapsulate ECoG signals with information relevant to decoding phonemes. C) Ranking plots reveal the relative amount of information content in specific time samples within the matched filter windows for each cognitive task. Each line plots the median rank across subjects and phonemes for each cognitive task. Shaded areas show the extent of the 95% confidence intervals on the median (100 bootstraps with resampling). For hearing, the ranks peak toward the end of the window due to the increasing amount of cortical processing involved as the subjects prepare to repeat the stimulus word. The highest ranks for speaking surround the voice onset.

5.7 Spectral Diversity

The final dimension of the neural motif we study is frequency. Because it is generally accepted that there are physiological rhythms in several distinct frequency bands below 60Hz, here we examined the subparcellation of the frequencies above 60 Hz. Figure 5.10 contains exemplar matched filter plots and time traces for specific frequencies from a single subject and electrode while hearing three different phonemes. These plots reveal that there is spectral diversity above 60 Hz in the neural motifs correlated with each phoneme. The colored lines overlaid on the matched filter time-frequency plots for the phonemes M_N, K_N and T_N highlight the four frequencies of interest. The full time-frequency plots on the right subjectively illustrate diversity by showing all frequency bands analyzed independently. In contrast, the three spectral average time-frequency plots show the matched filters when power in all frequencies above 60 Hz is averaged. The time courses show each of the four frequencies independently as well the spectral average above 60 Hz for each of the three phonemes. The time courses illustrate the independence and

diversity of these four bands. First, there is no evidence of purely broadband, ***1/f*** power increases. In every phoneme, there are instances when higher frequencies have statistically significant power modulations while lower frequencies do not. Second, certain frequencies have power modulations specific to phonemes. As examples, consider the 290 Hz band which has similar time course characteristics for M_N and T_N, but no statistically significant activity for the phoneme K_N. The 190 Hz band has little significant activity for M_N, but has 250 ms duration power increases for both T_N and K_N, which happen at different times during the respective phonemes. Also consider the differences between the four frequency bands of interest and the spectral average trace. There are subtleties for each individual spectral example trace that are not captured in the average spectral trace. Next we seek to quantify this diversity.

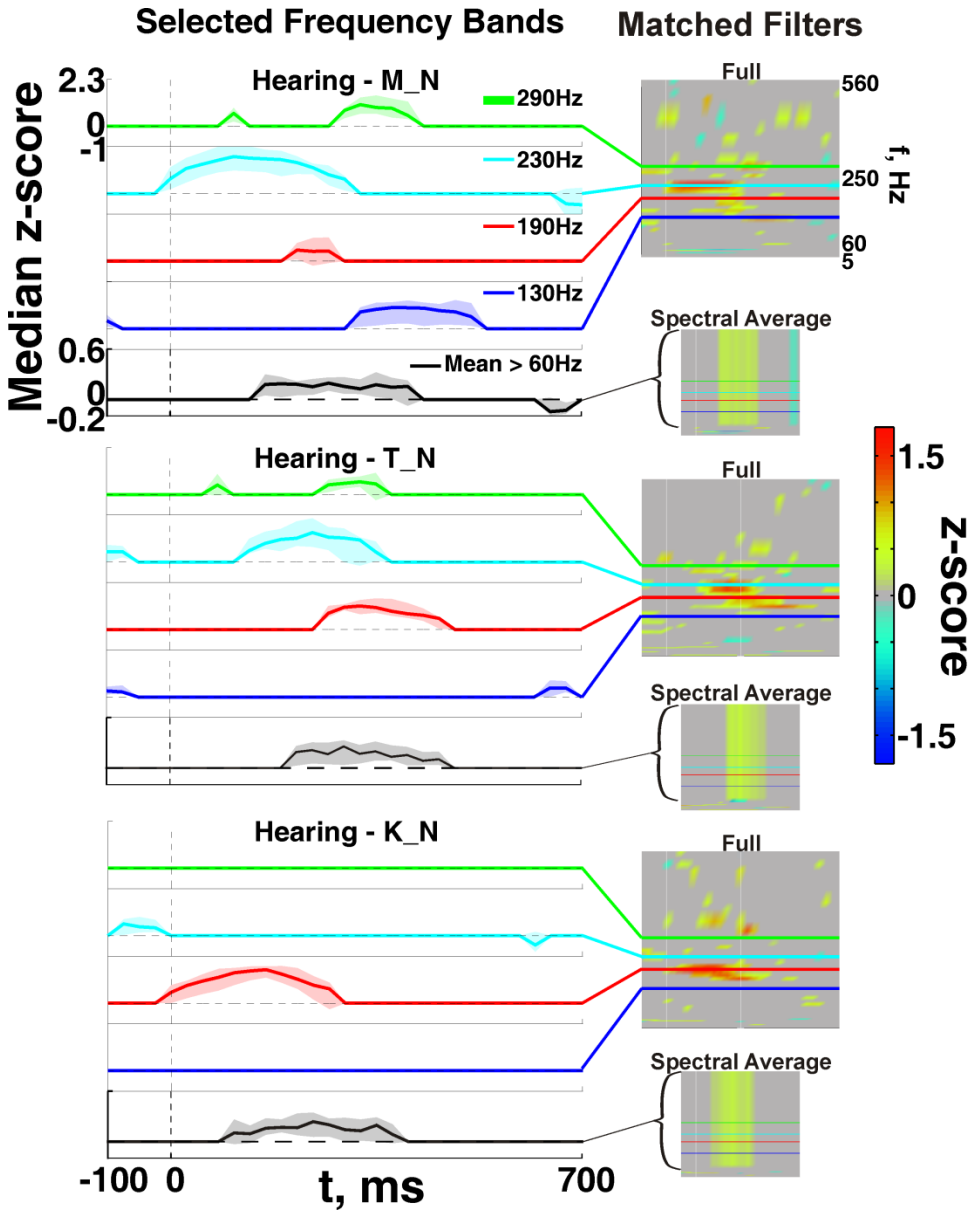

Figure 5.10 Spectral diversity exemplar
Matched filter variants and time courses of power in four frequency bands of interest illustrate spectral diversity. Full matched filters on the right from a single electrode and three different consonant classes (M_N: N=22, T_N: N=23, K_N: N=22). These plots have been thresholded so that all colored areas are statistically significant (Wilcoxon sign-rank, $p<0.05$). The colors show median z-score across all trials on the scale shown by the color bar at the right. The four colored lines (green, cyan, red, blue) highlight the frequency bands of interest. Spectral Average matched filters were constructed by averaging the power in all frequency bands above 60 Hz. Frequency bands below 60Hz were still considered independently. The sections of the plot with color are significant (Wilcoxon sign-rank, $p<0.05$) and use the same scale as the full matched filters. Time courses of power z-scores for each of the frequencies of interest and spectrally averaged power illustrate the diversity in the frequency bands above 60 Hz. Solid lines are the median power levels for significant (Wilcoxon sign-rank, $p<0.05$) power changes across trials. Shaded regions indicate the 95% confidence intervals on the median (100 bootstraps with resampling). All time courses for the four frequencies of interest have a common ordinate scale (-1.0 to 2.3). The spectral average traces (black) are also

plotted on a common ordinate scale (-0.2 to 0.6) that is different from the exemplar frequencies. These plots reveal that power modulation in bands above 60 Hz occurs independently within and across phonemes.

The first analysis of high frequency spectral diversity was the ANOVA which used the three matched filter variants contrasting differing levels of spectral diversity. The three reference waveform variants included the truncated version which omitted the high frequencies and only used the bands below 60 Hz, the smoothed version which used the spectral average for frequencies above 60 Hz, and the discrete bands version with full spectral diversity. The results of Chapter 4 demonstrated that there were only certain subjects that exhibited the dissociation band phenomena in frequencies above 60 Hz. Similarly, only a subset of subjects exhibited high frequency spectral diversity in the neural motif analysis. Therefore, this analysis was only performed data from seven of the 10 subjects (Subjects 1, 4, 5, 7, 8, 9, 10). The results of the ANOVA contrasting these three high frequency spectral variants on this subset of subjects are contained in Table 5.4. All of the single factors were significant and again, the high frequency factor accounted for more variance in the model than either cognitive task or phoneme. The paired interactions that included frequency accounted for less variance than frequency as a single factor. These results indicate that in this group of subjects, spectral diversity in bands above 60 Hz is more prevalent in the neural motif and depends less on the cognitive task or phonemic content. The following analyses help illustrate the sources and distribution of the temporal diversity in the neural motif.

Table 5.4 ANOVA for spectral variants of frequencies above 60 Hz on seven subjects with high frequency diversity

Source		Sum Squares	Degrees of Freedom	Mean Squared Error	F Statistic	Prob>F
Single Factors	Subject	22.8066	9	2.5341	331.1225	0
	Task	0.26839	1	0.26839	35.0705	3.3548e-009
	Phoneme	2.4707	12	0.20589	26.9036	3.6943e-060
	>60	4.756	2	2.378	310.7268	3.5573e-129

Interactions	Subject*Task	3.5704	9	0.39671	51.8373	3.3918e-091
	Subject*Phoneme	7.9914	108	0.073995	9.6688	6.8379e-139
	Subject*>60	2.7474	18	0.15263	19.9445	3.3379e-063
	Task*Phoneme	0.53308	12	0.044423	5.8047	4.301e-010
	Task*>60	0.051216	2	0.025608	3.3461	0.035285
	Phoneme*>60	0.12826	24	0.0053442	0.69832	0.85843
	Error	46.2391	6042	0.0076529		
	Total	91.6433	6239			

The summary analyses in Figure 5.11 quantify the difference in the spectral diversity above 60 Hz and illustrate the differences between generic cognitive tasks and those for specific phonemes. Figure 5.11A contains the results of the non-parametric ANOVA and shows the difference between the AUC scores for matched filters in the three variants that contrasted signal content above 60 Hz for a selected group of subjects. The matched filters with no frequency content above 60Hz have AUC scores with the lowest median and a significant portion of the interquartile range below the chance line. Because this variant contained the least amount of information (only the 16 frequencies below 60 Hz), lower scores are expected. The two remaining variants used all 43 frequency bands. The ***Spectral Mean*** variant uses the average power for frequencies above 60 Hz in each time sample as the common matched filter pattern for all of those frequencies. In contrast the ***Discrete Bands*** variant allows independent temporal variation for each frequency above 60 Hz. The inset to Panel A reveals that the ***Discrete Bands*** variant is significantly higher than the ***Spectral Mean*** variant in this population of subjects. This result shows that there is information correlated with specific phonemes encoded in the independent time varying dynamics of multiple frequency bands above 60 Hz. Conversely, treating the frequency range above 60Hz as a single entity results in a decrease of information contained in the matched filter as shown by the drop in median AUC score.

There are two other trends in Panel A that must be addressed. The fact that the interquartile range for the ***Spectral Mean*** variant is above the chance line reveals that treating the frequencies above 60Hz as a uniform entity contains a significant amount of information. Second, the ***Discrete Bands*** variant was only better than the ***Spectral Mean*** variant in seven of the 10 subjects. This is consistent with the results of Chapter 4 and our previously published results in which activity above 60 Hz dissociated cognitive tasks and anatomic locations in most, but not all, subjects (Gaona, Sharma et al. 2011).

Figure 5.11B shows how adding individual frequency bands to the matched filter impacts the information content. When added in order of decreasing r^2, nearly all of the frequency bands improve the matched filter AUC scores. For phonemes, 70% or more of the frequency bands improve the AUC scores, while for the general cognitive tasks, 56% or more of the frequency bands improve the scores. In contrast to the spatial summary, adding frequency bands beyond the optimal point does not significantly decrease AUC score. Figure 5.11C reveals the spectral distribution of information by plotting the median rank (best r^2 highest) versus frequency. As expected from the ECoG functional mapping literature, the frequencies with consistently highest ranks occur between 10-30 Hz (alpha/beta bands) and 70-100 Hz (traditional high gamma bands) (Crone, Miglioretti et al. 1998; Leuthardt, Miller et al. 2007; Wu, Wisneski et al. 2010). Notice that for generic cognitive tasks, the median ranks and confidence intervals for the best frequencies are between 70-100 Hz and exceed those of the phoneme ranks. This illustrates that for discriminating generic cognitive tasks, the typical frequency bands are consistently more important in the matched filters. Notice also, that the frequencies above 380 Hz have consistently higher rankings for the phoneme specific matched filters. This result may

indicate that the dynamics of higher frequencies may inform decisions on specific phonemic content. However, recall from Panel B that only 70-74% of the frequency bands improve the AUC scores. The median rankings fall below the 30th percentile at approximately 300 Hz. This indicates that above the 300 Hz mark, these frequency bands do not appear to improve the matched filter AUC scores.

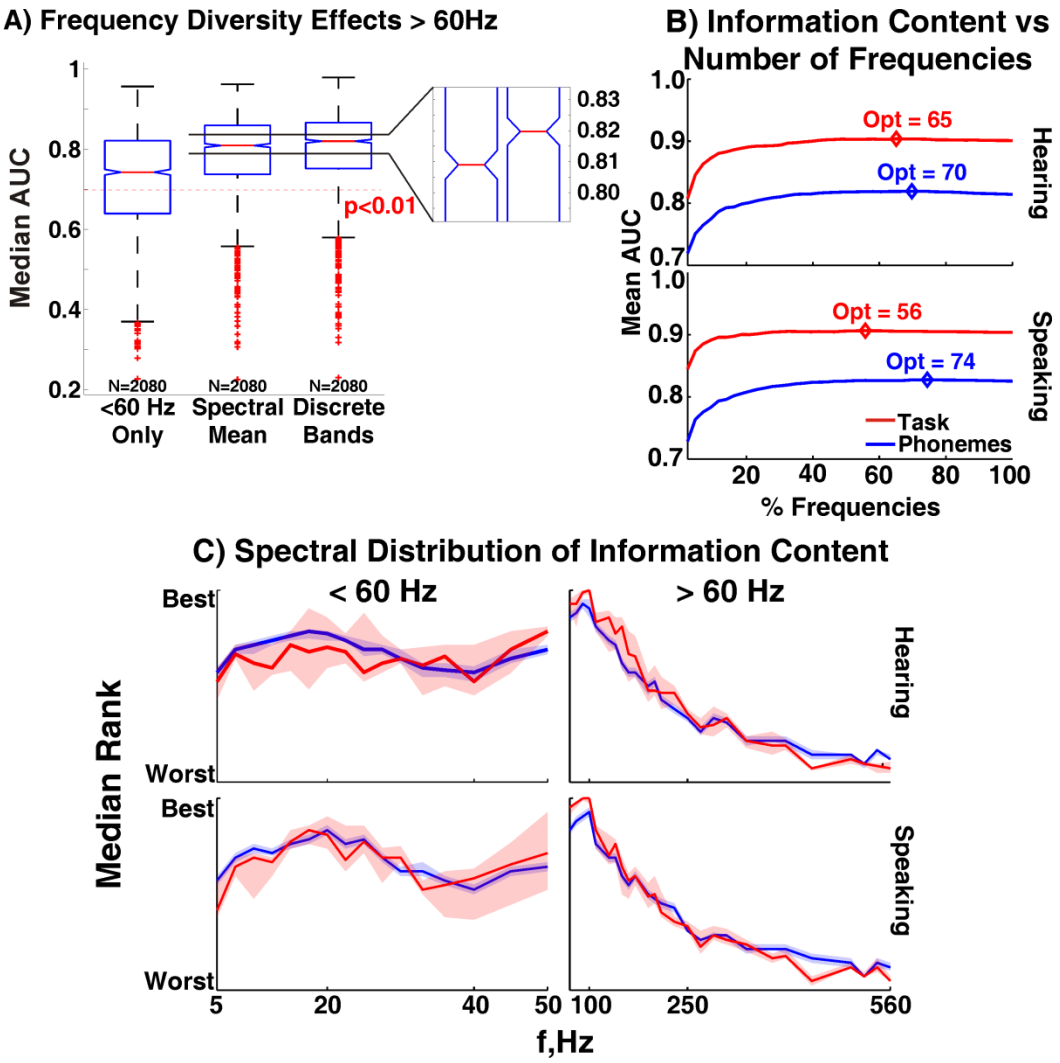

Figure 5.11 Spectral diversity summary
Quantitative results show that information content is encoded diversely in multiple frequency bands above 60 Hz in most subjects. A) The results of nonparametric ANOVA tests (Kruskal-Wallis) showing the range of the data (whiskers), interquartile range (boxes), median (red line) and 95% confidence intervals on the median (notches around red line) for 7 subjects and all cognitive tasks, phonemes and crossfolds on the test data. The three different data series contrast matched filters AUC scores for which frequency bands above 60 Hz were ***Not Included***, used the ***Spectral Mean*** of all 27 frequency bands above 60Hz, or used all 27

frequencies above 60Hz as ***Discrete Bands***. The confidence intervals on the medians for all three populations were above chance; however only the ***Spectral Mean*** and ***Discrete Bands*** populations had interquartile ranges above the chance line. The inset shows that the 95% confidence intervals on the medians between these populations were nonoverlapping and that the ***Discrete Bands*** population had the highest median AUC score. B). Analysis of the information content in the matched filter as a function of the number of frequency bands used to predict phonemes and general cognitive tasks. When added in decreasing order of correlation (best frequency band first), the mean AUC scores for cognitive tasks and phonemes increases as the majority of the spectrum is added to the matched filter. This indicates that power modulation in 70% or more of the available frequency bands encapsulate ECoG signals with information relevant to decoding phonemes. C) Ranking plots reveal the relative amount of information content in specific frequency bands within the matched filter spectrum. Each line plots the median rank across subjects, phonemes and crossfolds. Shaded areas show the extent of the 95% confidence intervals on the median (100 bootstraps with resampling). Rank traces for frequencies above and below 60 Hz are plotted separately for readability. For both cognitive tasks, rankings are highest in the 10-30 Hz (alpha/beta) and 70-100 Hz (high gamma) ranges, traditionally associated with functional mapping.

5.8 Conclusion

We have shown that the neural motifs captured by ECoG contain sufficient information in several subjects to discriminate specific phonemic content. The information exists in at least the three dimensions studied here: anatomic location, time and center frequency of power modulation. We used the matched filter to capture and quantify the diversity of information content in the neural motif. Spatially, we have shown that approximately 9-24 cm^2 of cortex provide an optimal representation of phonemic information and that information is broadly represented within this area. We have also clearly shown the importance of including temporal dynamics on a time scale of at least as fine as 26.7 ms. Temporally, the windows most important for discriminating phonemes during hearing occur 50 to 700 ms after stimulus onset, and during speaking they occur from 400 ms pre- to 560 ms post-voice onset. Spectrally we have shown that, in the majority of subjects, allowing diversity in the frequency bands above 60 Hz improves AUC score. While the alpha, beta and high gamma ranges have the highest ranks, including frequencies in discrete bands up to approximately 300Hz provides the greatest amount of information for decoding specific phonemes.

5.9 References

Binder, J. R., J. A. Frost, T. A. Hammeke, R. W. Cox, S. M. Rao and T. Prieto (1997). "Human brain language areas identified by functional magnetic resonance imaging." J. Neurosci. **17**(1): 353-362.

Bullock, T. H., M. C. McClune, J. Z. Achimowicz, V. J. Iragui-Madoz, R. B. Duckrow and S. S. Spencer (1995). "Eeg coherence has structure in the millimeter domain: Subdural and hippocampal recordings from epileptic patients." Electroencephalography and Clinical Neurophysiology **95**(3): 161-177.

Canolty, R. T., M. Soltani, S. S. Dalal, E. Edwards, N. F. Dronkers, S. S. Nagarajan, H. E. Kirsch, N. M. Barbaro and R. T. Knight (2007). "Spatiotemporal dynamics of word processing in the human brain." Frontiers in Neuroscience **1**: 11.

Church, J. A., R. S. Coalson, H. M. Lugar, S. E. Petersen and B. L. Schlaggar (2008). "A developmental fmri study of reading and repetition reveals changes in phonological and visual mechanisms over age." Cereb. Cortex **18**(9): 2054-2065.

Crone, N., D. Boatman, B. Gordon and L. Hao (2001). "Induced electrocorticographic gamma activity during auditory perception." Clinical Neurophysiology **112**(4): 565-582.

Crone, N. E., D. L. Miglioretti, B. Gordon, J. M. Sieracki, M. T. Wilson, S. Uematsu and R. P. Lesser (1998). "Functional mapping of human sensorimotor cortex with electrocorticographic spectral analysis. I. Alpha and beta event-related desynchronization." Brain **121**(12): 2271-2299.

Edwards, E., M. Soltani, W. Kim, S. S. Dalal, S. S. Nagarajan, M. S. Berger and R. T. Knight (2009). "Comparison of time-frequency responses and the event-related potential to auditory speech stimuli in human cortex." J Neurophysiol **102**(1): 377-386.

Gaona, C. M., M. Sharma, Z. V. Freudenburg, J. D. Breshears, D. T. Bundy, J. Roland, D. L. Barbour, G. Schalk and E. C. Leuthardt (2011). "Nonuniform high-gamma (60–500 hz) power changes dissociate cognitive task and anatomy in human cortex." The Journal of Neuroscience **31**(6): 2091-2100.

Gómez, C., J. Marco-Pallarés and C. Grau (2006). "Location of brain rhythms and their modulation by preparatory attention estimated by current density." Brain Research **1107**(1): 151-160.

Jäncke, L., S. Mirzazade and N. Joni Shah (1999). "Attention modulates activity in the primary and the secondary auditory cortex: A functional magnetic resonance imaging study in human subjects." Neuroscience Letters **266**(2): 125-128.

Leuthardt, E., K. Miller, N. Anderson, G. Schalk, J. Dowling, J. Miller, D. Moran and J. Ojemann (2007). "Electrocorticographic frequency alteration mapping: A clinical technique for mapping the motor cortex." Neurosurgery **60**(4): 260.

Ojemann, G., J. Ojemann, E. Lettich and M. Berger (1989). "Cortical language localization in left, dominant hemisphere." Journal of Neurosurgery **71**(3): 316-326.

Petersen, S. E., P. T. Fox, M. I. Posner, M. Mintun and M. E. Raichle (1989). "Positron emission tomographic studies of the processing of singe words." Journal of Cognitive Neuroscience **1**(2): 153-170.

Salmelin, R. (2007). "Clinical neurophysiology of language: The meg approach." Clinical Neurophysiology **118**(2): 237-254.

Ulanovsky, N., L. Las, D. Farkas and I. Nelken (2004). "Multiple time scales of adaptation in auditory cortex neurons." The Journal of Neuroscience **24**(46): 10440.

Woldorff, M. G., C. C. Gallen, S. A. Hampson, S. A. Hillyard, C. Pantev, D. Sobel and F. E. Bloom (1993). "Modulation of early sensory processing in human auditory cortex during auditory selective attention." Proceedings of the National Academy of Sciences of the United States of America **90**(18): 8722.

Wu, M., K. Wisneski, G. Schalk, M. Sharma, J. Roland, J. Breshears, C. Gaona and E. Leuthardt (2010). "Electrocorticographic frequency alteration mapping for extraoperative localization of speech cortex." Neurosurgery **66**(2): E407.

6 High Gamma Diversity in Microarray ECoG

In the previous two chapters we examined the heterogeneity and diversity that exists in the high frequency bands of ECoG signals from clinical grids with 2.3mm diameter electrodes and 10mm spacing. We conclude this research by examining spectral nonuniformities and information diversity in ECoG microarrays one order of magnitude smaller than the clinical grids. This chapter is divided into two sections. We start by examining the nonuniformity of high frequency signals and determine whether spectral nonuniformities in bands above 60 Hz can dissociate cognitive tasks and anatomic locations. This analysis concludes by quantifying the amount of information encoded in the spatial, temporal and spectral domains of the microarray ECoG signals.

Three subjects (11, 12 and 13 from Table 3.1) received ECoG microarray implants and therefore participated in this portion of the study. The microarrays were implanted without interfering with clinical recordings. Each subject received the microarray implant in a different location putatively associated with speech processing. Subject 11's microarray was implanted on the pars triangularis (Broca's Area), Subject 12's microarray was placed on the anterior superior temporal gyrus (STG) and Subject 13's microarray was placed on the posterior STG. These three areas have different putative roles in auditory single word repetition experiments (Petersen and Fiez 1993; Binder, Frost et al. 1997) and should therefore have unique responses to the different cognitive tasks involved within the experiment.

6.1 Dissociation Bands in Microarray ECoG

The results of the study of spectral nonuniformities in microarray ECoG were somewhat different than those from the clinical ECoG arrays. While all of the subjects had electrodes with significant power modulation correlated to activity, none of the electrodes had power changes in specific bands that dissociated cognitive tasks. One of the subjects did have several pairs of electrodes in which specific bands were able to distinguish the specific cortical location (1 mm to 4 mm separation). Figure 6.1 contains exemplar data from Subject 13. The median normalized spectra, single trial normalized spectra and time-course of normalized spectral power all demonstrate distinct power modulations that dissociate the two electrodes separated by 2.24 mm while hearing words.

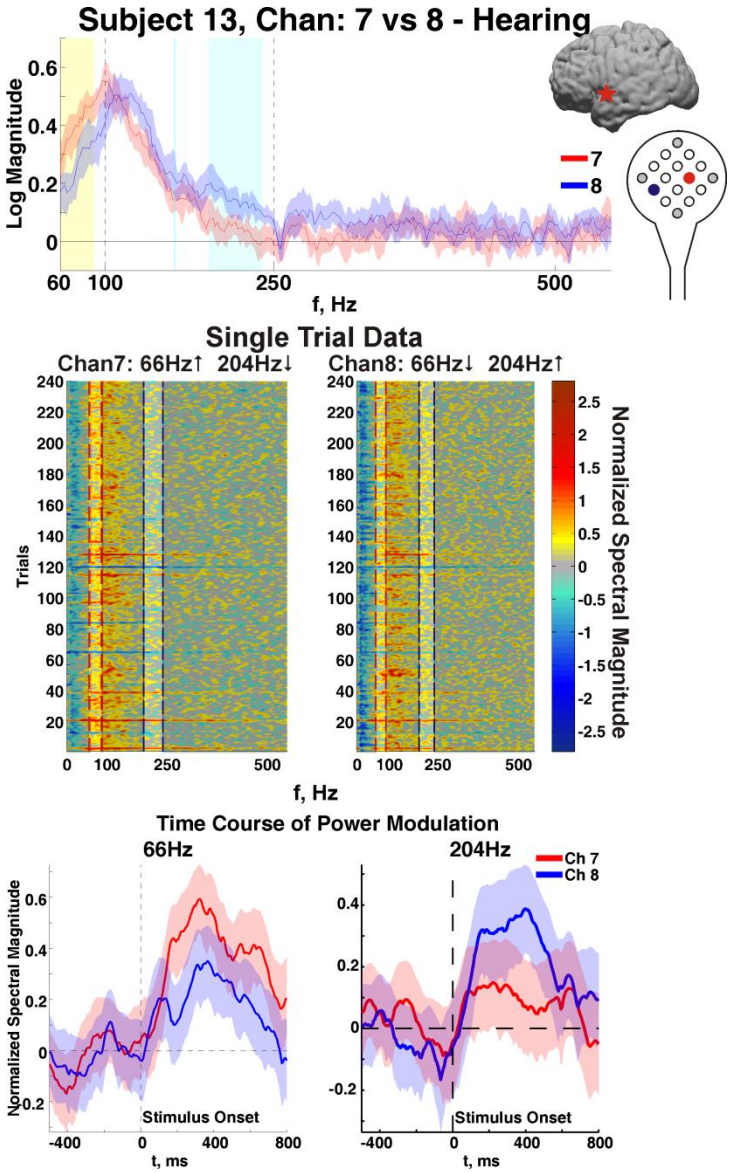

Figure 6.1 Microarray ECoG dissociation band dynamics

An exemplar pair of electrodes that dissociated two cortical locations separated by approximately 2.24 mm on the posterior STG. The top panel shows the median normalized spectra with 99% confidence intervals (100 bootstraps with resampling) over 240 trials. The dashed lines show typical high gamma analysis boundaries. The gold and blue shaded regions highlight selected frequency bands in which the median normalized spectra for these two channels were statistically different (Wilcoxon rank-sum, $p<0.01$ with FDR correction). The regions highlighted span 60-90 Hz and 192-240 Hz. The middle panel shows single trial normalized spectra from the two exemplar channels. The dashed lines demark the gold and blue highlighted frequency bands in the top panel. Opaque rectangles were placed over the nonrelevant bands to highlight the trends in the dissociation bands. The single trial spectra for channel 7 had consistently greater magnitudes (warmer colors) in the bands marked by the red dashed lines, whereas the single trial spectra for channel 8 had consistently greater magnitudes (warmer colors) in the bands marked by the blue dashed lines. The bottom panels illustrate that over the time course of this cognitive task, power modulation reversed between in the two bands also reverses (Gabor wavelet transforms centered at 66 Hz and 204 Hz).

The normalized spectra in the top panel of Figure 6.1 show that the power modulations in channel 7 fell below the noise floor at approximately 250 Hz, however on channel 8 they rose above the noise floor and were statistically significant as high as 540 Hz.

Using the same criteria to identify dissociation bands as described in Chapter 3, we quantified the total number of microarray electrode pairs with dissociation bands. The exemplar data from Figure 6.1 was used in a Monte Carlo simulation to determine the actual rate of Type I errors (false positives) in randomly labeled data. Table 6.1 contains the quantitative analysis of the total number of comparisons across all three subjects in the microscale study. Based on the Monte Carlo simulation, the single electrode dissociation band tests at all three significance levels and the electrode pair tests at 0.01 and 0.001 had familywise Type I error rates below 0.05.

Table 6.1 - Familywise Type I Error Rate computations for microscale data

Dissociation Band Test p-value	**0.05**	**0.01**	**0.001**
Permutations with dissociation bands	**16**	**0***	**0***
Single Channel Activity Comparisons	**3 – Subjects 11,13 10 – Subject 12**		
Channels with Significant Power	**Subjects: (11) (12) (13) 6 + 0 + 12 = 18**	**Subjects: (11) (12) (13) 3 + 0 + 12 = 15**	**Subjects: (11) (12) (13) 1 + 0 + 12 = 13**
Single Channel Type I Error Rate	**16x ((3 x 6) + (10 x 0) + (3 x 12))/100,000 = 0.0086**	**1 x ((3 x 3) + (3 x 12))/100,000 = 0.0005**	**1 x ((3 x 1) + (3 x 12)) /100,000 = 0.0004**
Channel Pair Activity Comparisons	**3 – Subjects 11,13 5 – Subject 12**		
Channel Pairs with Significant Power	**6 x 5 + 0 + 12 x 11 = 162**	**3 x 2 + 12 x 11=138**	**12 x 11 = 132**
Channel Pair Type I Error Rate	**16 x (3x6x5 +3x12x11) /100000 = 0.0778**	**1 x (3x3x2 + 3x12 x11) /100000 = 0.0041**	**1 x (3x12x11)/100000 = 0.004**

* There were no random occurrences after 100,000 permutations, therefore we used a 1/100,000 rate for the rest of the calculations.

The results in Figure 6.2 show the total number of dissociation bands detected in this group of three subjects. As mentioned earlier, none of the subjects with microarray data exhibited single electrode dissociation bands. One of the subjects had dissociation bands between pairs of microarray electrodes at the 0.05 and 0.01 significance tests. Although according to Table 6.1 the 0.05 tests had a familywise Type I error rate that was 0.116, the results are still shown in Figure 6.2B in gray because the correction factor used from Table 6.1 may be too stringent and in fact may result in Type II errors (false rejections).

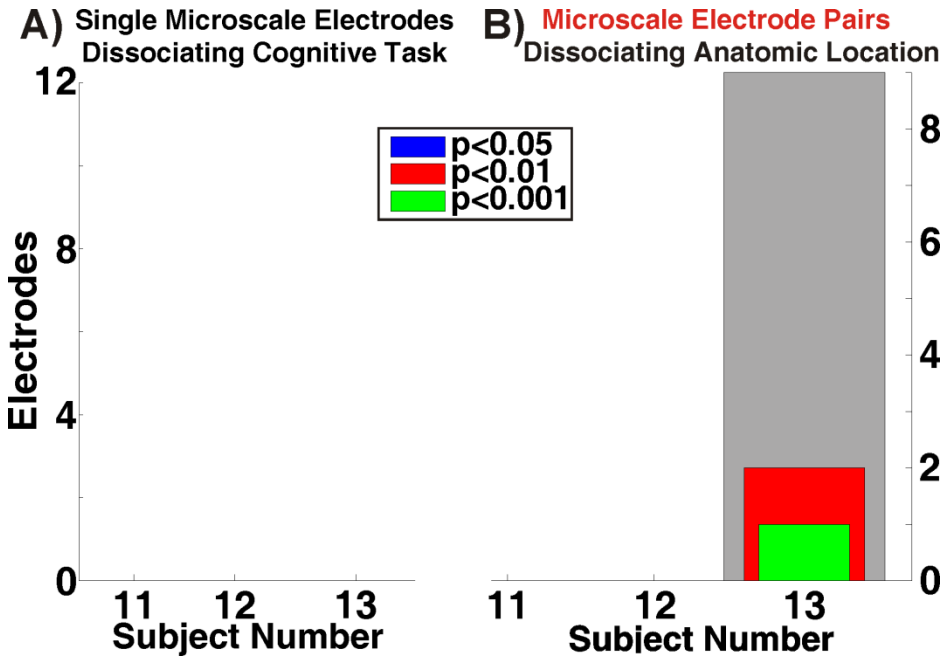

Figure 6.2 Quantitative summary of microarray ECoG dissociation bands
Graphic similar in format to the results shown in Chapter 4. The quantitative summary shows by p-value of the individual dissociation band tests the quantity of microscale electrodes with dissociation bands. All data shown here has been corrected so the familywise Type I error rate for each colored bar is less than 0.05 as shown in Table 6.1. The bar for the 0.05 test has been grayed out since the familywise Type I error rate for this level of test was 0.0778.

To visualize a summary of the results over different cognitive task and anatomic locations, Figure 6.3 and Figure 6.4 show the median normalized spectra and 95% confidence intervals for each microelectrode during hearing and speaking respectively. Figure 6.3 shows that during hearing, only the posterior STG microarray had significant power modulations. It is notable that the majority of the dissociation bands came from Subject

13 during Hearing. While the general shape of the normalized spectra are similar across the microarray, there were enough differences in these spectral patterns to yield 9 different electrode pairs with specific frequency bands dissociating the specific location. It is not surprising that the Broca's area microarray yielded little if any significant power changes. As discussed in Chapter 4, Broca's area is not normally implicated in functional imaging or scalp electrophysiology studies of hearing alone. As shown in Figure 4.5, Broca's area macro electrodes had the least number of significant power changes during hearing as well. The anterior STG has been attributed a role in processing words(Binder, Frost et al. 2000), however, this subject was congenitally blind and had some reorganization of speech areas. Notably, this subject showed no evidence of speech arrest in the areas surrounding the microarray during cortical stimulation mapping. Since these tasks contained no semantic analysis, it is not surprising that Subject 12's microarray had no significant power modulation during hearing. Subject 12 also performed several other experimental paradigms that involved hearing, including a verb generation task, a concept generation task and task that required discrimination of motion in environmental sounds. None of these paradigms induced significant power changes during hearing.

Figure 6.4 contains the median normalized spectra for Subjects 11 and 13 during speaking. As mentioned earlier, Subject 12's data was corrupted by the microphone signal, therefore only the hearing phase was studied. Both subjects had some significant normalized power change across a wide range of frequencies as high as 540 Hz. However, none of these spectra were consistently distinct enough to dissociate pairs of microarray electrodes, nor were they significantly different enough from the normalized spectra for hearing to dissociate cognitive tasks. The peak response frequency for Subject 11 appears to be approximately 200 Hz, with significant power modulations as high as 450 Hz. However

the confidence intervals reveal a significant amount of variability in the signals. Subject 13's normalized spectra for speaking appear to be an attenuated version of the hearing response which is in keeping with studies finding that posterior STG responds to the subjects own voice in an attenuated fashion (Creutzfeldt, Ojemann et al. 1989; Flinker, Chang et al. 2010). However, there is more inhomogeneity in the microarray response during speaking than hearing. Specifically, the microarray has a focal response at channel 5 to speaking. In contrast during hearing, while there are certainly differences in the normalized spectra, the electrodes in the microarray respond more uniformly.

The microarray responses to these two cognitive tasks are certainly physiologically plausible. Since Subject 13's microarray was located near the posterior STG, this is likely due to neural responses to both the auditory stimuli and the subject's self-monitoring during speaking (Demonet, Thierry et al. 2005; Binder, Desai et al. 2009). Subject 11's normalized spectra had the strongest response during speaking, but the wider confidence intervals on the normalized spectra indicate that the response was more variable. Researchers noted that this subject was not attentive to the task during portions of the experiment and was involved in a side conversation at times. Verbal communication uncorrelated with the experimental paradigm could have corrupted the experimental data. Additionally, the microarray was placed near Broca's area which should be more active with speech preparation and production (Petersen and Fiez 1993; Binder, Frost et al. 1997). Consistent with the results shown in Chapter 4, Subject 11's traces for speaking appear to have higher overall levels during speaking than hearing.

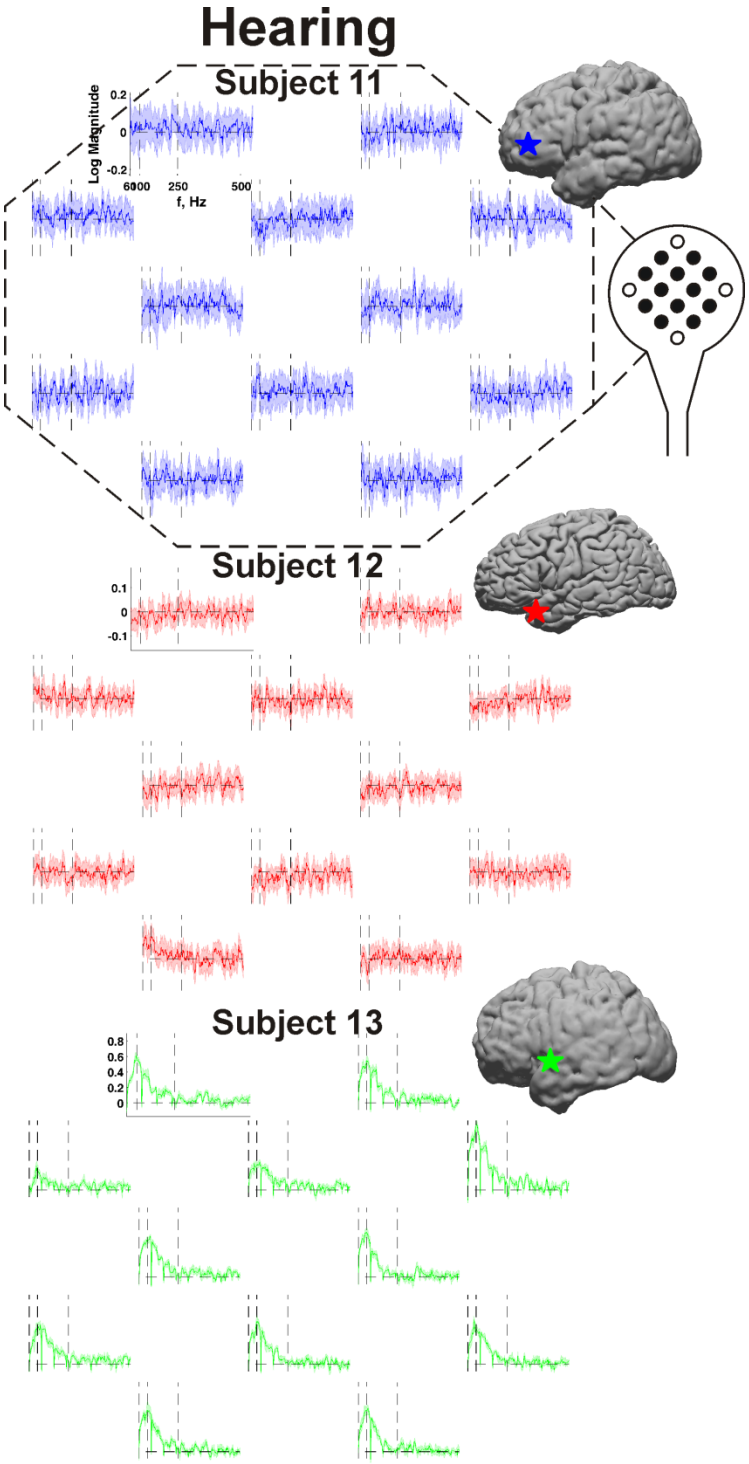

Figure 6.3 Summary of normalized spectra for Hearing by anatomic location
Data from Subject 11 is on the top row (**blue** traces), Subject 12 on the middle row (**red** traces) and Subject 13 is on the bottom row (**green** traces). At the far right, the colored stars on each brain display the approximate location of each microarray on either the subject's gyral anatomy (11 and 13), or the MNI model brain (12). The individual traces are arranged in the same spatial pattern as the microarray shown on the right. The 12 signal capture electrodes shown in black correspond to the 12 traces shown in each plot. The median normalized spectra are plotted from 60-550Hz. Dashed lines at 60, 100 and 250 Hz are plotted for reference. The ordinates for all normalized spectra for a given subject and cognitive activity have identical

ranges and are shown for the first electrode for reference. Each trace shows the median over trials with 95% confidence intervals on the median (5000 bootstraps with resampling). The posterior STG microarray exhibited the greatest power modulations for this cognitive task.

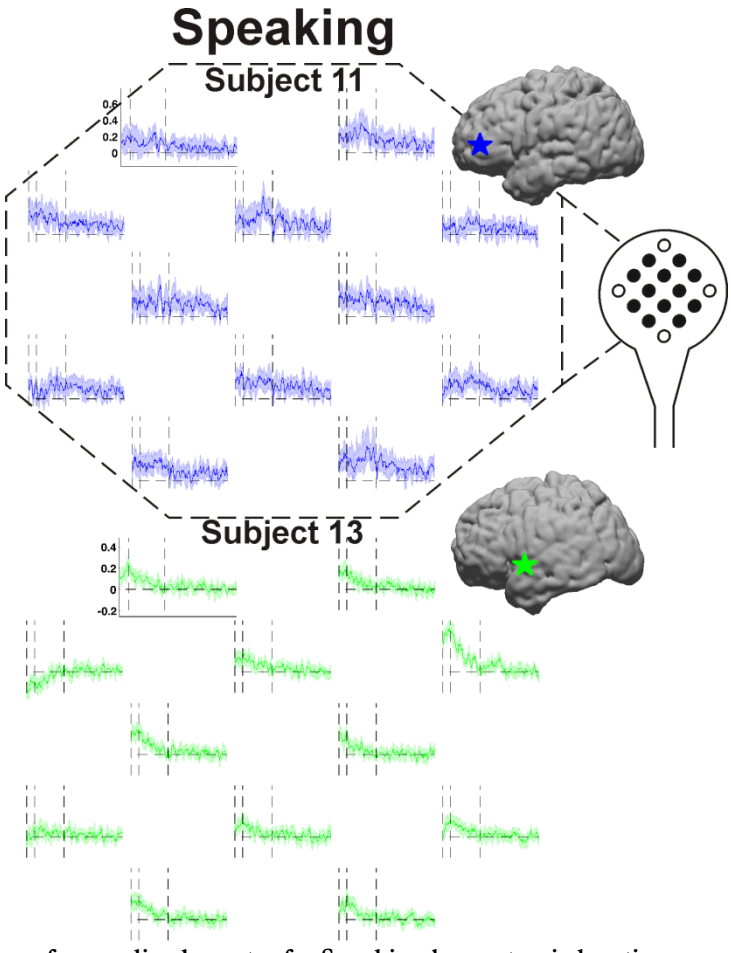

Figure 6.4 Summary of normalized spectra for Speaking by anatomic location
Data from Subject 11 is on the top row (**blue** traces) while Subject 13 is on the bottom row (**green** traces). At the far right, the colored stars on each brain display the approximate location of each microarray on either the subject's gyral anatomy after the same format as Figure 6.3. The median normalized spectra are plotted from 60-550Hz with 95% confidence intervals on the median (5000 bootstraps with resampling). Both microarrays show significant power modulations for this cognitive task; however, the posterior STG microarray exhibited more consistent power modulations as shown by the tighter confidence intervals.

In summary, the results of the dissociation band analysis on the microscale array data have shown that in this data set, there is sufficient nonuniformity to dissociate cortical regions separated by as little as 1mm in one subject. This is in keeping with previous spatial analyses of pial recordings in humans that showed there is sufficient spatial diversity in surface cortical recordings to require spatial sampling at least every 1.25 mm (Freeman,

Rogers et al. 2000). Independent high frequency power modulations resulting in dissociation bands were not present in two of the subjects. There are at least two reasons for this finding including microarray location and corruption of the ECoG recordings. The cortical location of the microarrays may have been toward the periphery of primary speech areas. Additionally, there were problems with the data collection for Subject 12 which corrupted all of the speaking tasks. Finally, as discussed earlier, Subject 13 had some difficulty attending to the task, and also performed the fewest trials of the experiment. These results should at this point be considered preliminary. They provide motivation to collect more data with which to test the hypothesis; however, conclusions should not be made based on this population of subjects.

6.2 Diversity in Microarray ECoG

The second half of this chapter examines the level of spatial, temporal and spectral diversity in microarray ECoG signals. This section flows in the same fashion as chapter 5, but where necessary, the analyses are modified to account for the smaller spatial scale.

6.2.1 Data Driven Analysis of Microarray Data

A preliminary analysis used data driven machine learning techniques to determine whether microarray ECoG data contained sufficient information to classify specific phonemic content in the context of a specific cognitive task. Figure 6.5 contains the results of the classification analysis. These show that only the consonants were discriminable. Given the results of the microarray dissociation band study, it is not surprising that only two subjects had classification scores above chance.

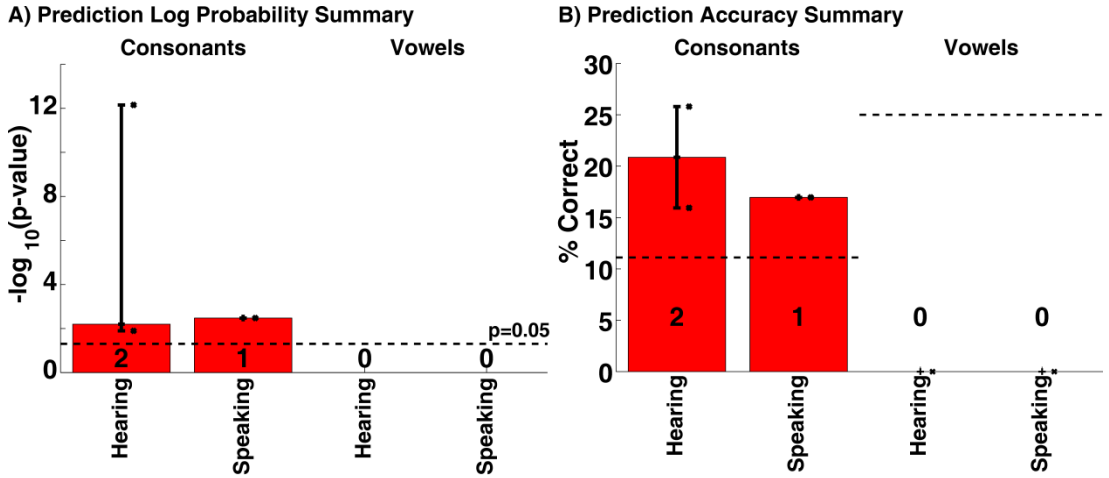

Figure 6.5 Summary of microarray phoneme classification
Bars plotting the median prediction log probabilities and accuracies for microarray subjects with performance above chance. Error bars illustrate the 95% confidence intervals on the median generated by 100 bootstraps. Digits in each bar indicate the number of subjects (out of 3) that were above chance ($p<0.05$). Individual data points are plotted as a scatter plot with 'x' marks. A) Bars indicate the median negative log probabilities for subjects with p-values < 0.05 for each cognitive task and phonemic category (consonants / vowels). The dashed line shows the threshold at $-\log_{10}(0.05)$. B) Bars show the median accuracy for subjects with p-values < 0.05 for each cognitive activity and phonemic category. Chance accuracies are shown by the dotted lines for each phonemic category. These results show that when using a data driven classification approach, there is sufficient information in the power modulation dynamics of microarray ECoG signals to predict consonant content within a specific cognitive task above chance.

Figure 6.6 shows the exemplar confusion matrices for hearing and speaking consonants. Again, these indicate that there is significant information encoded in the 3 mm x 3 mm cortical footprint covered by the microarrays. These results provided a basis for the subsequent matched filter analysis of diversity in the high frequency bands of the microarray data.

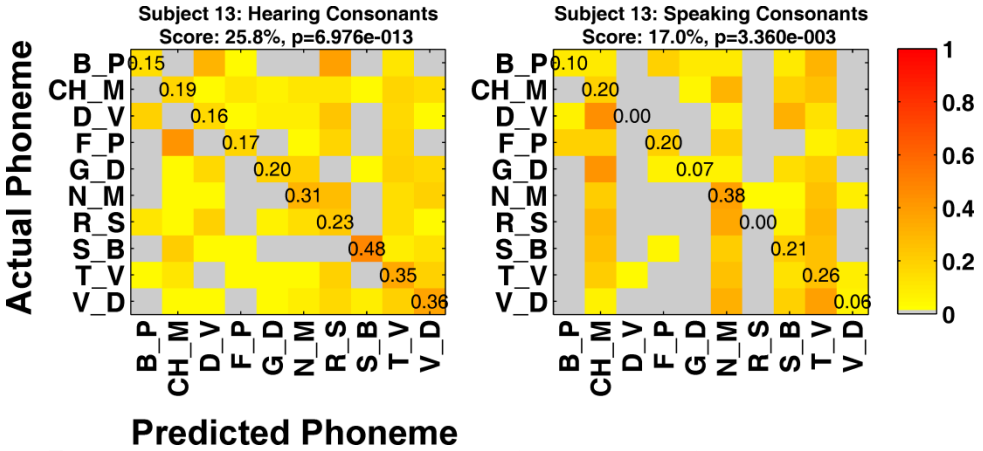

Figure 6.6 Exemplar microarray confusion matrices by cognitive task and phonemic category

These confusion matrices show the distribution of predicted versus actual phoneme labels. Microarray ECoG from each of these subjects contained enough information to predict several phonemes from each category above chance levels (10% for consonants, 25% for vowels). Each exemplar indicates the accuracy over all crossfolds and the associated p-value.

6.2.2 Receiver Operating Curve Characteristic

As in the macroscale data diversity analysis, we used the matched filter correlator to evaluate and quantify the amount of information in the neural motif; however in this chapter, it is applied to the microarray ECoG. As a first step, we evaluate the separability of the microarray reference waveforms for each cognitive task and phoneme. Figure 6.7 contains the normalized dot product matrices comparing the relative differences between the neural motifs for each phoneme within a specific cognitive task. Based on the heat maps in these matrices, the reference waveforms between different phonemes were less distinct.

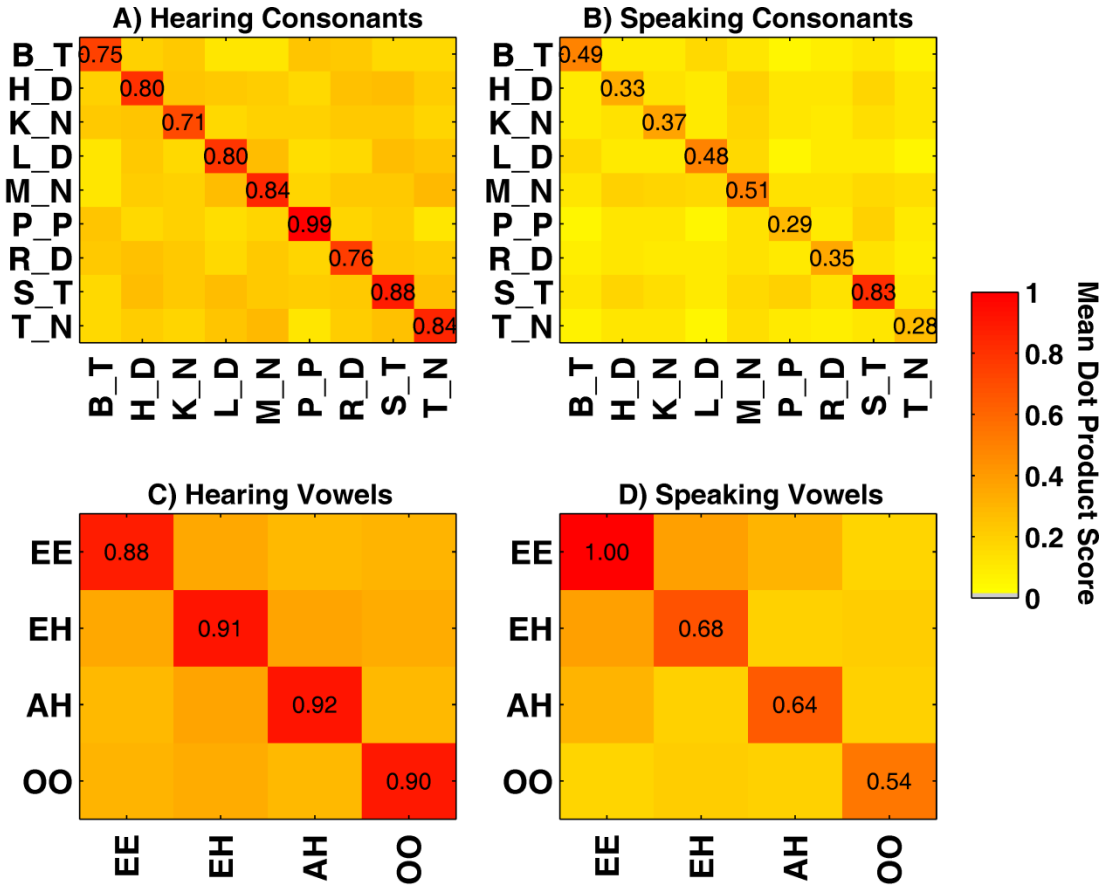

Figure 6.7 Summary of microarray matched filter dot product matrices
The dot products between matched filters representing different phonemes within specific cognitive tasks and phonemic categories reveal specificity in the neural motifs. Shown in the same format as Figure 5.3. For each subject, task and category, matched filters from the training data were created for each phoneme. Pairwise dot products between matched filters for all phonemes were normalized by dividing by the greatest dot product score within a cognitive task and phonemic category. Each panel shows the average normalized dot product score across 10 subjects for each cognitive task and phonemic category.

An exemplar set of dot product matrices from Subject 11's data shows that the neural motifs captured by the matched filter reference waveforms have significant preferences toward specific cognitive tasks and phonemes. Figure 6.8 illustrates that in this subject, the reference waveforms were very distinct for hearing, and for saying vowels. However the speaking consonants matrix reveals that there was a large difference in reference waveform energy between S_T and the other phonemes.

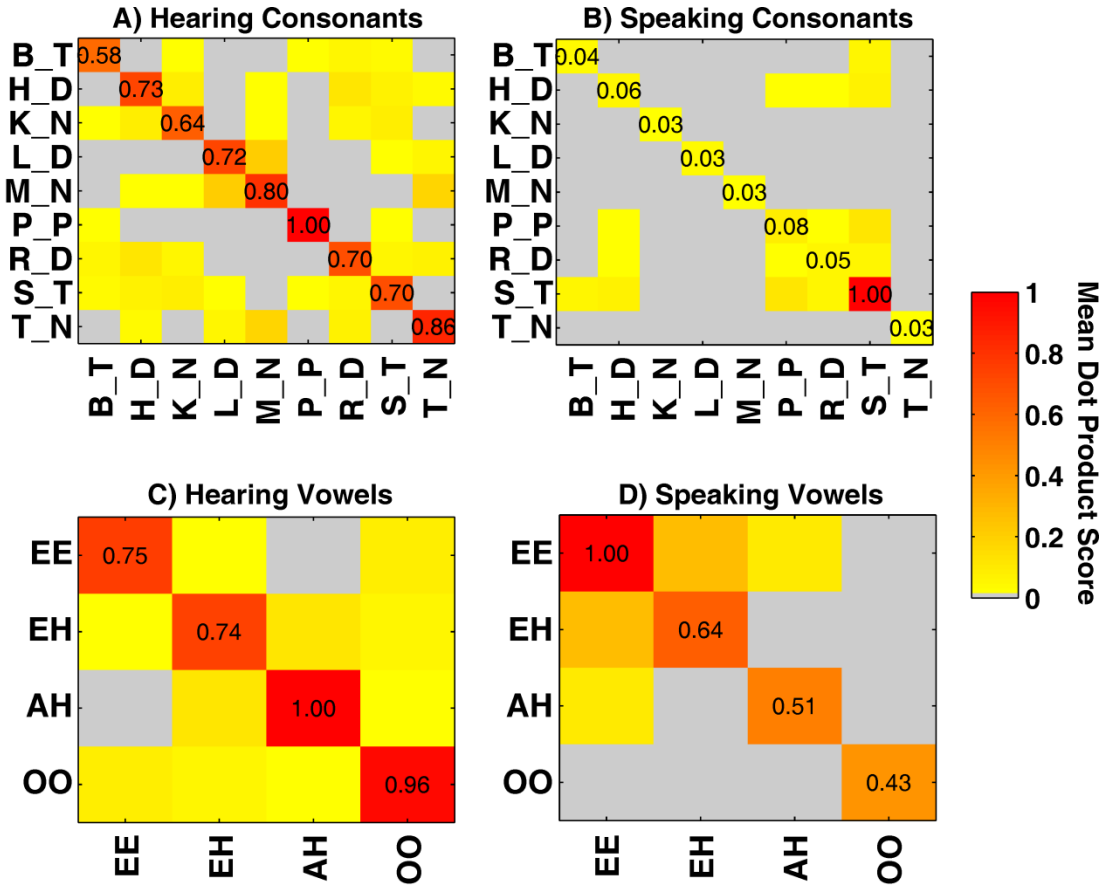

Figure 6.8 Single subject microarray matched filter dot product matrices
Data from Subject 13 only, in the same format as Figure 6.7. This figure shows the differences in response from the microarray data between cognitive tasks and phonemes. While the reference waveforms for hearing appear to be quite diverse, this cortical location appears to have a preferential responses during speaking to vowel sounds and saying the phoneme S_T.

The reference waveforms were used to generate matched filter scores for both training and testing data as before. Then, ROC curves and AUC scores were generated. Exemplar data in Figure 6.9 displays the level of accuracy in the matched filter for a typical subject's microarray data. Even though the test data AUC score is somewhat lower than the training data, the area is still greater than that of the diagonal chance line.

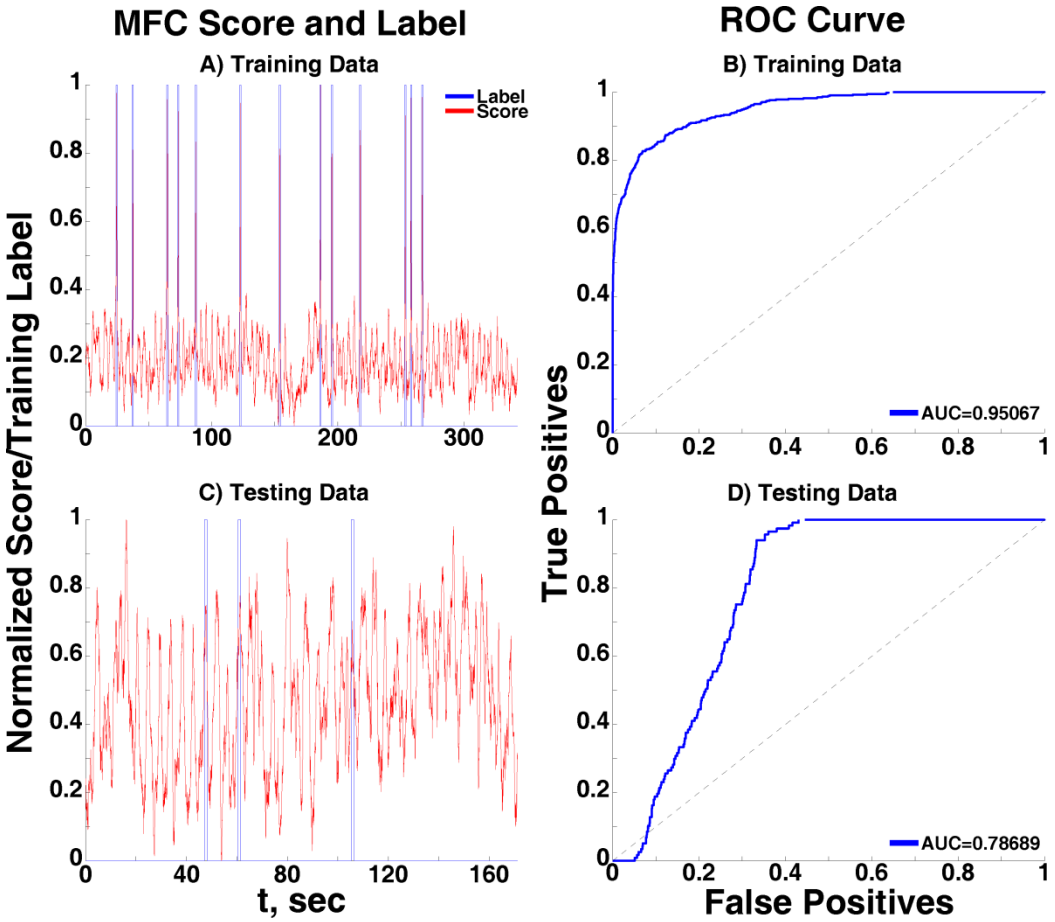

Figure 6.9 Exemplar microarray receiver operating curve analysis
Exemplar data from Subject 11 illustrates that the microarray matched filter for saying the vowel 'EE' has above chance accuracies both the training and testing data. This subject performed three runs of the experiment; therefore two runs were used for training and the other for testing. A) The time course of training scores (**red**) and labels (**blue**) demonstrates the matched filter can localize instances of saying EE phonemes in the midst of hearing and saying all different phonemes. B) ROC for saying EE phonemes on the training data set has an AUC of 95.1%, (above the chance level of 50%). C) Time course of testing scores (**red**) and labels (**blue**) shows that the matched filter continues to localize saying EE phonemes well even on the test data. D) ROC for saying EE words on the testing data has an AUC of 78.7%.

As seen in the macroscale data, there is a rhythmic component in the matched filter score. To determine whether the matched filter was capable of separating phonemic content, a single trial out classification experiment using on the matched filter scores as classifiers as described in Chapter 5. Figure 6.10 contains the results of this experiment, which clearly illustrate the efficacy of the matched filter approach to discriminating phonemic content from within a single cognitive task. The classification performance for the matched filter approach is significantly better than data driven approach reported above. There are two

factors in the data driven approach that could be adversely impacting classification performance. First, information is lost in the dimensionality reduction step. It is possible that approaches besides principal component decomposition may improve performance. Second, the data driven approach was computed using a one run out crossfold validation. Nonstationarity in the cortical signals between runs is also likely decreasing performance. In spite of the relatively poor data driven classification scores, these results show that the matched filter captures a meaningful representation of the neural motif associated with phonemic content within a specific cognitive task. In the following sections we examine how the different dimensions of the matched filter representation (space, time and frequency) encode phonemic correlates.

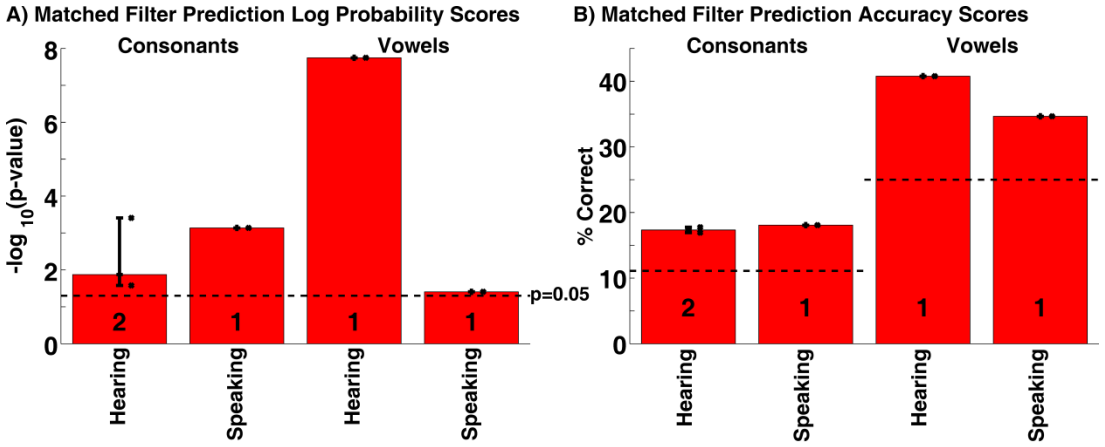

Figure 6.10 Summary of matched filter microarray classification scores
The results of one trial out classification using microarray matched filter scores only. Bars plot the median prediction log probabilities and accuracies for those patients with above chance performance. Error bars illustrate the 95% confidence intervals on the median generated by 100 bootstraps. Digits in each bar indicate the number of subjects (out of 3) that were above chance ($p<0.05$). Individual data points are plotted as a scatter plot with 'x' marks. A) Bars indicate the median negative log probabilities for subjects with p-values < 0.05 for each cognitive task and phonemic category (consonants / vowels). The dashed line shows the threshold at $-\log_{10}(0.05)$. B) Bars show the median accuracy for subjects with p-values < 0.05 for each cognitive activity and phonemic category. Chance accuracies are shown by the dotted lines for each phonemic category. These results show that the matched filter approach applied to microarray data can classify phonemic content within single cognitive tasks without machine learning algorithms.

6.2.3 Analysis of Variance

The full ANOVA on the microarray ECoG matched filter scores provides insight into the specific factors of the matched filter analysis that affected the scores most. Table 6.2 contains the results. Although all single factors were significant ($p<5e-5$), the greatest single factor in affecting the matched filter scores was the specific subject. Because the subjects performed the experiments with different stimulus sets and because subject 12 had no speaking data, the phoneme and cognitive task factors were omitted from the model. This may be the reason the sum of squares for the error term is twice the magnitude of the largest single factor. The single diversity factors with the largest impact on the model were time and channel indicating that even within the microarray data, anatomic location was an important factor. Between the two frequency diversity factors, both appeared to be significant, however diversity in the frequency bands above 60 Hz had a larger impact on the model. It is also interesting that the sum of squares for the interactions between subject and the frequency diversity factors had larger influence than any single factor. Based on the results of the dissociation band analysis in the previous section, this is likely because some subjects in this portion of the study did not have significant power modulations in the high frequency bands. Each of these factors was examined more closely on an individual basis using additional analyses.

Table 6.2 Microarray ECoG Analysis of Variance Results
Abbreviations: <60: frequency bands below 60 Hz, >60: frequency bands above 60 Hz

	Source	Sum Squares	Degrees of Freedom	Mean Squared Error	F Statistic	Prob>F
Single Factors	Subject	162.6394	2	81.3197	6048.7344	0
	<60	0.22222	1	0.22222	16.529	4.8054e-005
	>60	0.61544	1	0.61544	45.7776	1.3529e-011
	Time	1.2652	2	0.63262	47.0555	3.9904e-021
	Channel	1.2187	2	0.60936	45.3256	2.237e-020
Interaction	Subject*<60	2.3541	4	0.58852	43.7756	1.1195e-036

	Subject*>60	3.1751	4	0.79378	59.0433	1.0462e-049
	Subject*Time	1.118	4	0.27949	20.7891	3.9768e-017
	Subject*Channel	0.099613	4	0.024903	1.8524	0.11581
	<60*>60	0.063152	3	0.021051	1.5658	0.19537
	<60*Time	0.7584	4	0.1896	14.1029	1.6914e-011
	<60*Channel	0.45084	4	0.11271	8.3837	9.3715e-007
	>60*Time	0.64845	4	0.16211	12.0583	8.6146e-010
	>60*Channel	0.10463	4	0.026157	1.9456	0.09992
	Time*Channel	0.04613	4	0.011532	0.85781	0.48842
	Error	348.7665	25942	0.013444		
	Total	569.2442	25991			

6.2.4 Spatial Diversity

The first analysis of diversity focuses on the three matched filter variants that contrasted differing levels of spatial diversity. The three reference waveform variants included the single best channel, the optimal number of channels based on the training data and all 12 channels on the microarray. The best and optimal channel variants were selected for each cognitive task, phoneme and crossfold. The results of the ANOVA contrasting these three variants with full diversity in the temporal and spectral dimensions are contained in Table 6.3. These results indicate that over the entire population, spatial diversity was not a significant factor.

Table 6.3 Microarray ANOVA for spatial variants only

Source	Sum Squares	Degrees of Freedom	Mean Squared Error	F Statistic	Prob>F
Subject	12.3711	2	6.1856	511.8304	9.9056e-157
Channel	0.04836	2	0.02418	2.0008	0.13573
Subject*Channel	0.0098322	4	0.0024581	0.2034	0.93656
Error	12.9432	1071	0.012085		
Total	25.3846	1079			

Since only certain subjects had significant power modulations, the ANOVA was repeated for individual subjects as well. In this analysis, only the ANOVA for Subject 13 had a

channel as a significant factor. Therefore a more detailed analysis was carried out on Subject 13's data. The summary of the spatial diversity analysis Figure 6.11 illustrates the results of the analysis of variance on all three subjects as well as a more focused analysis on Subject 13. Since the ANOVA assumes a linear model of the factors with normally distrusted errors, and the actual error histograms were non-Gaussian, we used a nonparametric analysis to compare the AUC scores between the three spatial variants. Figure 6.11A shows that across the three microarray subject, none of the three variants had medians that were significantly above the chance levels ($p<0.05$ Monte Carlo analysis). The right plot in Panel A shows that for Subject 13, all three variants had medians above chance; however, none of the three variants were significantly different from each other. Since these results contained both cognitive tasks, and the normalized spectra during hearing for this subject were stronger and more consistent than the speaking tasks, we studied the tasks separately. Figure 6.11B shows the effect of adding single channels in order of decreasing r^2 as in Chapter 5. The results show that there is a slight inflection in the hearing curves for both individual phonemes as well as general cognitive tasks for either 2 or 3 microarray channels, however the curves are relatively flat. Researches also noted that 4-6 channels (depending on the run) appeared noisy while recording Subject 13's data. Upon closer inspection of intra-operative photos, it appeared that the microarray was situated on top of blood vessels that could have obscured the recordings. Therefore it is not appropriate to draw conclusions regarding the optimal regions that encode phonemic content in microarray data from this data set.

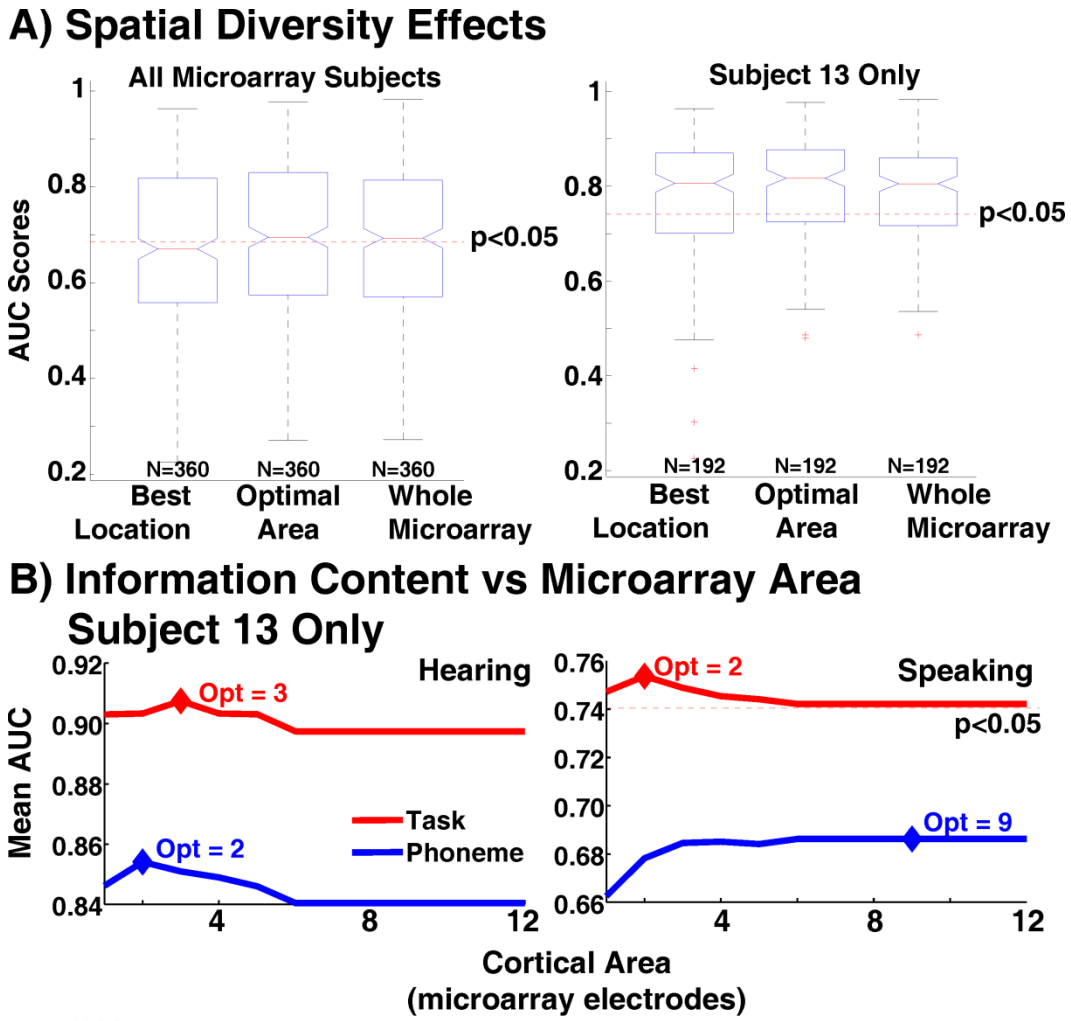

Figure 6.11 Microarray spatial diversity summary
The summary of the spatial diversity analysis are inconclusive in this group of subjects. A). The results of nonparametric Kruskal-Wallis tests showing the range of AUC scores for reference waveform variants contrasting spatial diversity at three levels show that across all subjects (Left), none of the population medians were significantly better than chance. The same test on Subject 12's data reveals that the scores were significantly better than chance, however none of the variants were different from each other. However, several of the channels may have been obscured by blood vessels (see text for details). B) Analysis of the information content as a function of microarray channels included in the matched filter also indicated that spatial diversity plays little if any role in this subject. All hearing tasks were above chance ($p<0.05$, Monte Carlo), however the speaking tasks were either borderline in significance or not significant.

Although the summated AUC scores across cognitive tasks and phonemes were not significant for Subjects 11 and 12, the single subject matched filter dot product matrices showed indications of phoneme and task specificity within the microarray (see Appendix C). Therefore, we performed a single channel matched filter analysis. Here, AUC scores from reference waveforms using single microarray channels were compared to the Monte

Carlo results for random performance ($p<0.05$). The numbers of phonemes or general cognitive tasks with AUC scores above chance were counted for each individual channel. The results in Figure 6.12 show that specific locations in the microarray preferentially encoded specific phonemes and cognitive tasks. For example, in Subject 12, channels 1, 2 and 4 did not predict any single auditory phonemes better than chance; however, these locations were able to predict hearing as a general task above chance. This is consistent with single unit studies in human subjects in which neurons on the STG have been correlated with a variety of different speech parameters, many of which were general auditory responses and not correlated with specific phonemes (Engel, Moll et al. 2005). Additionally, Subject 11's microarray had certain channels that responded preferentially to either hearing or speaking (compare channels 6, 7 and 12). It is interesting that neither Subject 11 nor 12 had very strong normalized power changes during hearing in the dissociation band analysis (see Figure 6.3), yet Subject 12 had several channels that could predict hearing in general above chance. There are two possible sources for this apparent difference. First, the dissociation band analysis did not account for temporal diversity, and instead averaged the power changes over 500ms. This analysis technique may have obscured brief power changes in high frequencies. The second and more likely source of the difference is the use of the low frequency bands (<60 Hz) in the diversity analysis which have been reported in the functional mapping literature as a correlate of cognitive task engagement (Crone, Miglioretti et al. 1998; Leuthardt, Miller et al. 2007; Wu, Wisneski et al. 2010).

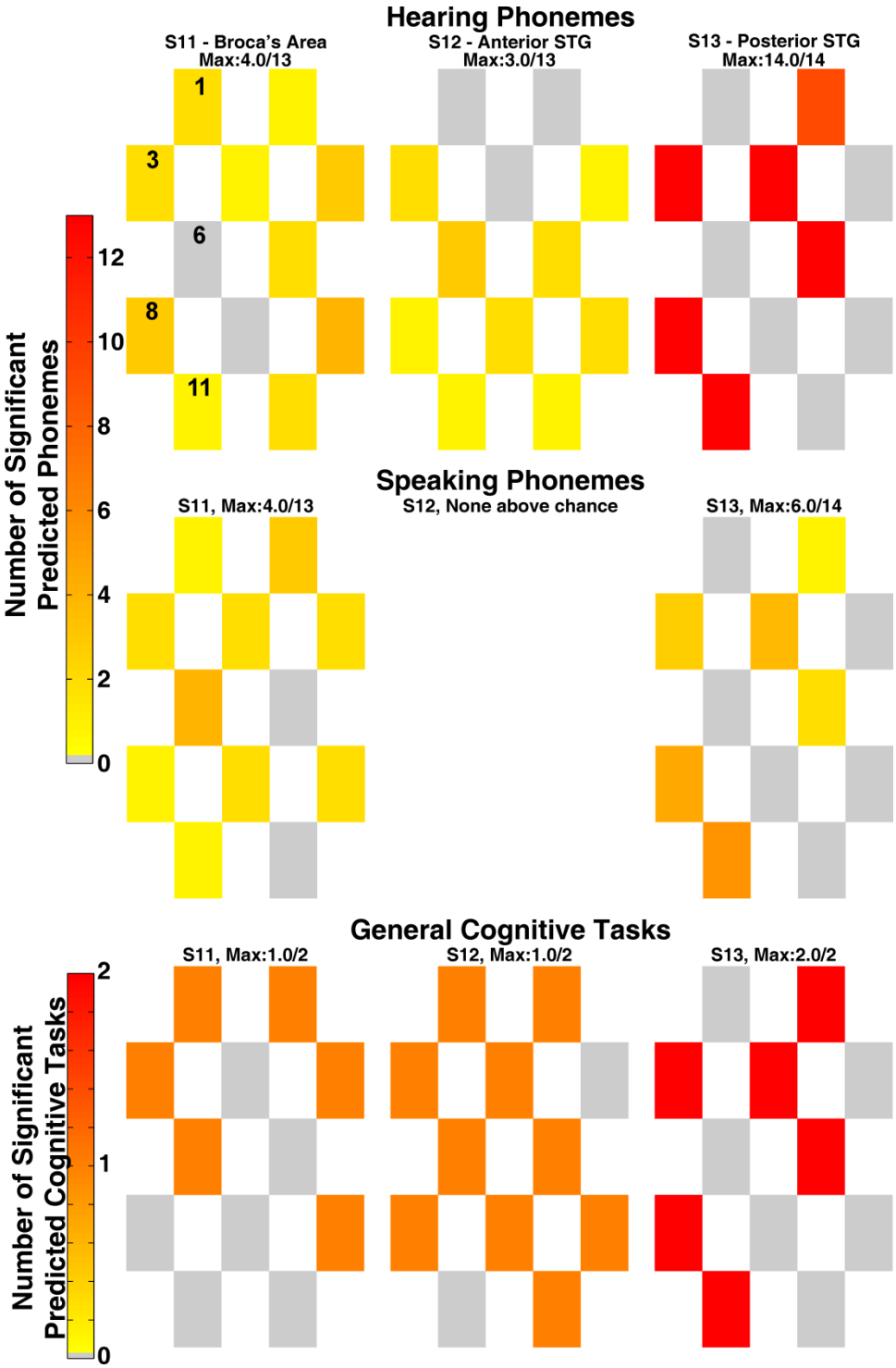

Figure 6.12 Microarray single channel spatial analysis

The results of a single channel matched filter analysis illustrate spatial inhomogeneity in microarray ECoG signals. Rows of microarray plots correspond to cognitive tasks. Columns correspond to the microarrays for specific subjects. Channel numbers are shown for reference in the Subject 11's microarray plot for Hearing. Heat maps for each microarray plot shows the number of phonemes or general cognitive tasks that had above chance ($p<0.05$ Monte Carlo) performance. The maximum for each subject and cognitive task is annotated above each microarray plot. Color bars for phoneme specific tasks and general tasks are separated

to since there were only two general cognitive tasks. Note that microscale anatomy appears to process information preferentially for specific task and phonemes.

In summary, the spatial analysis was for the most part carried out on data from a single subject. In this data set, neither the ANOVA nor the nonparametric score analysis demonstrated a significant difference between the three spatial matched filter reference waveform variants. Because of potential vasculature blockage, the rank order analysis was inconclusive as well. In spite of these difficulties, the single channel analysis did show indications of spatial inhomogeneity even at this small spatial scale across this group of subjects. These diverse patterns of cortical activity in microarray ECoG are consistent with previous reports of spatial patterns in microscale pial recordings correlated with behavior by Freeman et al. (Freeman 1979; Freeman and van Dijk 1987).

6.2.5 Temporal Diversity

The analysis of temporal diversity in microarray ECoG data also started with an ANOVA. Table 6.4 contains the ANOVA on the three matched filter reference waveform variants contrasting different levels of temporal diversity. In this multi-subject analysis, time was a significant factor, however it accounted for much less variance than the subject factor or residuals.

Table 6.4 Microarray ANOVA for spatial variants only

Source	Sum Squares	Degrees of Freedom	Mean Squared Error	F Statistic	Prob>F
Subject	10.7447	2	5.3724	408.8126	9.7465e-133
Time	0.10426	2	0.052131	3.9669	0.01921
Subject*Time	0.0986	4	0.02465	1.8757	0.11242
Error	14.1138	1074	0.013141		
Total	25.1817	1082			

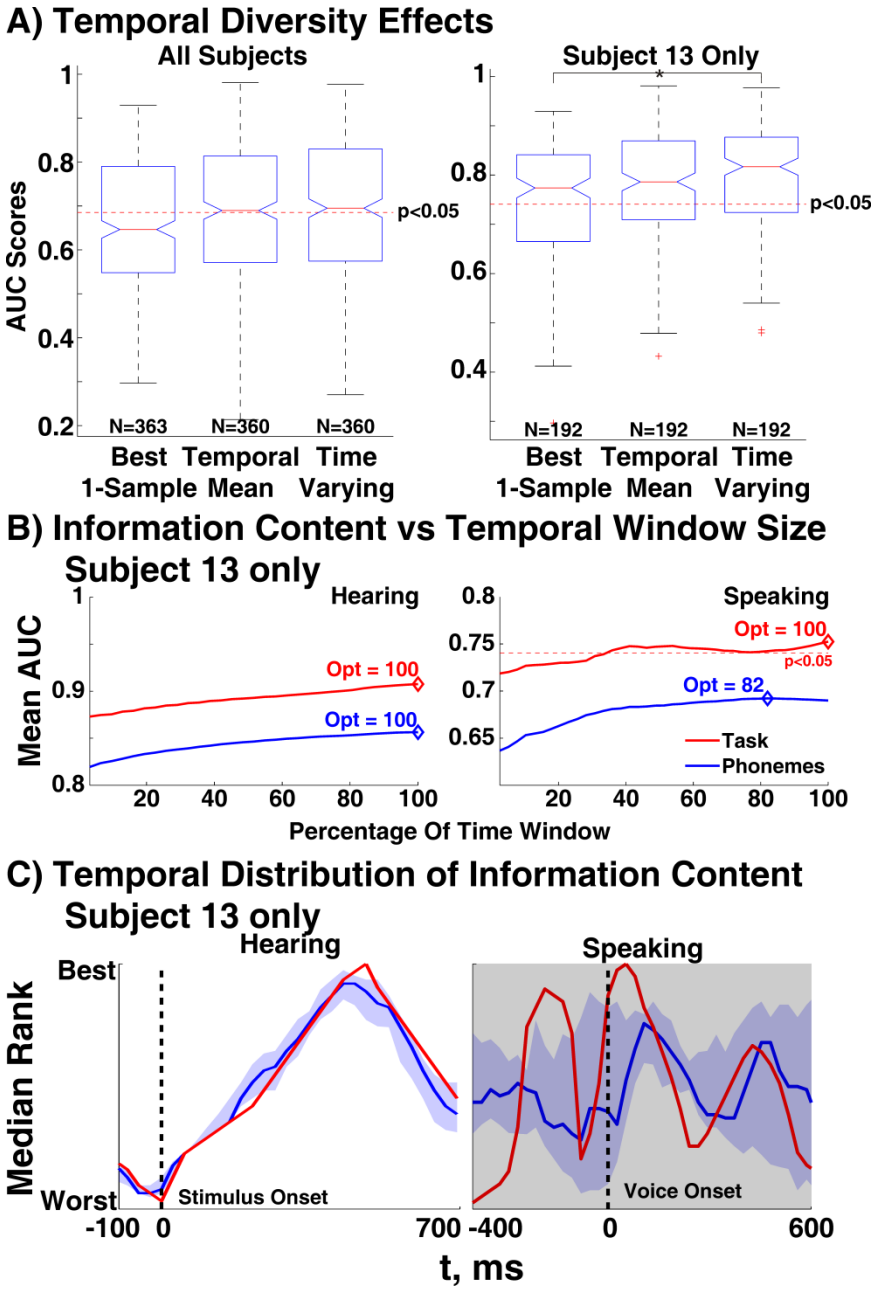

Figure 6.13 Microarray temporal diversity summary

Three different analyses illustrate the presence of temporal diversity in microarray ECoG. A) The results of nonparametric Kruskal-Wallis tests show that the median AUC scores in the analysis of all subjects failed to rise above significance. The data from Subject 13, however, had medians significantly above chance for all three contrasts. Additionally, the medians between the ***Time Varying*** and ***Best 1-Sample*** populations had nonoverlapping confidence intervals. B) Analysis of the information content in the matched filter as a function of the percentage of time samples used to predict phonemic content. When added in decreasing order of correlation (best time sample first), the mean AUC scores for Subject 13 increased throughout the time window for each task. Note that the speaking task AUC scores only rose slightly above chance levels while the speaking phoneme scores did not achieve significance. These results indicate that for this subject, the entire temporal window aided in the prediction outcome. C) Ranking plots reveal the relative amount of information content in specific time samples for each cognitive task. Each line plots the median rank across phonemes for each cognitive task. Color shaded areas show the extent of the 95% confidence intervals on the median (100 bootstraps with resampling). For hearing, the ranks peak toward the end of the window due

to the increasing amount of cortical processing involved as the subject prepares to repeat the stimulus. Although the highest ranks for speaking are just following voice onset as in the macrogrid analysis, note that the ranking plot for speaking is grayed out. The AUC scores were only slightly better than chance for the speaking task, and not better than chance for speaking phonemes.

The summary results in Figure 6.13 provide some significant evidence for temporal diversity. Panel A shows the nonparametric analysis of the three temporal reference waveform variants. As in the spatial analysis, the subject population AUC scores are not significantly better than chance ($p<0.05$ Monte Carlo), therefore, the remaining analyses are performed only on Subject 13's data. The Kruskal-Wallis test on Subject 13's data illustrates that all three spatial variants had above chance AUC Scores and that there was an increasing trend in the scores with increasing amounts of information in the matched filter reference waveforms. Panel B shows that the entire window improves Subject 13's AUC score for both for the hearing task and hearing phonemes. The AUC scores for the speaking task were only slightly above chance and the scores for speaking phonemes did not reach significance. Therefore, it is difficult to draw broad conclusions from this data. Panel C shows the relative ranks of the time samples in the matched filter window have similar shapes to those reported in Chapter 5. There is one additional feature in the ranking plot for hearing in Panel C that deserves comment. In the nonword experiment performed by Subject 13, the stimuli were all normalized to have 500 ms durations. It is clear from the hearing plot in Panel C that the relative ranks peak between 450-480 ms, then gradually drop off as the subject was preparing to say the stimulus words. The time samples at the beginning of the hearing do not reach the rank levels of the time samples at the end of the stimulus until 186 ms after stimulus onset. This seems to indicate that cortical representation of auditory phonemic information is strongest between 200 ms after stimulus onset to 200 ms after stimulus offset. This does not mean that there is no meaningful phonemic encoding at the beginning of the temporal window. The evidence in

Panel B suggests that even in advance of the stimulus, the cortical signals encode information regarding the cognitive task and phoneme. While this may seem counter intuitive, recall that in this analysis, the matched filter is discriminating a specific task and phoneme from all other tasks and phonemes. Since the trial has a regular temporal structure, it is likely that preparatory attention aided in predicting the onset of the specific cognitive task {Gómez, 2006 #604}. While the results are not yet generalizable across multiple subjects or tasks, they represent strong preliminary evidence of temporal diversity in microarray ECoG signals.

6.2.6 Spectral Diversity

Table 6.5 shows the results of the ANOVA contrasting the three spectral variants of the matched filter reference waveforms. The factor accounting for spectral diversity was significant, but accounted for a small amount of variance in the model. The factors for specific subjects and error were three orders of magnitude larger.

Table 6.5 Microarray ANOVA for spectral variants only
Abbreviations: >60: frequency bands above 60Hz

Source	Sum Squares	Degrees of Freedom	Mean Squared Error	F Statistic	Prob>F
Subject	10.8823	2	5.4412	524.4418	1.6299e-159
>60	0.076695	2	0.038348	3.6961	0.025137
Subject*>60	0.064147	4	0.016037	1.5457	0.18676
Error	11.1118	1071	0.010375		
Total	22.2038	1079			

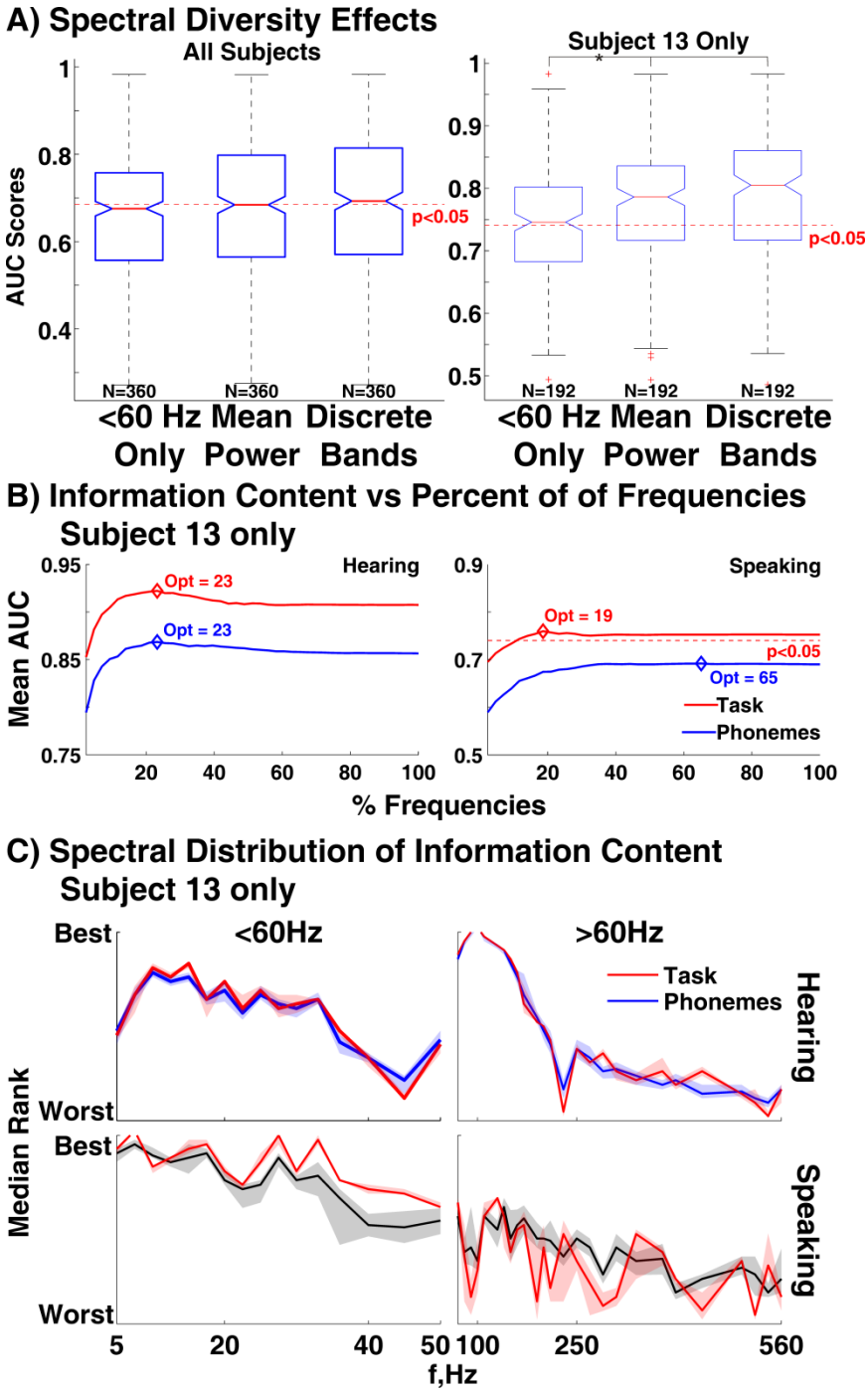

Figure 6.14 Microarray spectral diversity summary

Quantitative results show the extent of microarray diversity in multiple frequency bands above 60 Hz in one subject. A) The results of nonparametric ANOVA tests (Kruskal-Wallis) on all three subjects show that none of the variants were significantly greater than chance ($p<0.05$ Monte Carlo). The analysis of Subject 13's data illustrates a clear trend of increasing AUC score with increasing spectral diversity above 60Hz. The AUC scores using only frequencies less than 60Hz are not significantly greater than chance. The 95% confidence intervals on the medians (100 bootstraps with resampling) for the ***Mean Power*** and ***Discrete Bands*** variants were nonoverlapping with <60 Hz variant. B). Analysis of the information content in the matched filter for Subject 13 as a function of the number of frequency bands used to predict phonemes and general cognitive tasks. When added in decreasing order of correlation (best frequency band first), the mean AUC scores for

cognitive tasks and phonemes increases until approximately 23% the available frequency bands are added to the matched filter. Note again that the speaking task AUC scores are slightly above chance, while speaking phonemes does not reach significance. C) Ranking plots reveal the relative amount of information in specific frequency bands. Each line plots the median rank across phonemes and crossfolds for Subject 13. Shaded areas show the extent of the 95% confidence intervals on the median (100 bootstraps with resampling). The shading and traces for speaking phonemes are grayed out because they did not reach significance. Rank traces for frequencies above and below 60 Hz are plotted separately for readability. For hearing, the top 23% of rankings fall between 10-15 Hz (alpha) and 70-160 Hz (high gamma) ranges, traditionally associated with functional mapping.

The quantitative analyses in Figure 6.14 elucidate the findings from the ANOVA. Panel A contrasts the nonparametric Kruskal-Wallis test on the AUC Scores from all subjects with those from Subject 13 alone. Again, the median scores from the summary across subjects do not reach significance ($p<0.05$, Monte Carlo). The results from Subject 13, however, reveal an increasing trend in AUC score with increasing spectral diversity above 60 Hz. The 95% confidence intervals on the medians for the ***Mean Power*** and ***Discrete Bands*** do not overlap with the chance line, or the ***< 60 Hz*** variant. While the median for the ***Discrete Bands*** variant is higher than the ***Mean Power*** variant, the confidence intervals do overlap. One of the reasons these variants are not more different is that the analysis was performed on both the hearing and speaking tasks. As shown below, the AUC scores for speaking phonemes were not above chance. Using only the scores above chance may reveal a more significant difference between these two variants. Panel B quantifies how many frequency bands helped improve AUC score performance by cognitive task. As the frequency bands were added in order of decreasing r^2, the hearing scores peaked after 23% of the frequencies (10 bands) were included. As discussed previously, the speaking task scores were only slightly higher than the significance threshold while the speaking phonemes scores were significantly above chance. Panel C illustrates specifically which frequencies tend to produce the best AUC scores and therefore encode the most information in microarray ECoG signals. The top ten ranked frequency bands were

between 10-15 Hz and 70-160 Hz in Subject 13. These results are in concert with those from functional mapping studies which highlight the high gamma band as a reliable focal indicator of cortical activity (Crone, Miglioretti et al. 1998; Crone 2000; Leuthardt, Miller et al. 2007; Wu, Wisneski et al. 2010). There curves for both the hearing task and hearing phonemes are very similar and do not appear to reveal any band specificity for phonemes versus tasks. Although the dissociation band results for the microarray data showed consistent high frequency modulations as high as 540 Hz in the dissociation band section of this study, those frequencies were not highly ranked in this analysis. While the ANOVA results and quantitative study of Subject 13's data provide preliminary evidence that spectral diversity in high frequency microarray ECoG signals improves AUC scores, additional patients and further analyses are necessary to generalize conclusions.

6.3 Conclusion

We have examined microarray ECoG signals in the context of auditory single word repetition paradigms in three cortical areas associated with speech with the goals of determining: 1) whether spectral diversity could dissociate cognitive tasks and anatomic locations, and 2) whether the spatio-temporal dynamics of spectral diversity in frequency bands above 60 Hz contain signals correlated with phonemic content. Although these results must be considered preliminary, in one subject the results clearly support both of our original hypotheses. In Subject 13, we reported several anatomic locations within a 3 mm x 3 mm microarray, some separated by only 1 mm, which were dissociated by nonuniform power modulations in different frequency bands above 60 Hz. The anatomic dissociations were present at the strongest statistical test ($p<0.001$, FDR corrected) and in bands as high as 550 Hz.

In that same subject, using the matched filter correlator as a foundation for the diversity analysis, we reported evidence that supports spatial, temporal and spectral diversity above 60 Hz. Most notably, we found the matched filter reference waveforms to be a consistent and predictive indicator of the neural motif associated with phonemic content. Spatially, while we were unable to quantify the optimal microarray region associated with phonemic content, we have reported several inhomogeneities between cognitive task and phoneme representation in ECoG microarrays. Temporally, we showed in that subject, all samples were beneficial in identifying auditory phonemic information. The best samples were in the window from 200 ms post stimulus onset to 200 ms post stimulus offset, peaking at approximately 480 ms. Spectrally, the preliminary evidence from one subject indicates that treating the frequencies above 60 Hz as discrete bands yields a slight, though not statistically significant, improvement in AUC Scores. The optimal frequency bands during hearing for this subject appear to be in the alpha (10-15 Hz) and high gamma ranges (70-160 Hz). In summary, as preliminary results, these findings are encouraging and justify gathering additional microarray data to study the spectral diversity in microarray ECoG.

6.4 References

Binder, J., J. Frost, T. Hammeke, P. Bellgowan, J. Springer, J. Kaufman and E. Possing (2000). "Human temporal lobe activation by speech and nonspeech sounds." Cerebral Cortex **10**(5): 512.

Binder, J. R., R. H. Desai, W. W. Graves and L. L. Conant (2009). "Where is the semantic system? A critical review and meta-analysis of 120 functional neuroimaging studies." Cereb. Cortex **19**(12): 2767-2796.

Binder, J. R., J. A. Frost, T. A. Hammeke, R. W. Cox, S. M. Rao and T. Prieto (1997). "Human brain language areas identified by functional magnetic resonance imaging." J. Neurosci. **17**(1): 353-362.

Creutzfeldt, O., G. Ojemann and E. Lettich (1989). "Neuronal activity in the human lateral temporal lobe. Ii: Responses to the subjects own voice." Experimental Brain Research **77**(3): 476-479.

Crone, N., D. Miglioretti, B. Gordon and R. Lesser (1998). "Functional mapping of human sensorimotor cortex with electrocorticographic spectral analysis. Ii. Event-related synchronization in the gamma band." Brain **121**(12): 2301-2315.

Crone, N. E. (2000). "Functional mapping with ecog spectral analysis." Neocortical Epilepsies **84**: 343-351.

Crone, N. E., D. L. Miglioretti, B. Gordon, J. M. Sieracki, M. T. Wilson, S. Uematsu and R. P. Lesser (1998). "Functional mapping of human sensorimotor cortex with electrocorticographic spectral analysis. I. Alpha and beta event-related desynchronization." Brain **121**(12): 2271-2299.

Demonet, J.-F., G. Thierry and D. Cardebat (2005). "Renewal of the neurophysiology of language: Functional neuroimaging." Physiol. Rev. **85**(1): 49-95.

Engel, A. K., C. K. Moll, I. Fried and G. A. Ojemann (2005). "Invasive recordings from the human brain: Clinical insights and beyond." Nature reviews. Neuroscience **6**(1): 35-47.

Flinker, A., E. Chang, N. Barbaro, M. Berger and R. Knight (2010). "Sub-centimeter language organization in the human temporal lobe." Brain and Language.

Freeman, W. (1979). "Eeg analysis gives model of neuronal template-matching mechanism for sensory search with olfactory bulb." Biological cybernetics **35**(4): 221-234.

Freeman, W. J., L. J. Rogers, M. D. Holmes and D. L. Silbergeld (2000). "Spatial spectral analysis of human electrocorticograms including the alpha and gamma bands." Journal of Neuroscience Methods **95**(2): 111-121.

Freeman, W. J. and B. W. van Dijk (1987). "Spatial patterns of visual cortical fast eeg during conditioned reflex in a rhesus monkey." Brain Research **422**(2): 267-276.

Leuthardt, E., K. Miller, N. Anderson, G. Schalk, J. Dowling, J. Miller, D. Moran and J. Ojemann (2007). "Electrocorticographic frequency alteration mapping: A clinical technique for mapping the motor cortex." Neurosurgery **60**(4): 260.

Petersen, S. and J. Fiez (1993). "The processing of single words studied with positron emission tomography." Annual Review of Neuroscience **16**(1): 509-530.

Wu, M., K. Wisneski, G. Schalk, M. Sharma, J. Roland, J. Breshears, C. Gaona and E. Leuthardt (2010). "Electrocorticographic frequency alteration mapping for extraoperative localization of speech cortex." Neurosurgery **66**(2): E407.

7 Summary and Conclusions

The central hypothesis advanced at the start of this work was that the high gamma band in ECoG signals contained behaviorally relevant information in multiple sub-bands above 60 Hz. To that end, we have shown evidence that proves that hypothesis in macroscale subdural recordings through the first two aims. First, we showed that nonuniform power changes in multiple frequency bands above 60 Hz could dissociate either cognitive tasks from the same cortical location or anatomic locations during the same cognitive task. Second, by using the matched filter construct, we showed that adding information in the spatial, temporal and spectral domains of ECoG signals above 60Hz improved the classification of specific phonemes and cognitive tasks. Additionally, we demonstrated that the neural motif captured using the matched filter classified specific phonemes within the context of a single cognitive task at levels better than chance. Finally, in microarray ECoG recordings, we have provided preliminary evidence supporting that our central hypothesis hold in microscale recordings as well. In the following sections we address related findings from the scientific literature and present directions for future studies.

7.1 Discussion

7.1.1 Spatial Diversity

The evidence of spatial diversity in the ECoG signals is not only consistent with studies of human language organization and microscale electrophysiology studies, but may also be an explanatory factor in the presence of dissociation bands.

7.1.1.1 Support from Human Language Studies

Overall, cortical functions reported in human language studies using other modalities support the findings reported here. Studies of human language using a variety of different modalities have shown robust and widespread responses to both receptive and productive speech tasks. Here we examine the consistency of the results we reported with those published from other studies.

The patterns of cortical activity reported in Figure 4.5, Figure 6.3 and Figure 6.4 are consistent with previous studies examining sensorimotor cortex, Broca's area and STG. Sensorimotor cortex had strong activations in all four cognitive tasks. While its role during receptive speech is the subject of much debate (Scott, McGettigan et al. 2009), our findings are in line with likely roles of phonetic encoding, formulation of motor articulatory plans, and other motor control activities (Petersen and Fiez 1993; Salmelin 2007; Towle, Yoon et al. 2008) as well as multisensory integration (Ghazanfar and Schroeder 2006). Broca's area had robust cortical activations during speaking tasks, moderate activations during reading, and minimal activations during hearing. These activations are likely attributable to the grapho-phoneme conversion process during reading (Jobard, Crivello et al. 2003; Salmelin 2007) and late pre-articulatory responses in preparation for speech (Indefrey and Levelt 2004; Towle, Yoon et al. 2008), which may occur late in the hearing phase. The activations in left STG were strongest during hearing and speaking but were minimal during reading. Primary auditory perception, phonological processing (Binder, Desai et al. 2009) and self-monitoring (Demonet, Thierry et al. 2005) are likely the functions causing activations during hearing and speaking. While electrophysiological studies have reported high-frequency power increases during reading associated with lexical and semantic processing (Salmelin 2007; Mainy, Jung et al. 2008), the weaker response during reading in Figure 4.5

is most likely because the read and repeat paradigm used here required little lexical or semantic processing.

The diversity analyses in Chapters 5 and 6 relied on the ability of the matched filter reference waveforms to discern specific phonemes and cognitive tasks in the context of the trial structure from both macro- and microscale electrophysiology. Previous studies have also reported electrophysiological correlates of phonemic activity. Single unit studies in human temporal lobe have identified neurons that fired preferentially for specific phonemic combinations during both perceptive and productive speech (Creutzfeldt, Ojemann et al. 1989; Creutzfeldt, Ojemann et al. 1989; Engel, Moll et al. 2005). Several studies using macroscale subdural recordings have also reported electrophysiological correlates of phonemic processing and production in the temporal lobe (Liégeois-Chauvel, de Graaf et al. 1999; Flinker, Chang et al. 2010) and inferior frontal cortex (Blakely, Miller et al. 2009). Studies using MEG have also phonemotopic organization in the human temporal lobe (Shestakova, Brattico et al. 2004). It is interesting that this research implicated a relative large cortical area (as much as 18-24 cm2) that included posterior STG, middle temporal gyrus, angular gyrus, sensorimotor and premotor cortex during hearing phonemes. While these results could be used to support the motor representation of speech theory (Scott, McGettigan et al. 2009), it is important to remember that the matched filter analysis was used in the context of an auditory word repetition task. It is not clear when pre-articulation coding and motor planning begin in this experimental paradigm. In order to more clearly test the motor representation of speech hypothesis, the analysis should be repeated using a passive hearing paradigm or auditory discrimination task requiring a non-verbal response.

7.1.1.2 Support from Microscale Pial Recordings

Ours is not the first report of spatial diversity correlated with specific behaviors. Several microscale electrophysiological studies in animals have reported that spatial patterns of power modulation have been correlated with olfactory (Freeman 1979; Freeman and Baird 1987), visual (Freeman and van Dijk 1987), and barrel cortex sensory processing (Simons 1985). Additionally, a study of a single human subject with an ECoG microarray reported the single electrodes spaced 1mm apart responded distinctly during spoken words (Kellis, Miller et al. 2010). While the results of the spatial analysis in Chapter 6 were not quantitatively conclusive, there was preliminary evidence of spatially diverse cognitive task and phonemic representation in three subjects. Additionally, we reported the presence of multi-electrode dissociation bands in microarray ECoG signals. This phenomena indicated that different microscale cortical areas, separated by as little as 1 mm, had evoked power changes in different frequency bands independent enough to dissociate the two locations during the same cognitive task. This could be indicative of a columnar tuning phenomenon in which specific cortical locations have preferred or resonant frequencies. If this is the case, it may account for the single electrode dissociation bands reported in macroscale recordings in Chapter 4. Since the results of Chapter 6 are still considered preliminary, this hypothesis will need to be tested with additional data.

7.1.2 Temporal Diversity

In the matched filter analysis of the macro- and microscale ECoG there was strong evidence for temporal diversity. In addition to the neural correlates of specific phonemes reported above, there is other evidence of temporal coding of language. Single unit and macroscale recordings from temporal cortex have been correlated with voice onset time,

which is a subtle temporal parameter that differentiates phonemes (Liégeois-Chauvel, de Graaf et al. 1999; Mukamel, Gelbard et al. 2005). Single unit studies of auditory working memory in human temporal lobe have also reported a spatially and temporally distributed cycle of encoding (Ojemann, Schoenfield-McNeill et al. 2008). Given that speech is constructed from temporally sequenced blocks of phonemes and syllables (Doupe and Kuhl 1999), and the prevalence of neural correlates of these speech parameters, it is not surprising that time varying information in a broad window yielded the greatest AUC scores.

The presence of temporally diverse power modulations correlated with phonemic content may also explain the apparent differences in the microarray study between the dissociation band and matched filter studies. While it was reported that the normalized spectra for Subjects 11 and 12 were not significant during hearing (see Figure 6.3), the single channel matched filter analysis in Figure 6.12 revealed that there were several electrodes capable of discerning specific phonemes and cognitive tasks at above chance levels. While these appear to be in conflict, temporal diversity and phonemic correlation could explain the difference. If power modulations are only correlated with specific phonemes and not to speech in general (Creutzfeldt, Ojemann et al. 1989), and they only occur in a brief temporal window corresponding to the presence of that phoneme (Mesgarani, David et al. 2008), then averaging the spectral power change over all phonemes and a broad temporal window, as done in the dissociation band analysis, may not necessarily be significant.

7.1.3 Spectral Diversity

This dissertation presents evidence of spectral diversity in ECoG using both the dissociation band and matched filter analyses. The presence of dissociation bands showed

that sub-band power modulations were independent enough to dissociate cognitive tasks and anatomic locations. In the diversity analysis, the matched filter reference waveforms that used discrete bands above 60 Hz significantly improved AUC scores compared to variants that used the average power in all bands above 60 Hz. This evidence supports the hypothesis that there are nonuniform power modulations in the high gamma band in contrast to the hypothesis that high gamma band power modulation is strictly uniform. These findings are consistent with previously published results from many modalities and significantly alter the perspective on the extent and nature of high-gamma band power changes in macro-scale electrophysiology.

7.1.3.1 Evidence in Previously Published Literature

Previous studies have demonstrated that physiologically relevant cortical power changes can occur at various high frequencies. Single-unit local field potential recordings in rodents have reported gamma oscillations up to 150Hz (Sirota, Montgomery et al. 2008). Macroscale recordings from ECoG, EEG and MEG have also reported the independence of cortical power changes between low-gamma (roughly 30-60Hz) and high-gamma (>60Hz) bands (Herculano-Houzel, Munk et al. 1999; Crone, Boatman et al. 2001; Edwards, Soltani et al. 2005; Wyart and Tallon-Baudry 2008). Our results (Figure 4.4 and Figure 4.5) further extend this subparcellation to the high-gamma band above 60Hz. While many studies have identified unitary power changes in the high-gamma band associated with cognitive behavior, the results presented here show that there is behavioral information encoded in sub-bands above the 60Hz marker.

Gamma band activity has been attributed to a variety of cellular mechanisms, both normal and pathologic. Low-gamma (30-60Hz) oscillations are purportedly caused by alternating

excitatory and inhibitory post synaptic potentials (Sukov and Barth 1998). The physiological underpinnings of oscillations between 60-200Hz are less clear. Single-unit studies in non-human primate somatosensory cortex have correlated local field potentials between 60-200Hz and average firing rates (Ray, Crone et al. 2008). EEG studies in primate primary visual cortex have shown gamma power (30-100Hz) coupled to delta phase (2-4Hz) can predict multiunit firing rates (Whittingstall and Logothetis 2009). Higher frequency oscillations (up to 600Hz) caused by peripheral nerve stimulation have been reported in non-human primate epidural and single-unit recordings (Baker, Gabriel et al. 2003) and human scalp EEG/MEG (Curio 2000). Higher oscillatory frequencies (200-600Hz) appear to be correlated with summated action potential spiking (Jones, MacDonald et al. 2000; Baker, Gabriel et al. 2003). It may be that the 60-200Hz range of the high-gamma band power increases are associated with asynchronous increases in multiunit firing rates, while gamma band power above 200Hz indicates synchronous firing activity. In addition to natural physiological processes, evidence of high-frequency "fast ripples" (250-500Hz) have been reported in human epileptic hippocampus (Bragin, Wilson et al. 2002). Since all subjects in this study underwent treatment for epilepsy, it is possible that some power change patterns in our data are pathologies of the disease. However, the strength of the statistical tests used to correlate power changes with specific cognitive tasks as well as the single-trial and time-course data indicate that these high-frequency power changes are not random occurrences. Taken together, these studies show that there are physiological bases for power changes between 60-500Hz.

7.1.3.2 Absence in Previously Published Literature

There are several legitimate reasons that previous ECoG studies have not identified distinct, non-uniform high-gamma power change patterns that dissociate cognitive tasks or locations. Choice of behavioral task, data collection method, or analysis technique could obscure these differences. Many ECoG studies of language utilize experimental paradigms designed to illuminate cortical changes caused by subtle differences in cognitive behaviors (e.g., phonological processing, semantic processing, lexical processing, etc.). The paradigms often focus on cortical responses to input stimuli with relatively simple behavioral responses (e.g., button press) (Mainy, Jung et al. 2008) or passive stimulation alone (Edwards, Soltani et al. 2005). While differences in high-gamma activity may have been present, they may have been subtle or considered irrelevant. Additionally, studies of relatively simple motor tasks (e.g., hand clasping, finger movements) that have reported uniform power increases correlated with movement (Miller, Zanos et al. 2009) may involve different physiologies. Functional imaging studies of finger movements implicate much smaller regions of BOLD signal change (Cunnington, Windischberger et al. 2002) than those for the language tasks studied here (Church, Coalson et al. 2008). The difference between a more focal versus a more networked cortical process may result in genuinely different electrophysiological responses. Thus, broadband responses to motor tasks may also be behavior- and location-specific, but may not necessarily generalize to other tasks or cortical areas.

Signal-to-noise ratios and frequency analysis techniques may also explain why other research has not reported the high-frequency behavior shown here. The raw power spectral density of electrical cortical activity drops off geometrically in proportion to the observation frequency (Nunez and Srinivasan 2006); therefore, when analyzing high

frequencies, practices that improve signal-to-noise ratio are critical. Recordings for this work used intracranial and non-cortical (skull-facing) reference electrodes, which are less susceptible to noise than scalp or cortical electrodes. Biosignal amplifiers used in this study have 24-bit analog to digital converters. Equipment with lower precision (using fewer bits) will have higher quantization noise levels, which may obscure low power fluctuations at high frequencies. Linear time-frequency analysis techniques (wavelet and Fourier transforms) inherently trade time resolution for frequency resolution (Hlawatsch and Boudreaux-Bartels 1992). Selecting analysis parameters that favor fine time resolution can obscure narrowband changes because of coarse frequency resolutions at higher ranges.

7.1.3.3 Alternative Explanations

While there is agreement between our results and corresponding findings in microscale high-gamma studies and language studies from multiple modalities, we acknowledge there are possible alternative explanations. The normalization technique used here removes noise characteristics that may change over time; however, as a result the ITI spectra are explicitly included in the comparisons between tasks. Therefore it is possible that some of the dissociation band phenomenon reported here could also have been caused by differences in the ITI spectra either between experimental tasks (single electrodes) or between pairs of electrodes during the same cognitive task. There is a finite precision in the electrode registration method used here (approximately 1cm) that directly affects Brodmann area assignment (Miller, Makeig et al. 2007). Additionally, it is well known that there are significant individual differences in the organization of cortical language areas (Ojemann, Ojemann et al. 1989). Regardless of possible inaccuracies in Brodmann area categorization or subject-specific differences in functional anatomy, the vast agreement

between the existing language literature and our results supports the credibility of the results presented here and amplify the dissociation band findings.

7.1.4 Neural Motifs Captured by Matched Filters

One of the most striking findings of this research was the predictive value of the matched filter. We used the matched filter correlator in two different contexts to classify specific behaviors. We first showed that matched filter reference waveforms discriminated phonemic content within a specific cognitive task. The matched filter scores in the ROC analysis also demonstrated significant sensitivities and specificities to combinations of cognitive tasks and phonemes. The AUC scores revealed that these combinations could be reliably detected over the course of the testing data using the matched filter construct. Given the evidence of spatial, temporal and spectral diversity reported in this dissertation, these findings indicate that the matched filter reference waveforms are a reliable representation of the multi-dimensional neural motifs associated with specific phonemes and tasks. We have shown that the matched filter is capable of identifying fine grained cognitive processing (saying or hearing a specific phoneme) on a fine time scale.

Other studies have identified neural correlates of relatively detailed cognitive processing using other modalities as well. Studies of object representation have revealed neural correlates of object representation in specific inferior and ventral temporal lobe locations using functional imaging (Haxby, Gobbini et al. 2001), and electrophysiology (Hung, Kreiman et al. 2005). Studies of semantic representation have shown spatially diffuse BOLD correlations with different categories as well (Mitchell, Shinkareva et al. 2008). A recent EEG study has even applied the matched filter construct to classify imagined consonant-vowel combinations using multiple electrodes and temporal envelopes of the

theta, alpha and beta frequency bands (D'Zmura, Deng et al. 2009). The results reported here are novel in two respects. First it is the first study the author is aware of, that has shown the ability to classify specific phonemic content from whole words. Additionally, it is the first time that specific combinations of tasks and phonemes were detected from data including multiple tasks (hearing, speaking, resting) and phonemes embedded in words.

7.2 Future Research

While we believe these findings to be significant, they also inspire further questions that remain to be answered. There is still research to be done to explore spectral power modulations, the diversity in neural motifs, and microarray ECoG.

While we have shown that there are indeed nonuniform power changes in frequencies above 60 Hz, the phenomena still has many avenues to examine. There is a need to identify the specific cortical areas in which dissociation bands occur. It may be that they occur in associative areas, and that spectral nonuniformities are a sign of information integration. The search for dissociation bands should also be expanded to other types of cognitive tasks (motor, attention, semantic, spatial navigation, mental computation). This study may also help shed light on the specific cortical areas that exhibit dissociations. On a finer scale, research could be done to identify the bandwidths of the dissociation bands and any correlations with cortical areas or tasks. Finally, further research should seek to identify reasons for subject specificity in high frequency diversity.

Using the matched filter construct, we identified a portion of the neural motif correlated with specific cognitive tasks and phonemes; however, there are several open directions for research in this area as well. The matched filter construct implemented for this research used only the amplitude of power modulations. However, it has been shown that there are

various phase-related phenomena associated with auditory stimuli (Edwards, Soltani et al. 2005; Canolty, Soltani et al. 2007). An adaptation of the matched filter to account for phase synchrony should be explored as well. Application of the matched filter to other cognitive tasks is another opportunity. Previous work in non-human primates used a similar construct and illustrated robust and stable features correlated with motor kinematics (Chao, Nagasaka et al. 2010). This work could be expanded in humans, as well as adaptation to semantic and object representation. Given the classification performance and the sensitivity and specificity of the matched filter, it also seems appropriate to use the matched filter in the context of an online BCI control algorithm. The study by Chao et al, showed that continuous kinematic information was well correlated with the matched filter (Chao, Nagasaka et al. 2010), and here we show that discrete information is also well detected by the matched filter. The combination of discrete and continuous signals in a BCI could multiply the degrees of freedom and information bit rates achievable. Additionally, since the matched filter is a simple dot product between the reference waveforms and incoming signals, the classification scheme should computationally efficient.

The microarray results we reported in Chapter 6 offer support for the hypotheses we proposed regarding microscale spectral diversity. However, this analysis remains incomplete. In addition, research to improve the recording techniques would aid this study. The addition of a head stage amplifier in close proximity to the microarray would likely improve the signal to noise ratio, and may reveal even more spectral diversity than reported here.

7.3 Conclusion

In conclusion, these findings indicate a new approach is necessary to evaluate high-gamma range macroscale electrophysiology. In addition to time and location of power changes, the specific frequency band within the high-gamma range is another fundamental dimension of cortical electrophysiology. Though the cellular underpinnings of these phenomena require further study, we posit that these distinct, frequency-specific changes represent a mixture of asynchronous increases in multiunit activity as well as synchronous oscillatory activity and action potential firing. Regardless of the source of these spectral nonuniformities, the discovery of frequency diversity in the high-gamma range provides the opportunity to explore the dynamics of these narrow frequency bands and their behavioral and neuronal correlates which may better facilitate the continuing synthesis of cellular, ensemble, and behavioral neuroscience.

7.4 References

Baker, S., C. Gabriel and R. Lemon (2003). "Eeg oscillations at 600 hz are macroscopic markers for cortical spike bursts." The Journal of Physiology **550**(2): 529.

Binder, J. R., R. H. Desai, W. W. Graves and L. L. Conant (2009). "Where is the semantic system? A critical review and meta-analysis of 120 functional neuroimaging studies." Cereb. Cortex **19**(12): 2767-2796.

Blakely, T., K. J. Miller, S. P. Zanos, R. P. N. Rao and J. G. Ojemann (2009). "Robust, long-term control of an electrocorticographic brain-computer interface with fixed parameters." Neurosurgical FOCUS **27**(1): E13.

Bragin, A., C. L. Wilson, R. J. Staba, M. Reddick, I. Fried and J. E. Jr. (2002). "Interictal high-frequency oscillations (80-500hz) in the human epileptic brain: Entorhinal cortex." Annals of Neurology **52**(4): 407-415.

Canolty, R. T., M. Soltani, S. S. Dalal, E. Edwards, N. F. Dronkers, S. S. Nagarajan, H. E. Kirsch, N. M. Barbaro and R. T. Knight (2007). "Spatiotemporal dynamics of word processing in the human brain." Frontiers in Neuroscience **1**: 11.

Chao, Z., Y. Nagasaka and N. Fujii (2010). "Long-term asynchronous decoding of arm motion using electrocorticographic signals in monkeys."

Church, J. A., R. S. Coalson, H. M. Lugar, S. E. Petersen and B. L. Schlaggar (2008). "A developmental fmri study of reading and repetition reveals changes in phonological and visual mechanisms over age." Cereb. Cortex **18**(9): 2054-2065.

Creutzfeldt, O., G. Ojemann and E. Lettich (1989). "Neuronal activity in the human lateral temporal lobe. I. Responses to speech." Experimental brain research. Experimentelle Hirnforschung. ExpÃ rimentation cÃ rÃ brale **77**(3): 451.

Creutzfeldt, O., G. Ojemann and E. Lettich (1989). "Neuronal activity in the human lateral temporal lobe. Ii: Responses to the subjects own voice." Experimental Brain Research **77**(3): 476-479.

Crone, N., D. Boatman, B. Gordon and L. Hao (2001). "Induced electrocorticographic gamma activity during auditory perception." Clinical Neurophysiology **112**(4): 565-582.

Cunnington, R., C. Windischberger, L. Deecke and E. Moser (2002). "The preparation and execution of self-initiated and externally-triggered movement: A study of event-related fmri." Neuroimage **15**(2): 373-385.

Curio, G. (2000). "Linking 600-hz "spikelike" eeg/meg wavelets ("sigma-bursts") to cellular substrates: Concepts and caveats." J Clin Neurophysiol **17**(4): 377-396.

D'Zmura, M., S. Deng, T. Lappas, S. Thorpe and R. Srinivasan (2009). "Toward eeg sensing of imagined speech." Human-Computer Interaction. New Trends: 40-48.

Demonet, J.-F., G. Thierry and D. Cardebat (2005). "Renewal of the neurophysiology of language: Functional neuroimaging." Physiol. Rev. **85**(1): 49-95.

Doupe, A. J. and P. K. Kuhl (1999). "Birdsong and human speech: Common themes and mechanisms." Annual Review of Neuroscience **22**(1): 567-631.

Edwards, E., M. Soltani, L. Y. Deouell, M. S. Berger and R. T. Knight (2005). "High gamma activity in response to deviant auditory stimuli recorded directly from human cortex." J Neurophysiol **94**(6): 4269-4280.

Engel, A. K., C. K. Moll, I. Fried and G. A. Ojemann (2005). "Invasive recordings from the human brain: Clinical insights and beyond." Nature reviews. Neuroscience **6**(1): 35-47.

Flinker, A., E. Chang, N. Barbaro, M. Berger and R. Knight (2010). "Sub-centimeter language organization in the human temporal lobe." Brain and Language.

Freeman, W. (1979). "Eeg analysis gives model of neuronal template-matching mechanism for sensory search with olfactory bulb." Biological cybernetics **35**(4): 221-234.

Freeman, W. J. and B. Baird (1987). "Relation of olfactory eeg to behavior: Spatial analysis." Behavioral Neuroscience **101**(3): 393.

Freeman, W. J. and B. W. van Dijk (1987). "Spatial patterns of visual cortical fast eeg during conditioned reflex in a rhesus monkey." Brain Research **422**(2): 267-276.

Ghazanfar, A. A. and C. E. Schroeder (2006). "Is neocortex essentially multisensory?" Trends in Cognitive Sciences **10**(6): 278-285.

Haxby, J. V., M. I. Gobbini, M. L. Furey, A. Ishai, J. L. Schouten and P. Pietrini (2001). "Distributed and overlapping representations of faces and objects in ventral temporal cortex." Science **293**(5539): 2425-2430.

Herculano-Houzel, S., M. Munk, S. Neuenschwander and W. Singer (1999). "Precisely synchronized oscillatory firing patterns require electroencephalographic activation." Journal of Neuroscience **19**(10): 3992.

Hlawatsch, F. and G. F. Boudreaux-Bartels (1992). "Linear and quadratic time-frequency signal representations." Signal Processing Magazine, IEEE **9**(2): 21-67.

Hung, C. P., G. Kreiman, T. Poggio and J. J. DiCarlo (2005). "Fast readout of object identity from macaque inferior temporal cortex." Science **310**(5749): 863.

Indefrey, P. and W. J. M. Levelt (2004). "The spatial and temporal signatures of word production components." Cognition **92**(1-2): 101-144.

Jobard, G., F. Crivello and N. Tzourio-Mazoyer (2003). "Evaluation of the dual route theory of reading: A metanalysis of 35 neuroimaging studies." Neuroimage **20**(2): 693-712.

Jones, M. S., K. D. MacDonald, B. Choi, F. E. Dudek and D. S. Barth (2000). "Intracellular correlates of fast (>200 hz) electrical oscillations in rat somatosensory cortex." J Neurophysiol **84**(3): 1505-1518.

Kellis, S., K. Miller, K. Thomson, R. Brown, P. House and B. Greger (2010). "Decoding spoken words using local field potentials recorded from the cortical surface." Journal of Neural Engineering **7**: 056007.

Liégeois-Chauvel, C., J. B. de Graaf, V. Laguitton and P. Chauvel (1999). "Specialization of left auditory cortex for speech perception in man depends on temporal coding." Cerebral Cortex **9**(5): 484-496.

Mainy, N., J. Jung, M. Baciu, P. Kahane, B. Schoendorff, L. Minotti, D. Hoffmann, O. Bertrand and J.-P. Lachaux (2008). "Cortical dynamics of word recognition." Human Brain Mapping **29**(11): 1215-1230.

Mesgarani, N., S. David, J. Fritz and S. Shamma (2008). "Phoneme representation and classification in primary auditory cortex." The Journal of the Acoustical Society of America **123**: 899.

Miller, K. J., S. Makeig, A. O. Hebb, R. P. N. Rao, M. denNijs and J. G. Ojemann (2007). "Cortical electrode localization from x-rays and simple mapping for electrocorticographic research: The "location on cortex" (loc) package for matlab." Journal of Neuroscience Methods **162**(1-2): 303-308.

Miller, K. J., S. Zanos, E. E. Fetz, M. den Nijs and J. G. Ojemann (2009). "Decoupling the cortical power spectrum reveals real-time representation of individual finger movements in humans." J. Neurosci. **29**(10): 3132-3137.

Mitchell, T. M., S. V. Shinkareva, A. Carlson, K.-M. Chang, V. L. Malave, R. A. Mason and M. A. Just (2008). "Predicting human brain activity associated with the meanings of nouns." Science **320**(5880): 1191-1195.

Mukamel, R., H. Gelbard, A. Arieli, U. Hasson, I. Fried and R. Malach (2005). "Coupling between neuronal firing, field potentials, and fmri in human auditory cortex." Science **309**(5736): 951-954.

Nunez, P. L. and R. Srinivasan (2006). Electric fields of the brain : The neurophysics of eeg. New York, Oxford University Press.

Ojemann, G., J. Ojemann, E. Lettich and M. Berger (1989). "Cortical language localization in left, dominant hemisphere." Journal of Neurosurgery **71**(3): 316-326.

Ojemann, G. A., J. Schoenfield-McNeill and D. Corina (2008). "The roles of human lateral temporal cortical neuronal activity in recent verbal memory encoding." Cereb. Cortex: bhn071.

Petersen, S. and J. Fiez (1993). "The processing of single words studied with positron emission tomography." Annual Review of Neuroscience **16**(1): 509-530.

Ray, S., N. E. Crone, E. Niebur, P. J. Franaszczuk and S. S. Hsiao (2008). "Neural correlates of high-gamma oscillations (60-200 hz) in macaque local field potentials and their potential implications in electrocorticography." J. Neurosci. **28**(45): 11526-11536.

Salmelin, R. (2007). "Clinical neurophysiology of language: The meg approach." Clinical Neurophysiology **118**(2): 237-254.

Scott, S. K., C. McGettigan and F. Eisner (2009). "A little more conversation, a little less action [mdash] candidate roles for the motor cortex in speech perception." Nat Rev Neurosci **10**(4): 295-302.

Shestakova, A., E. Brattico, A. Soloviev, V. Klucharev and M. Huotilainen (2004). "Orderly cortical representation of vowel categories presented by multiple exemplars." Cognitive Brain Research **21**(3): 342-350.

Simons, D. J. (1985). "Temporal and spatial integration in the rat si vibrissa cortex." Journal of neurophysiology **54**(3): 615.

Sirota, A., S. Montgomery, S. Fujisawa, Y. Isomura, M. Zugaro and G. Buzsáki (2008). "Entrainment of neocortical neurons and gamma oscillations by the hippocampal theta rhythm." Neuron **60**(4): 683-697.

Sukov, W. and D. S. Barth (1998). "Three-dimensional analysis of spontaneous and thalamically evoked gamma oscillations in auditory cortex." J Neurophysiol **79**(6): 2875-2884.

Towle, V. L., H.-A. Yoon, M. Castelle, J. C. Edgar, N. M. Biassou, D. M. Frim, J.-P. Spire and M. H. Kohrman (2008). "Ecog gamma activity during a language task: Differentiating expressive and receptive speech areas." Brain **131**(8): 2013-2027.

Whittingstall, K. and N. K. Logothetis (2009). "Frequency-band coupling in surface eeg reflects spiking activity in monkey visual cortex." **64**(2): 281-289.

Wyart, V. and C. Tallon-Baudry (2008). "Neural dissociation between visual awareness and spatial attention." Journal of Neuroscience **28**(10): 2667.

A. Appendix: Supplemental Dissociation Band Figures

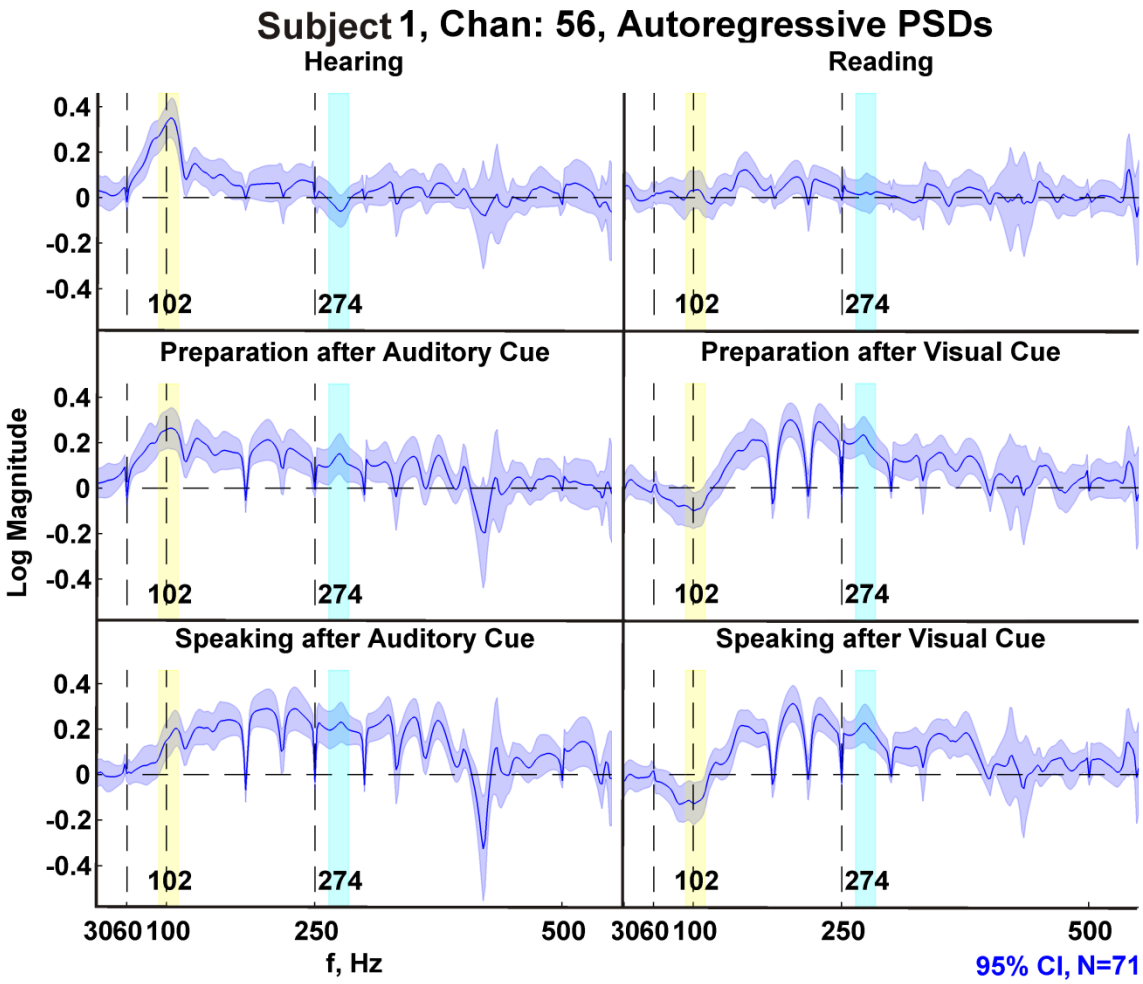

Figure A.1 Single subject autoregressive spectra

Normalized autoregressive spectra for single channel across all six cognitive activities. This data is shown using the same subject, electrode and format as Figure 3.1 in the primary work. The two frequency bands centered at 102Hz and 274Hz illustrate a dissociation band between Hearing and Speaking after the Visual Cue. These six normalized spectra illustrate that power in the two frequency bands of interest is modulated independently and do not reverse as an artifact of signal processing. Consider two examples. While Speaking after the Auditory Cue, both bands have significant power increases. During Reading, neither band is statistically different than rest, but a band centered at 150 Hz has a significant power increase.

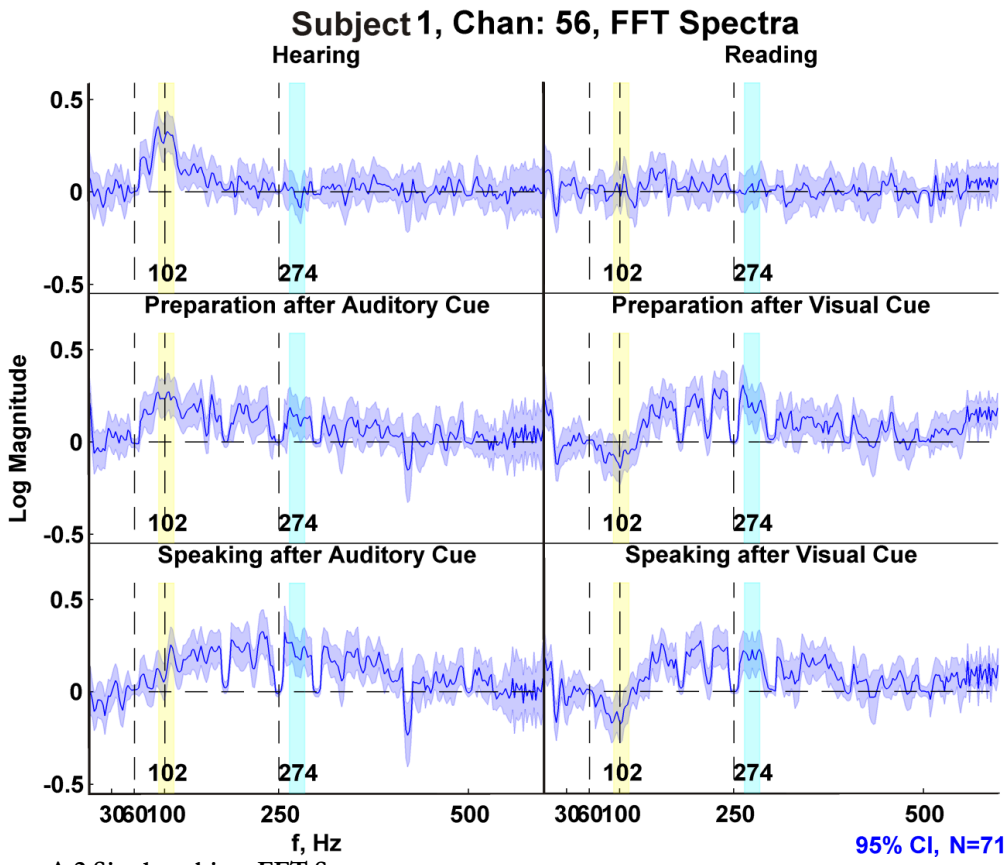

Figure A.2 Single subject FFT Spectra

Normalized Fast Fourier Transform (FFT) spectra for single channel across all six cognitive tasks. The data comes from the same subject, electrode and format as Figure 3.1 from the primary work and **Error! eference source not found.**Figure 1 above. To show that dissociation bands were not signal processing artifacts, normalized spectra are computed with the FFT instead of the autoregressive method. Task PSD estimates used the same sample blocks, window sizes, overlaps, and statistical methods cited in the Materials and Methods section. Individual PSDs were computed using 512-point FFTs with hamming windows. Direct comparison to Figure 1 shows the normalized spectra for each cognitive task are very similar and that the autoregressive spectral estimation method did not introduce the nonuniform high-gamma power changes discussed in this paper as a signal processing artifact.

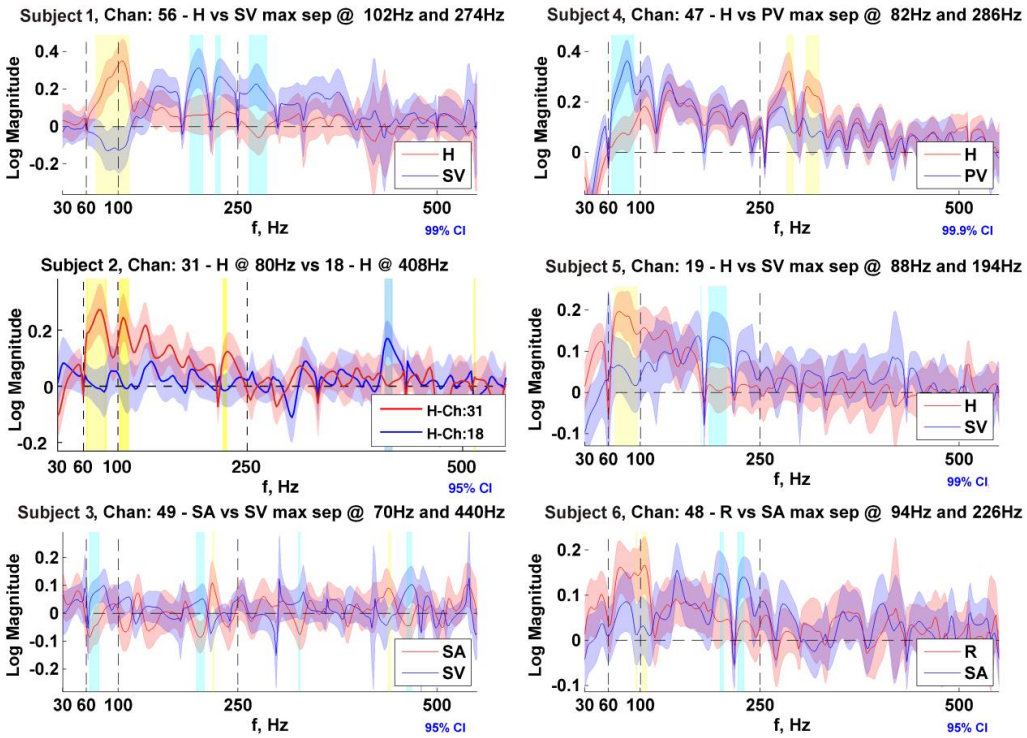

Figure A.3 Exemplar dissociation band normalized spectra

Exemplar individual subject normalized spectra illustrating dissociation bands for all subjects. Subject 2 did not have single electrode dissociation bands, so the exemplar comes from two different electrodes during the same cognitive task. Each plot shows the mean normalized spectra with varying confidence intervals and are in the same general format as Figure 3.2B in the primary work. Markers at 60, 100 and 250Hz outline typical gamma analysis bands. Yellow and blue bands highlight areas where confidence intervals do not overlap. Cognitive Task Key: H=Hearing, R=Reading, PA=Preparation after Auditory cue, PV=Preparation after Visual Cue, SA=Speaking after Auditory Cue, SV=Speaking after Visual Cue.

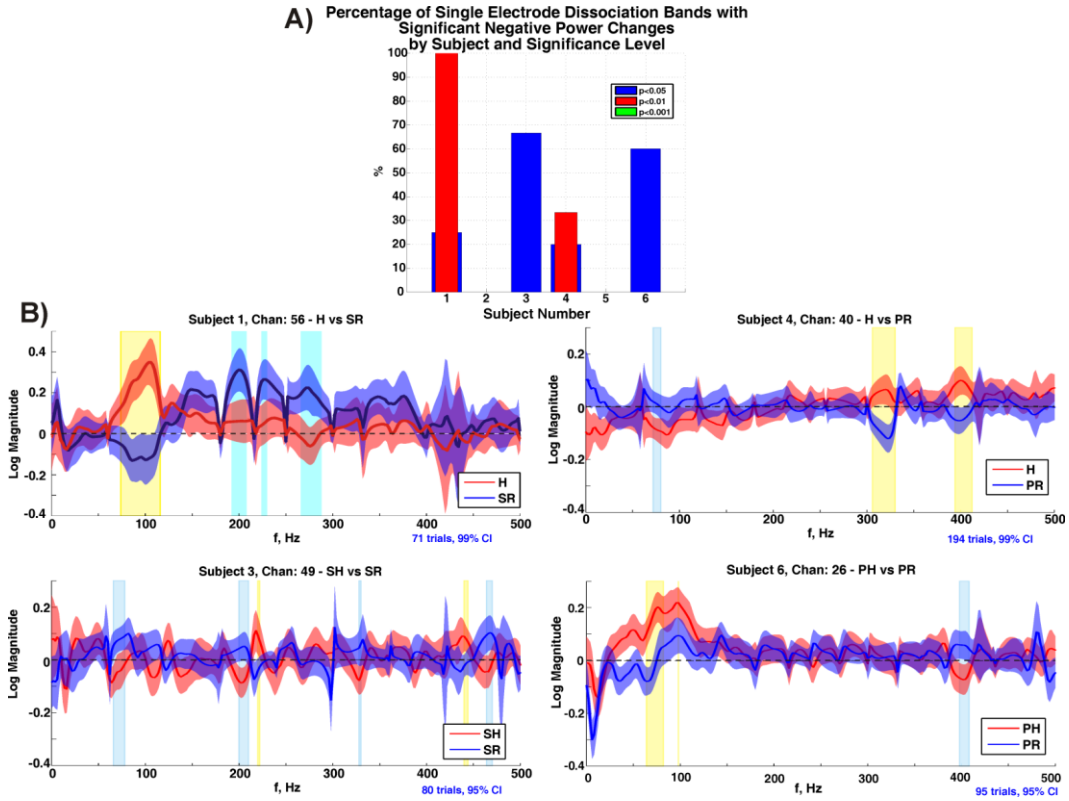

Figure A.4 Dissociation bands with negative power changes

A) The percentage of single electrode dissociation bands from Figure 1.4 of the main work that had statistically significant (confidence interval did not include zero) power decreases compared to the ITI. Subject 2 had no single electrode dissociation bands. B) Exemplar spectra from individual subjects illustrating dissociation bands with significant power decreases. Cognitive Task Key: H=Hearing, R=Reading, PA=Preparation after Auditory cue, PV=Preparation after Visual Cue, SA=Speaking after Auditory Cue, SV=Speaking after Visual Cue.

Table A.1 Kolmogorov-Smirnov test results for cortical activation plots

p-Values for Kolmogorov-Smirnov tests on the consolidated cortical activation plots from Figure 4.5 from the primary work. These values are the results of statistical tests of the null hypothesis that the shapes of the individual cortical activation plots came from the same distribution. Green blocks indicate that the null hypothesis can be rejected at the $p<0.05$ level. Bold lines outline the intra-region comparisons. Note that within STG none of the tests were rejected, in Broca's only one was rejected, and in Sensorimotor only two tests were rejected. This indicates that the spectral patterns of modulated power within each cortical region were generally distinct between cognitive tasks at the $p<0.05$ levels. Additionally, for each cognitive task, at least two cortical regions had activation plots that were statistically different ($p<0.05$).

		Sensorimotor				Broca's				STG		
		Hear	Speak (Aud)	Read	Speak (Vis)	Hear	Speak (Aud)	Read	Speak (Vis)	Hear	Speak (Aud)	Read
Sensori-motor	Hear											
	Speak Aud	1.26E-08										
	Read	6.58E-06	2.34E-04									
	Speak Vis	1.26E-05	5.87E-02	3.78E-01								
Broca's	Hear	7.70E-05	4.72E-08	6.10E-08	4.99E-06							
	Speak Aud	1.27E-18	2.90E-05	4.13E-21	1.18E-10	2.44E-10						
	Read	8.43E-06	2.58E-03	6.43E-01	9.27E-01	1.87E-06	3.09E-17					
	Speak Vis	3.08E-17	1.13E-03	5.01E-16	5.66E-08	6.17E-10	2.05E-01	9.16E-13				
STG	Hear	1.92E-07	1.92E-02	2.71E-02	9.04E-01	1.34E-07	1.42E-28	1.85E-01	5.20E-20			
	Speak Aud	1.17E-04	8.14E-08	2.69E-01	1.51E-02	6.42E-07	4.98E-42	6.14E-02	1.68E-32	2.19E-04		
	Read	1.73E-02	7.14E-12	5.71E-09	4.92E-09	1.04E-01	8.42E-23	2.11E-09	1.39E-21	5.26E-11	2.67E-07	
	Speak Vis	1.30E-09	8.15E-01	3.88E-07	2.28E-03	6.09E-08	2.51E-07	2.20E-05	2.13E-05	2.33E-05	1.01E-12	1.19E-13

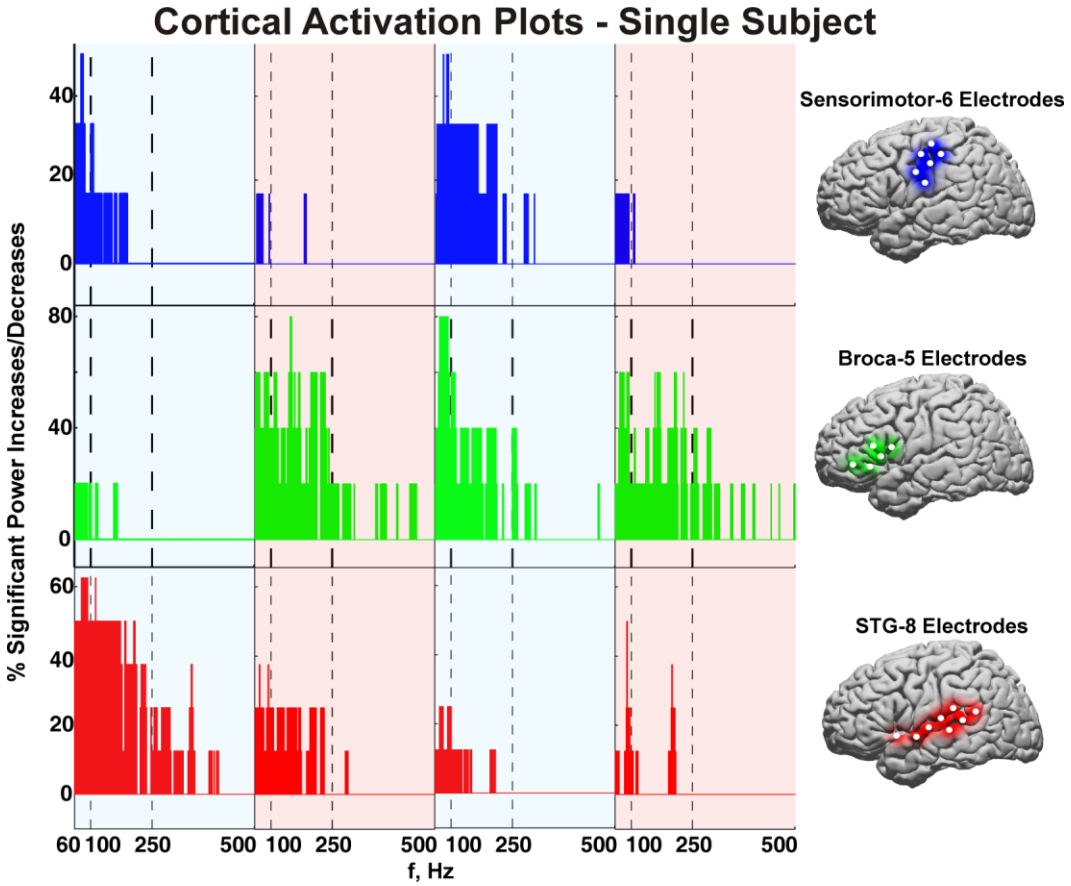

Figure A.5 Single subject cortical activation plot

Individual cortical activation plots for Subject 6 in the same format of Figure 3.5 of the main work. Each plot shows the percentage of electrodes in the region of interest that had statistically significant ($p<0.001$, FDR corrected for multiple comparisons) power changes at each frequency. Rows of activation plots correspond to anatomic locations, columns correspond to cognitive tasks. Markers at 100 and 250Hz outline typical gamma analysis bands. Electrode locations for each cortical region of interest are plotted on the MNI model brain for reference. Multiple peaks per plot, shifts in percentage of cortex active by cognitive task, and changes in active bandwidth within cortical populations are all evidence of nonuniform power changes in these high-gamma bands (60-500Hz).

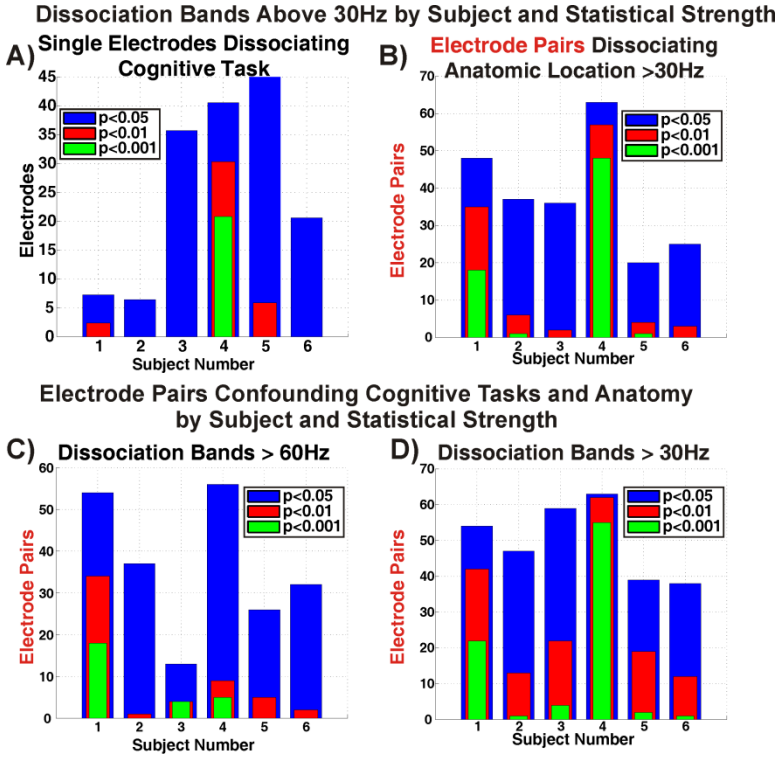

Figure A.6 Summary of dissocation band comparisons

A) & B) contain the numbers of electrodes and electrode pairs respectively between 30-500Hz by subject and p-value as shown in Figure 3.4 of the main work. These results verify the previously reported independence of low-gamma and high-gamma power modulations by showing that the number of dissociation bands increases when the low-gamma range is included. C) & D) report the number of electrode pairs in which dissociation bands confound the combination of cognitive task and anatomic location between 60-500Hz and 30-500Hz respectively. These results show that there are several pairs of electrodes that exhibit the dissociation band phenomena, which do not solely distinguish either cognitive task alone or anatomic location alone.

B. Appendix: Supplemental Information, Spatio-Temporal Dynamics of High Frequency ECoG

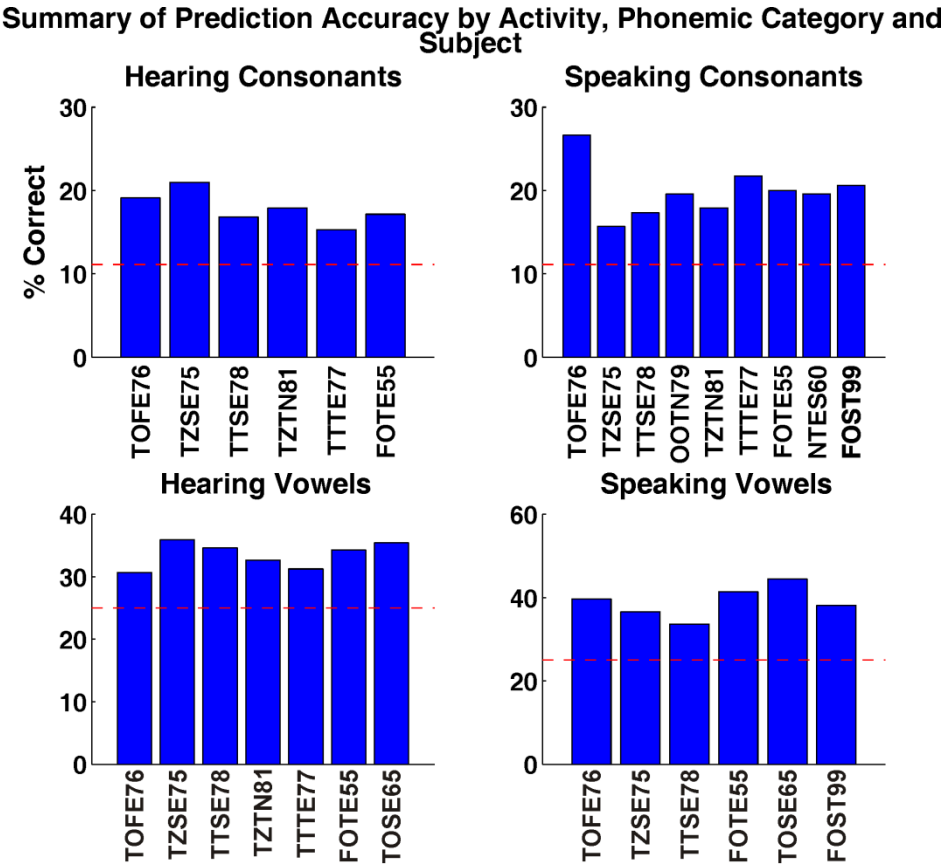

Figure B.1 Classification accuracy by subject
Bars plot the classification accuracy by cognitive task and phonemic category for each subject with above chance accuracy.

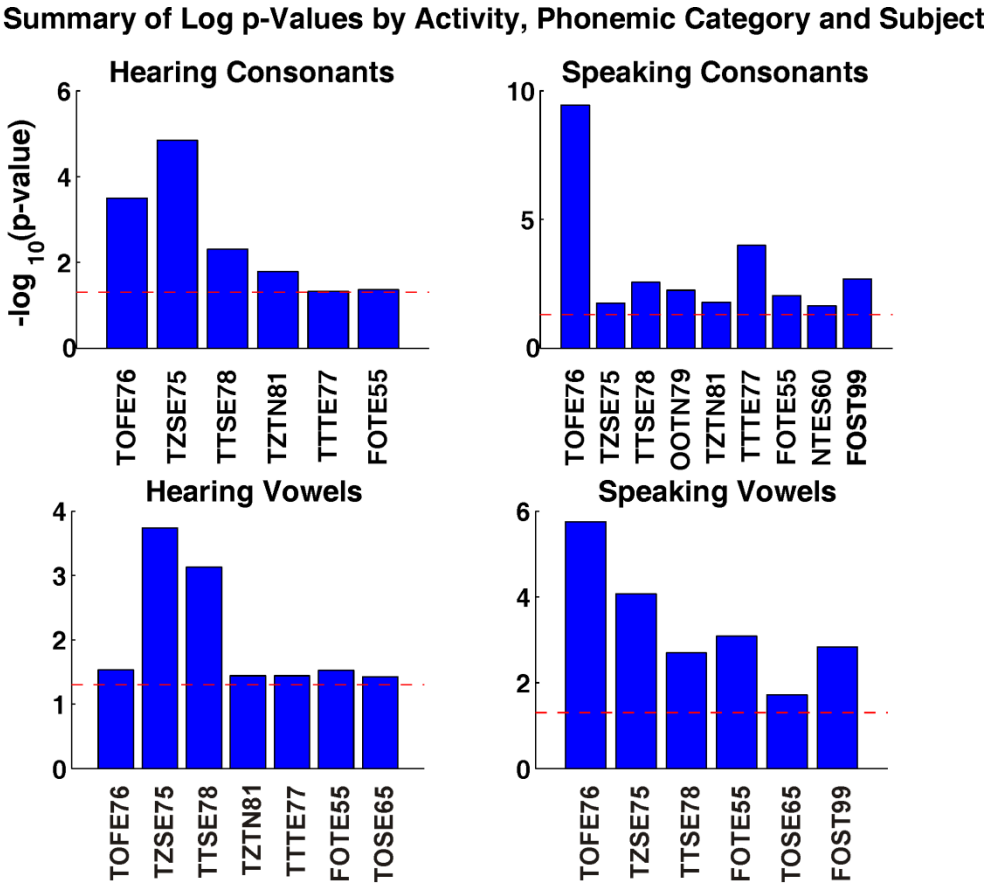

Figure B.2 Classification p-values by subject

Bars plot the associated negative log p-values for classification accuracies in **Error! Reference source ot found.** by cognitive task and phonemic category for each subject with above chance accuracy.

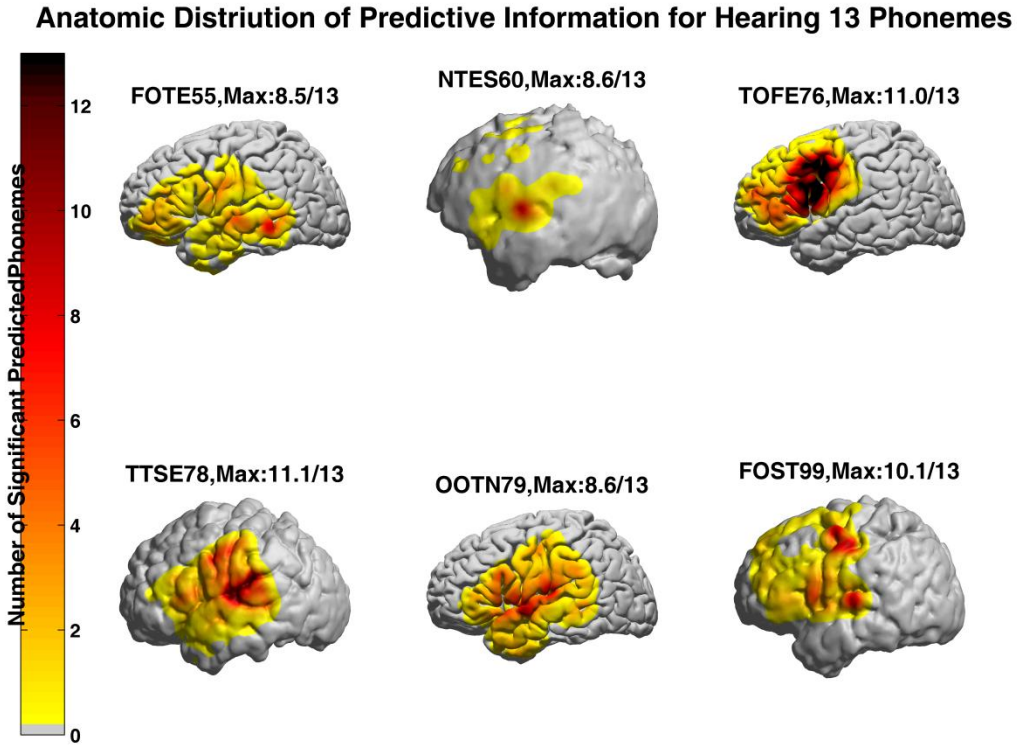

Figure B.3 Single electrode analysis results for hearing phonemes on single subjects
In a format similar to Figure 5.7, the results of the single electrode analysis show the spatial distribution of predicting auditory phonemes.

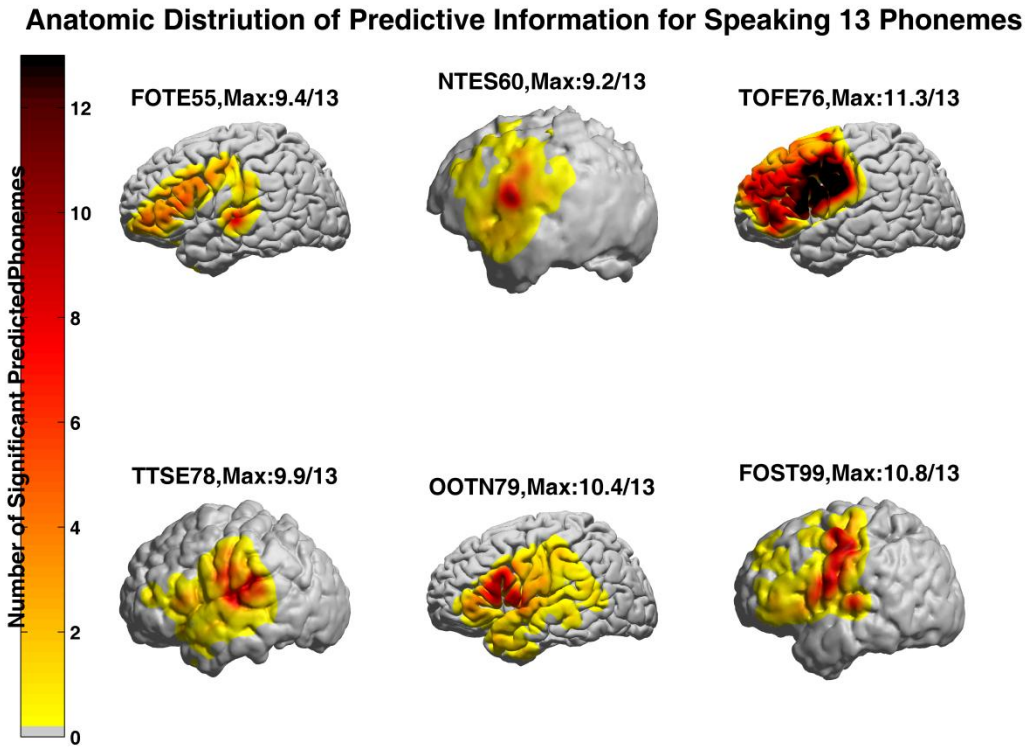

Figure B.4 Single electrode analysis results for speaking phonemes on single subjects
In a format similar to Figure 5.7, the results of the single electrode analysis show the spatial distribution of predicting spoken phonemes.

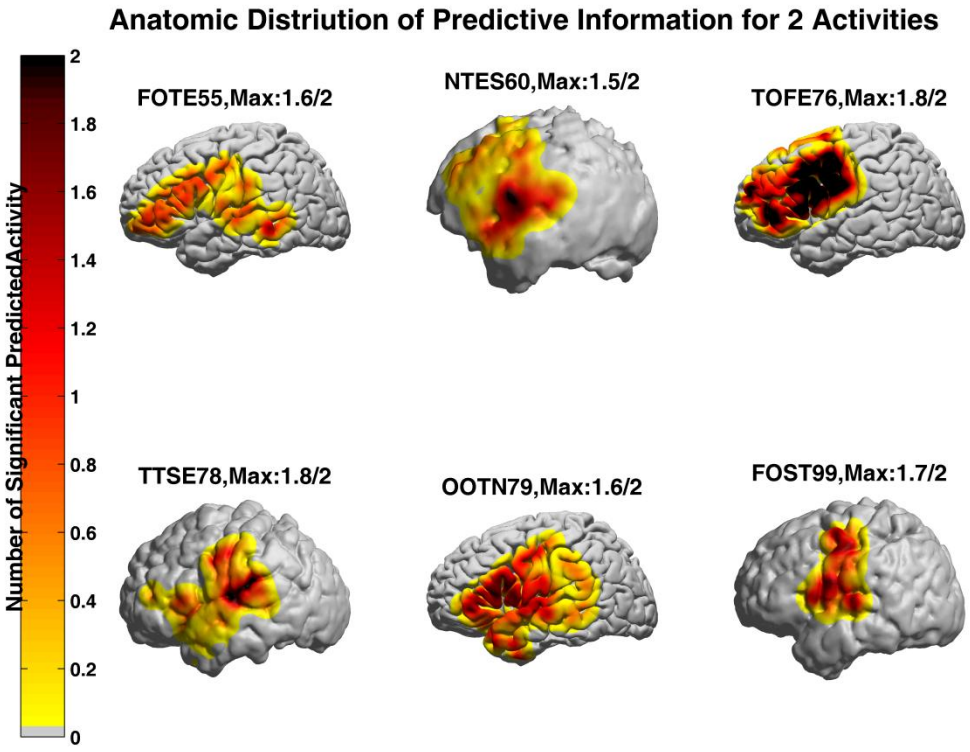

Figure B.5 Single electrode analysis results for general cognitive tasks on single subjects
In a format similar to Figure 5.7, the results of the single electrode analysis show the spatial distribution of both hearing and speaking in general.

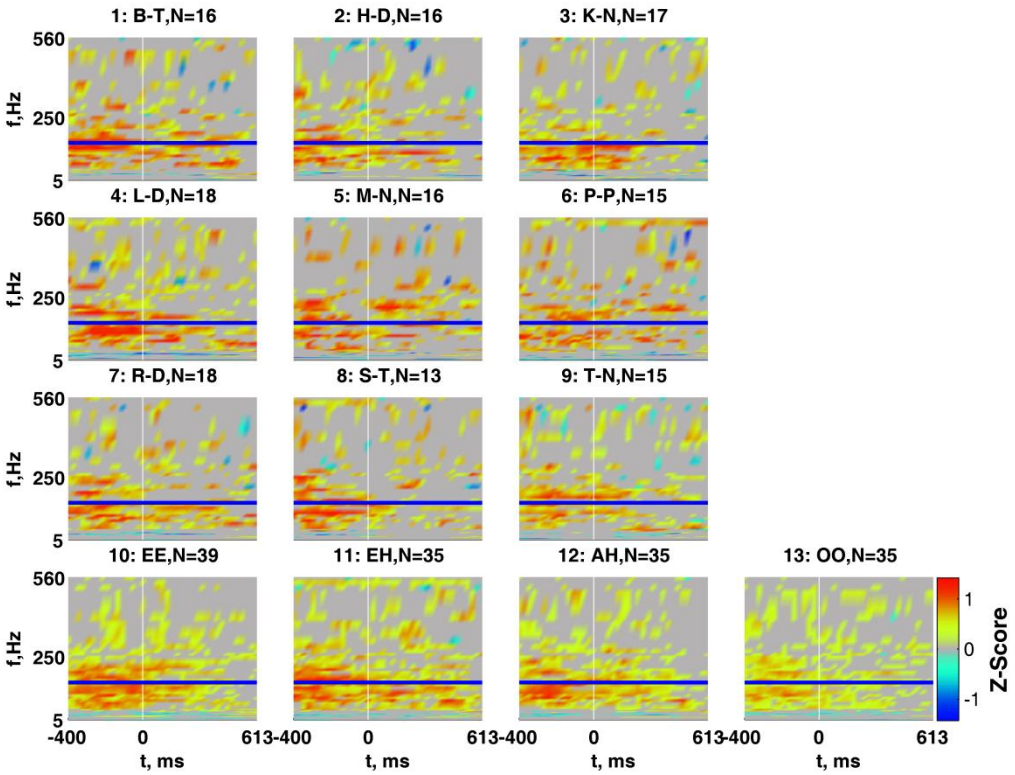

Figure B.6 Matched filters exemplars for all 13 phonemes highlighting temporal diversity
For the same subject and electrode as in Figure 5.8, these plots display matched filter excerpts for all 13 different phonemes. These plots show the spectral and temporal diversity between phonemes in a single cortical location. Statistics were computed as described in the caption for Figure 5.8.

C. Appendix: Supplemental Information, Microarray Diversity

Table C.1 Macroelectrode versus microelectrode impedance comparison
Using a saline bath and sample macro- and microarray ECoG grids, the impedance was calculated using g.USBamps manufactured by g.tec. Impedances were calculated by driving a 10mV sine wave at 10Hz. Channel 4 on the microarray was omitted from the calculations due to a broken connection.

Macroarray Electrode Impedances	Impedance (kΩ)	Microarray Electrode Impedances	Impedance (kΩ)
ch 17 (UA-2007.10.30/01):	65.2	ch 01 (UA-2006.09.10/01):	520.3
ch 18 (UA-2007.10.30/02):	50.8	ch 02 (UA-2006.09.10/02):	385.8
ch 19 (UA-2007.10.30/03):	32.7	ch 03 (UA-2006.09.10/03):	683.9
ch 20 (UA-2007.10.30/04):	36.7	ch 04 (UA-2006.09.10/04):	**4783.1
ch 21 (UA-2007.10.30/05):	20.7	ch 05 (UA-2006.09.10/05):	316.7
ch 22 (UA-2007.10.30/06):	18.5	ch 06 (UA-2006.09.10/06):	947.6
ch 23 (UA-2007.10.30/07):	16.7	ch 07 (UA-2006.09.10/07):	551.7
ch 24 (UA-2007.10.30/08):	15.8		
Mean:	32.1375	Mean:	567.6666667
SD:	18.0656689	SD:	226.4587439

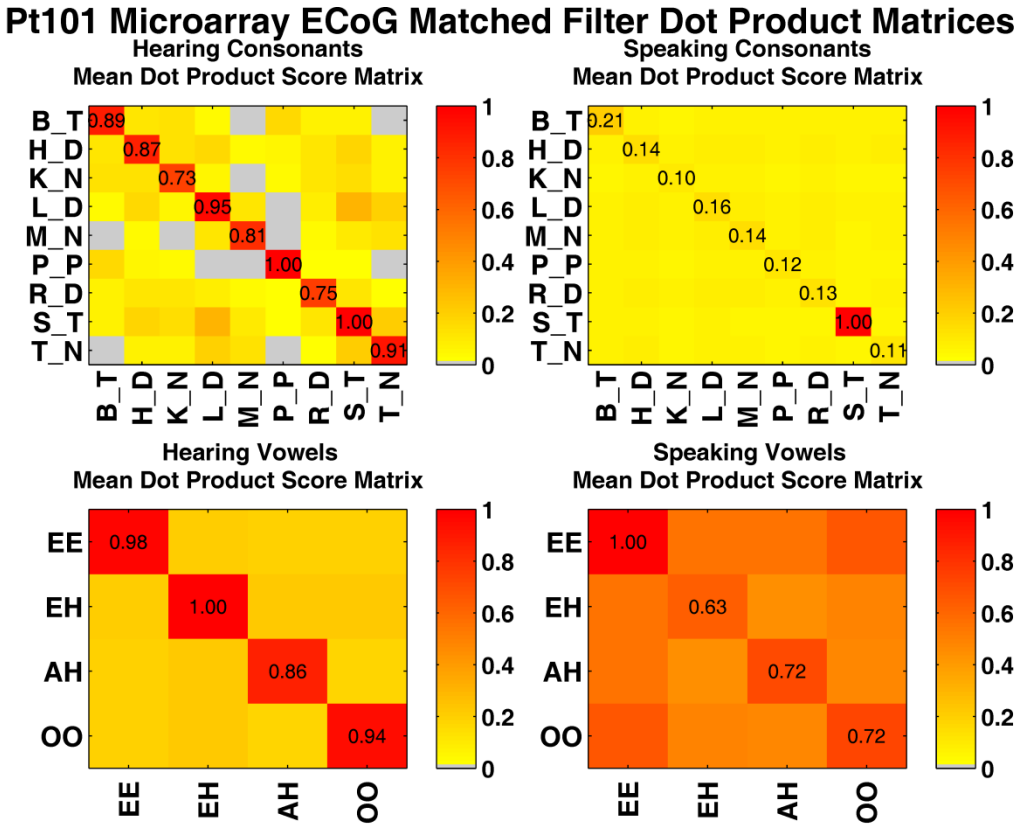

Figure C.1 Matched filter dot product matrices for Subject 12
Using the same format as Figure 6.7, these matrices illustrate the diversity and selectivity of the matched filter reference waveforms in microarray ECoG.

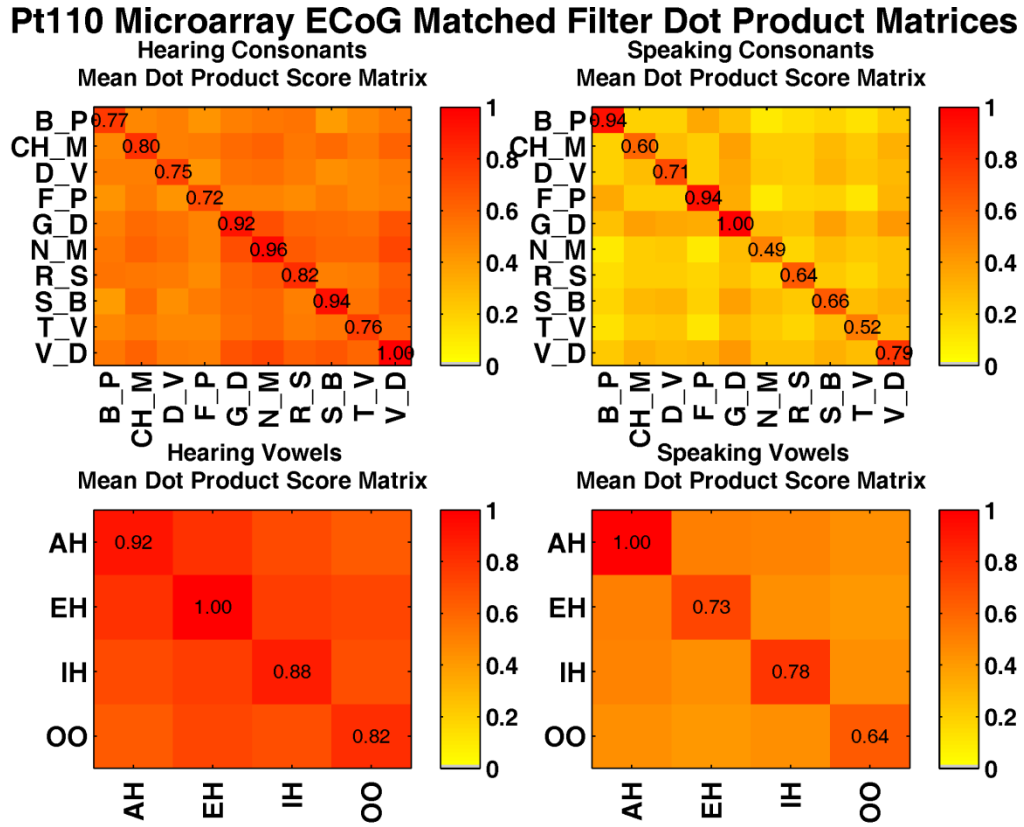

Figure C.2 Matched filter dot product matrices for Subject 13
Using the same format as Figure 6.7, these matrices illustrate the diversity and selectivity of the matched filter reference waveforms in microarray ECoG.

Vita

CHARLES M. GAONA

Education

PhD, Biomedical Engineering, Washington University in St. Louis, 2011
MS, Electrical Engineering, Air Force Institute of Technology, Ohio 2005
BS, Electrical Engineering, University of Colorado, Boulder, 1994
BA, Music, University of Colorado, Boulder, 1994

Employment (July 1994 – Present, Commissioned Officer, United States Air Force)

Jul 08 – Present	**PhD Candidate Air Force Institute of Technology, Civilian Institution Program Washington University in St. Louis, Missouri**
Mar 05 – Jul 08	**Assistant Professor, Communications Division, Department of Electrical and Computer Engineering, United States Air Force Academy, USAF Academy Colorado**
Aug 03 – Mar 05	**Masters Student, Air Force Institute of Technology, Wright-Patterson Air Force Base, Ohio**
Dec 00 – Aug 03	**Chief Engineer, Joint Multi-Platform Common Data Link Program, Reconnaissance System Program Office, Aeronautical Systems Center, Wright-Patterson Air Force Base, Ohio**
Jun 00 – Dec 00	**Flight Commander, Field Training, Lackland Air Force Base, Texas**
Jul 99 – Jun 00	**Flight Commander, Standardization and Evaluation, Lackland Air Force Base, Texas**
Dec 97 – Jul 99	**Operations Officer, 320th Training Squadron, Lackland Air Force Base, Texas**
Dec 96 – Dec 97	**Executive Officer, Aerospace Equipment Management Directorate, Kelly Air Force Base, Texas**
Jul 94 – Dec 96	**Project Engineer, Non-Destructive Inspection Program Office, San Antonio Air Logistics Center, Texas**

Teaching Experience (Academic Year)

Courses Taught

Introduction to Electrical Signals and Systems (2005, 2006)
Electromagnetics (2006)
Communications Systems (2007)
Capstone Design I & II (2007)

Design Projects Mentored

Therapeutic Joystick, Manipulus (AY 2007)
Therapeutic Balance System (AY 2007)

Principal Publications

- Gaona, C. M., M. Sharma, Z. V. Freudenburg, J. D. Breshears, D. T. Bundy, J. Roland, D. L. Barbour, G. Schalk and E. C. Leuthardt (2011). "Nonuniform high-gamma (60–500 hz) power changes dissociate cognitive task and anatomy in human cortex." The Journal of Neuroscience **31**(6): 2091-2100
- C.M. Gaona, R.F. Mills, M.A. Temple, T.B. Hale, "Spectrally Encoded, Multicarrier PSK Communication in a Multipath Channel," *Proceedings of the 24th Digital Avionics Systems Conference*, Washington D.C., November 2005.
- C.M. Gaona, "Performance of a Spectrally Encoded Multi-Carrier Phase Shift Keying Communications System in a Frequency-Selective, Slowly-Fading Multipath Channel," Masters Thesis, Air Force Institute of Technology, March 2005.

Additional Publications

- Breshears, J. D., J. L. Roland, M. Sharma, C. M. Gaona, Z. V. Freudenburg, R. Tempelhoff, M. S. Avidan and E. C. Leuthardt (2010). "Stable and dynamic cortical electrophysiology of induction and emergence with propofol anesthesia." Proceedings of the National Academy of Sciences 107(49): 21170-21175.
- Leuthardt, E. C., C. Gaona, M. Sharma, N. Szrama, J. Roland, Z. Freudenberg, J. Solis, J. Breshears and G. Schalk (2011). "Using the electrocorticographic speech network to control a brain–computer interface in humans." Journal of Neural Engineering 8: 036004.
- Liu, Y., M. Sharma, C. M. Gaona, J. D. Breshears, J. Roland, Z. V. Freudenburg, K. Q. Weinberger and E. C. Leuthardt (2010). Decoding ipsilateral finger movements from ecog signals in humans. Advances in Neural Information Processing Systems 23, MIT Press.
- Pei, X., E. C. Leuthardt, C. M. Gaona, P. Brunner, J. R. Wolpaw and G. Schalk (2011). "Spatiotemporal dynamics of electrocorticographic high gamma activity during overt and covert word repetition." Neuroimage 54(4): 2960-2972.
- Wu, M., K. Wisneski, G. Schalk, M. Sharma, J. Roland, J. Breshears, C. Gaona and E. C. Leuthardt (2010). "Electrocorticographic frequency alteration mapping for extraoperative localization of speech cortex." Neurosurgery 66(2): E407.

Scientific and Professional Societies

Tau Beta Pi
Eta Kappa Nu
Institute of Electronic and Electrical Engineers, Member
Society for Neuroscience, Member

Honors and Awards

Outstanding Academy Educator, Department of Electrical and Computer Engineering, United States Air Force Academy Academic Year 2006-2007

Best Paper in Session, Best Paper in Communications and Navigation Systems Track and Best Student Paper, 24th Digital Avionics Systems Conference, Nov 2005, Crystal City, Virginia

Edwin E. Aldrin, Sr. Award, Air Force Institute of Technology, March 2005

Institutional and Professional Service

Systems Engineering Working Group representative for Department of Electrical and Computer Engineering

Engineering Division Capstone Working Group representative for Department of Electrical and Computer Engineering

Dean's Creating Academically Rich Environment Initiative representative for Department of Electrical and Computer Engineering

Professional Development Activities

City University of New York Seminar on Just-in-Time-Teaching, George Mason University, June 2006

Courses Taken at University of Colorado, Colorado Springs:

Real-Time Digital Signal processing (ECE 5655), Spring 2006
Electromagnetic Wave Propagation (ECE 5110), Fall 2005
Microwave Measurement Lab (ECE 5150), Fall 2005

Departmental technical presentation on Just-in-Time-Teaching

High Gamma Band Diversity in ECoG, Gaona, PhD. 2011